A 400 Ma-long Nd-Hf isotopic evolution of melt-modified garnet-pyroxenites in an ancient subcontinental lithosphere (Lanzo North ophiolite, Western Alps)

Alessio Sanfilippo*[1,2], Giulio Borghini[3], Luisa Guarnieri[4], Eizo Nakamura[5], Giovanni B. Piccardo[4], Riccardo Vannucci[1,2], Alberto Zanetti[2]

[1]Università degli Studi di Pavia, Via Ferrata 1, 27100 Pavia, Italy.
[2]Istituto Geoscienze e Georisorse, CNR, Via Ferrata 1, 27100, Italy.
[3]Dipartimento di Scienze della Terra, Università degli Studi di Milano, via Botticelli 23, 20133 Milano, Italy
[4]Accademia delle Scienze di Torino, Via Accademia delle Scienze, 6, 10123 Torino, Italy
[5]The Pheasant Memorial Laboratory for Geochemistry and Cosmochemistry, Institute for Planetary Materials, Okayama University, Misasa, Tottori 682-0193, Japan
*correspondence to alessio.sanfilippo@unipv.it

ABSTRACT

Pyroxenite veining is widely preserved in peridotite massifs, and used to derive information on the origin and evolution of upper mantle domains. These lithospheric mantle sections can be isolated from the convecting mantle for > 1 Ga or more, suffering a long history of melting and/or melt-rock reaction processes, which modify their original chemical and isotopic compositions. Here, we show the effect of ancient process of melt-rock reaction in the chemistry of garnet pyroxenites from Lanzo North Massif, an iconic lithospheric mantle section exhumed during the opening of the Jurassic Alpine Tethys. Selected pyroxenites are more than 10 cm thick, and embedded within peridotites that have textures and chemical compositions indicative of a complex history of interaction with migrating melts. Whole rock and clinopyroxene Nd-Hf isotopes of the pyroxenites consistently indicate that the first melt-rock reaction event occurred at ~400 Ma, likely in combination with exhumation from the garnet to the spinel-facies mantle conditions. Two samples still retain textural relicts and chemical evidence of precursor garnet and have high ε_{Nd} (~12) for comparatively low ε_{Hf} (~10), when recalculated at 400 Ma, which suggest that they were less affected by this ancient percolation process. The chemical evidence of such a long history of melt-rock reactions was preserved from 400 Ma until present. Finally, two pyroxenites located within plagioclase peridotites show evidence for an event of re-equilibration at plagioclase-facies conditions, likely triggered by infiltration of melt in the host rock. These samples reveal the coexistence of two internal Sm-Nd isochrones at 152 ± 30 Ma and 149 ± 13 Ma, thereby providing temporal constraints to the event of melt impregnation of the host peridotites as consequence of the opening of the Ligurian Tethys ocean.

Keywords: pyroxenite; Nd-Hf isotopes; Lanzo ophiolite; melt-rock reaction; subcontinental lithospheric mantle

1. INTRODUCTION

The upper mantle is a heterogeneous mixture of domains having different geochemical signatures inherited from a long-history of melting, recycling and re-fertilization processes (e.g. Stracke, 2012). Due to their fertile character, geochemically enriched domains are preferentially melted and thereby rarely recovered amongst abyssal peridotites (Salters and Dick, 2002; Warren, 2016). Geochemically enriched lithologies, mainly represented by pyroxenite veining, are nonetheless preserved in subcontinental peridotite massifs (Garrido and Bodinier, 1999; Downes, 2007; Bodinier and Godard, 2014) and, locally, in ophiolites formed at slow spreading environments (e.g., Montanini et al., 2012; Borghini et al., 2016). Indeed, most orogenic peridotites contain a great variety of pyroxenites and some of them, called "garnet pyroxenites", are mostly constituted by pyroxene and garnet, proving to be equilibrated at high pressure (e.g. Bodinier et al., 1987; Pearson et al., 1991; Morishita et al., 2003; Montanini et al. 2012). Contrary to what observed for abyssal peridotites (Cipriani et al., 2004; Stracke et al., 2011), which on average retain isotopic compositions more depleted than the associated MORB, the isotopic ratios of garnet pyroxenites extends towards enriched values (that is low $^{143}Nd/^{144}Nd$ and $^{176}Hf/^{177}Hf$, and high $^{87}Sr/^{86}Sr$ isotopic ratios), covering the entire variability of melts erupted at ocean ridges. The variability of Sr-Nd-Hf isotopic compositions related to pyroxenites is often coupled with very old Re-Os model ages (>1 Ga), thus consistent with the expected isotopic variability and timescale for crustal recycling in the mantle (Blichert-Toft et al., 1999; Pearson and Nowell, 2004; Ackerman et al., 2016; Varas-Reus et al., 2018; Tilhac et al., 2020). These data support the hypothesis that enriched domains in the upper mantle mostly derive from recycled portions of oceanic or continental lithosphere, including igneous crust, lithospheric mantle and associated sediments (e.g. Stracke et al., 2003; Lambart et al., 2016).

Most peridotite massifs represent ancient lithospheric portions emplaced at crustal depths after being isolated form the convecting mantle for hundreds of millions of years, or more (Reisberg

and Lorand, 1995). During their exhumation, these mantle sequences commonly experience events of partial melting or interaction with migrating melts leading to changes in their original mineralogy, texture and composition (Le Roux et al., 2009; McCarthy and Müntener, 2015; Rampone et al., 2020; Rampone and Sanfilippo, 2021). While fast exhumation rates prevent any substantial perturbations in the long-lived radiogenic isotope systematics (such as Rb-Sr; Sm-Nd; Lu-Hf; U-Th-Pb) (Blichert-Toft et al., 1999; Pearson and Nowell, 2004; Varas-Reus et al., 2018), a long-lasting history of exhumation associated with melting and/or interactions with migrating melts may result in significant variation in parent/daughter isotope ratios, causing deviations from the original isotopic signature (Pearson et al., 1991; Tilhac et al., 2017).

Here, we focus on garnet-pyroxenites within melt-modified peridotites from a subcontinental mantle to discuss the chemical changes imposed by old melt migration and their effect on the long-term Nd-Hf isotopic evolution of pyroxenites. We use major-trace elements and Nd-Hf isotope compositions of decimetre-thick pyroxenites from the Lanzo North massif (Western Italian Alps), a well-studied lithospheric sub-continental mantle section exhumed at the ocean seafloor during the opening of the Ligurian Tethys, in the Middle Jurassic (Boudier, 1978; Lagabrielle et al., 1989). Previous studies on the host peridotites indicate that this mantle sequence suffered a multistage history of interaction with melts having an enriched (E)-MORB signature (Guarnieri et al., 2012). New chemical/isotopic compositions of the pyroxenites are here used to constrain an older event of migration and spinel-facies equilibration at 400 Ma. Geochemical modelling suggests that this event caused a shift towards low Hf isotope ratios for comparatively high Nd isotope ratios, producing unusual Nd-Hf isotope decoupling below the mantle array. We infer that the chemical response to this ancient history of melt-rock reaction is preserved until present. Moreover, two samples collected within plagioclase-bearing peridotites preserve Sm-Nd internal isochrones indicating that the equilibration at plagioclase-facies mantle conditions occurred at closed system, likely triggered by increase in temperature due to the infiltration of melts into the

host peridotite during the emplacement of the Lanzo North mantle sequence on the Jurassic seafloor.

2. LANZO NORTH PERIDOTITE MASSIF: PETROLOGICAL BACKGROUND

2.1 Peridotites

The Lanzo peridotite massif is part of the Sesia-Lanzo Zone, an accretionary prism of the Alpine orogeny formed by continental crustal rocks and subordinate subcontinental mantle slivers from the Adriatic plate (Fig. 1). The Sesia-Lanzo Zone represents the thinned and partially exhumed ocean-continent transition (OCT) along the Adriatic margin of the Alpine Tethys, and is bound to the east to the lower continental crustal rocks of the Adriatic plate (i.e., Ivrea-Verbano Zone, Southern Alps) by the Insubric line (the Peri-Adriatic lineament) and to west to meta-ophiolitic units of the Jurassic Piedmontese basin (i.e. Pennidic units; Fig. 1). The Lanzo ultramafic massif constitutes the southernmost portion of the Sesia-Lanzo Zone, and it has been subdivided in three domains, namely South, Central and North, on the basis of distinct geochemical characteristics (after Boudier, 1978; Bodinier et al., 1991). The Lanzo North massif exposes exceptionally well-preserved subcontinental mantle peridotites, locally intruded by ~160 Ma-old MORB-type gabbros (Piccardo et al., 2007a;b; Kaczmarek et al., 2008) and basalt dykes (**Fig. 1**). Primary contacts with a Jurassic sedimentary cover indicate the exhumation of the mantle section on the Alpine Tethys seafloor (Lagabrielle et al., 1989).

Several contributions described the overall characteristics of the different rock types in the Lanzo North (Boudier, 1978; Pognante et al., 1985; Bodinier, 1988; Bodinier et al., 1991; Piccardo et al., 2007a; Piccardo, 2010; Guarnieri et al., 2012); the main results are hereafter summarised. The older rock type is spinel lherzolite tectonite, which locally exceeds 10 vol% of porphyroclastic clinopyroxene (Cpx) and, in place, contain centimeter-size symplectitic clusters of spinel + orthopyroxene and minor clinopyroene (Spl+Px). Similar to other peridotite occurrences (e.g., Hoogerduijn Strating et al., 1993; Vannucci et al., 1993), these textures were considered products of

garnet breakdown after transition to spinel-facies mantle conditions, thus suggesting an early equilibration at garnet facies conditions. These spinel lherzolites retain PM-like PGE patterns and up to 1 Ga-old Re depletion ages (calculated after Becker et al., 2006) that are coupled with relatively fertile major and incompatible trace element compositions. They yielded Sm-Nd and Lu-Hf model ages up to 2.1 Ga (Bodinier et al., 1991; Guarnieri et al., 2012). Chemical and isotopic data, thus, indicate a geochemical affinity acquired after a long-time isolation from the convective mantle in a subcontinental lithosphere, and an early process of re-equilibration at garnet-facies conditions (Boudier, 1978; Bodinier et al., 1991; Guarnieri et al., 2012).

The Spl-Px cluster-bearing spinel lherzolite tectonite is partially replaced by pyroxene-poor spinel harzburgites, also called reactive harzburgite (Guarnieri et al., 2012). Indeed, microtextural and geochemical evidence indicate that these modally depleted rocks formed by reactive percolation of silica-undersaturated melts with a E-type MORB geochemical signature (Guarnieri et al., 2012). The high LREE contents and variable Nd-Hf isotopes are the distinctive signatures of these melt-modified rocks. Symplectitic Spl+Px clusters rarely occur in the harzburgites, suggesting that they were consumed during the melt-rock reaction process. The preservation of radiogenic Nd and Hf isotopic ratios at variable Sm/Nd and Lu/Hf in these Spl-harzburgites led Guarnieri et al. (2012) to suggest that the event of migration of olivine-saturated melts occurred in Paleozoic times.

Locally, both lherzolites and modally depleted harzburgites show plagioclase-orthopyroxene micro-veins that crosscut the spinel-facies mineral assemblage, associated with a consequent increase in bulk rock SiO_2, Al_2O_3 and CaO at decreasing MgO and NiO contents (Guarnieri et al., 2012). These plagioclase-bearing peridotites form hectometric-scale domains that suggest a localized event of migration of silica-saturated MORB-like melts uprising in response to the passive upwelling of the asthenospheric mantle and continental extension that led to the opening of the Ligurian Tethys ocean in Jurassic times (Piccardo et al., 2003; Muntener et al., 2004; Piccardo and Vissers, 2007; Piccardo et al., 2007a; b; Piccardo, 2010; Higgie and Tommasi, 2014; Piccardo, 2016). This process is common in the ophiolitic mantle sequences of the Alpine-Appenine

143 ophiolites and is referred to as “plagioclase-impregnation” (see Rampone and Sanfilippo, 2021 for a
144 review).
145
146 **2.2 Pyroxenites**
147 Pyroxenites are widespread in the Lanzo North mantle sequence where they occur as
148 centimeter- to decimeter-thick layers within the different rock types (**Fig. 2**). The pyroxenites are
149 often parallel or sub-parallel to tectonic foliation of host peridotite (**Fig. 2d,e**), although they
150 locally are intensely folded and boudinated (Boudier, 1978; Piccardo et al., 2007b, Piccardo, 2010)
151 (**Fig. 2c**). This is in agreement with the idea that thick pyroxenites represent long-lived
152 heterogeneities deformed at deep lithospheric conditions (Bodinier and Godard, 2014). Thick
153 pyroxenite layers occur within spinel lherzolites, spinel harzburgites and plagioclase(Pl)-
154 peridotites, as previously described by Boudier (1978), Piccardo et al. (2007b) and Guarnieri et al.
155 (2012).
156 In this study, we focused on samples from the inner portions of thick (>10 cm) pyroxenite
157 layers. Samples were distinguished in three types of pyroxenites, based on their host rock. (i)
158 cluster-bearing (Grt)-Spl pyroxenites were collected within spinel lherzolites (**Fig. 2a,b**), which
159 represent the oldest rock-type in Lanzo North massif (Guarnieri et al., 2012). These pyroxenites
160 contain exceptionally diffuse Spl-Px clusters (**Fig. 2a,b**), similar to those locally found in the host
161 fertile lherzolites (Guarnieri et al., 2012). These microstructures coupled with geochemical
162 characteristics of the pyroxenes, such as very high Sc and V contents and HREE (Yb at 40-60 x CI)
163 in spinel-bearing clinopyroxene porphyroclasts, indicate that they are the sub-solidus product of
164 spinel-facies recrystallization of precursor garnet pyroxenites (see also Piccardo et al., 2007b;
165 Guarnieri et al., 2009; 2012), suggesting that they originated at least at P > 1.5 GPa (Piccardo,
166 2010; Borghini and Fumagalli, 2018). (ii) (Grt)-Spl pyroxenites occur within modally depleted
167 spinel harzburgites, which formed by olivine-forming and pyroxene-dissolving reactions induced
168 by percolating melts (Guarnieri et al., 2012). They rarely show Spl-Px clusters and commonly have

porphyroclastic textures made by coarse clinopyroxene and orthopyroxene and sporadic large green spinel. Large olivine porphyroclasts are also locally present although commonly replaced by serpentine. In pyroxenite groups "i" and "ii", rare exsolutions of secondary pyroxene plus plagioclase into coarse-grained pyroxene porphyroclasts and thin plagioclase + olivine coronas around Spl indicate the incipient recrystallization at plagioclase-facies conditions ($P < 1.0$ GPa, Piccardo et al., 2007b). (iii) Spl-Pl pyroxenites occur within plagioclase-impregnated peridotites (**Fig. 2e**). They have websteritic composition and compared to the Grt-Spl pyroxenites contains higher amounts of serpentinized olivine. Spl-Px clusters are absent in the Spl-Pl pyroxenites that instead show much larger extent of plagioclase-bearing recrystallization. This latter is testified by large domains of plagioclase + olivine + pyroxene neoblasts and diffuse occurrence of pyroxene + plagioclase exolutions partially replacing the coarse pyroxene and spinel porphyroclasts (**Fig. 2f**). In place, one Spl-Pl pyroxenite sample also shows thin plagioclase + orthopyroxene coronas surrounding clinopyroxene porphyroclasts (Piccardo et al., 2007b). These textures testify an event of equilibration at Pl-facies conditions likely triggered by the melt impregnation of the host peridotite (Piccardo et al., 2007b). As noted in previous studies, the field and microstructural features of the Lanzo N pyroxenites provide evidence that these rocks experienced multiple stages of equilibration, ranging from garnet- to spinel- to plagioclase-facies, as response of the progressive exhumation of the Lanzo North peridotite massif on the Jurassic seafloor (see Piccardo et al. 2007b; Guarnieri et al., 2012 and references therein).

3. ANALITICAL METHODOLOGY

Samples for this study were selected from the innermost portions of thick (>10 cm) pyroxenite layers. Analytical methodologies are identical to those reported in Guarnieri et al. (2012) for the host peridotites from Lanzo North. Hereafter, we include a brief description of each method, the reader is referred to Guarnieri et al. (2012) for further details. Major and trace elements whole-rock analyses were performed at the Pheasant Memorial Laboratory for Geochemistry and

Cosmochemistry (PML), Institute for Study of the Earth's Interior (ISEI, reorganized into the current Institute for Planetary Materials, IPM, in 2016), Okayama University at Misasa, Japan. Whole-rock major element compositions were determined by X-ray fluorescence spectrometry (XRF) with a Phillips PW 2400, using lithium tetraborate glass beads (1:10 ratio of sample and flux; Takei, 2002). Fusion temperature for bead preparation was set at 1,050 ˚C to avoid loss of alkali metals (Willis, 2010). The LOI (loss on ignition) was obtained by gravimetric method, and FeO content was determined by titration (Yokoyama & Nakamura, 2002). Matrix correction follows Norrish & Chappell (1977). Instrumental calibration was performed using the reference igneous rocks (n = 13) provided from Geological Survey of Japan (GSJ); those include andesites (JA-2 and JA-3), basalts (JB-1b, JB-2 and JB-3), rhyolites (JR-1, JR-2 and JR-3), granites (JG-1a and JG-2), gabbros (JGb-1 and JGb-2), peridotite (JP-1), and hornblendite (JH-1). Major-element compositions of these reference rocks are from Imai et al. (1995, 1999) and Terashima et al. (1998). Accuracy of calibration is better than 1%, estimated from root mean square of residues.

Trace elements were analyzed by inductively coupled plasma-quadrupole mass spectrometry (Agilent 7500CS) using the techniques of Makishima and Nakamura (2006). For Rb, Sr, Y, Cs, Ba, REE, Pb, Th, and U analysis, samples were spiked with ^{149}Sm and dissolved following the method of Makishima and Nakamura (1997). For the HFSE (Zr, Nb, Hf, and Ta) analysis, a mixed ^{91}Zr-^{179}Hf spike was added to the samples. Samples were dissolved following the Teflon bomb method of Tanaka et al. (2003). The 2sigma reproducibility of the rock standard JB-2 is less than 7% (n=3), and procedural blanks were less than 13 pg (n=2) for Rb, Sr, Y, Cs, Ba, REE, Pb, Th, and U analysis. For the HFSE analysis, the 2sigma reproducibility of the rock standard JB-3 is less than 5% (n=3), procedural blanks were less than 150pg for Nb, Hf and Ta, 5.7ng for Zr. Blank correction was applied to all the obtained elemental concentrations, and was less than 1% for Rb, Sr, Y, Cs, Ba, REE, Pb, Th, and U. Since the aluminum addition method (Tanaka et al, 2003) was applied to the HFSE analysis, the high blank value in the analysis is attributed to the added Al solution corresponding to the decomposed sample amount (~50 mg).

Except for Nb in PY5 (9% correction), the blank corrections for Zr, Nb, and Hf were less than 4%; however, Ta resulted in corrections from 60 to 150%, and nearly 400% in PY5. Typical detection limits (3sigma) in the analyses are sub-ppt up to 30ppt, which corresponds to sub-ppb to 30ppb of elemental concentration in the sample.

Major elements compositions of clinopyroxene and plagioclase (Tables S2, S3): were determined using a JEOL 8200 SuperProbe at the Dipartimento di Scienze della Terra, Università degli Studi di Milano. Accelerating voltage was 15 kV, beam current 15 nA. Natural and synthetic minerals and glasses were used as standards. In-situ trace element analysis of clinopyroxenes and plagioclase was carried out by laser ablation inductively coupled plasma mass spectrometry (LA-ICP-MS) at the IGG-CNR of Pavia, Italy. The laser probe consisted of a Q-switched Nd:YAG laser, model Quantel (Brilliant); the spot diameter was typically of 50 um. The ablated material was analyzed using an Elan DRC-e quadrupole mass spectrometer. NIST SRM 610 synthetic glass was used as an external standard. The CaO content determined by electron microprobe analysis (EMPA) was used as an internal standard. Precision and accuracy were assessed from repeated analyses of the BCR-2 g standard and were usually better than ±10%.

Neodymium-Hf isotope determinations for whole-rock, clinopyroxene (Cpx) and plagioclase (Pl) were performed at the PML as described above (Table S4). Neodymium isotopic composition and Nd and Sm abundances were analyzed on whole-rock, clinopyroxenes and plagioclase, whereas Hf isotopes and Lu and Hf concentrations were obtained for whole rocks exclusively. Clinopyroxene and plagioclase separates were handpicked under a binocular microscope. Although the isotopic exchange between seawater and the original mineral assemblage during late-stage alteration is negligible for Nd and Hf, to minimize the possible effects of seawater alteration, clinopyroxenes and whole-rocks were leached following a multi-day and multi-stage procedure. Analyses of Sm-Nd isotope ratios and concentrations were performed by thermal ionization mass spectrometry (TIMS) following the techniques of Nakamura et al. (2003). Sample powders (100-130mg of whole rock, 10-60mg of Cpx, 80mg of Pl) were spiked with ^{150}Nd and

^{149}Sm prior to dissolution and Nd isotope ratios and abundances by isotope dilution were determined simultaneously on a Thermo Fisher Scientific Triton TIMS equipped with nine Faraday cups. Samarium abundances were determined by isotope dilution procedures using a Finnigan-MAT262 solid-source TIMS equipped with five Faraday cups following Nakamura et al. (2003). Mean value of ^{143}Nd/^{144}Nd and reproducibility obtained by analyses of the in-house standard PML-Nd was 0.511737 +/- 0.000013 (2sigma, n=15), and corresponded value of the La Jolla standard was 0.511872 +/- 0.000013 (2sigma). The result of the reference rock standards JB2 and JB3 were 0.513114+/- 0.000029 (2sigma, n=4) and 0.513078+/- 0.000013 (2sigma, n=5), respectively. Total procedural blanks of Nd and Sm were 0.7pg (n=5) and 0.1pg (n=5) for Cpx and Pl, 2pg (n=5) and 0.2 pg (n=5) for whole-rock, respectively.

For Lu and Hf abundance and Hf isotope ratio determination, MC-ICP-MS (Thermo Fisher Scientific Neptune) was used. Whole -rock powders (100-130mg) were spiked with ^{176}Lu and ^{179}Hf prior to decomposition and Hf isotope ratios and abundances by isotope dilution were determined simultaneously applying the techniques of Lu et al. (2007) and Makishima and Nakamura (2008). Lu contents were also measured following the procedures of Makishima and Nakamura (2008). Hafnium isotopic data were normalized to ^{176}Hf/^{177}Hf = 0.282192 for JMC 14374, which corresponds to ^{176}Hf/^{177}Hf = 0.282160 for JMC 475. The ^{176}Hf/^{177}Hf result of the reference rock standards JB3 was 0.283224+/- 0.000011 (2sigma, n=5). Total procedural blanks of Hf and Lu were 154pg (n=11) and 0.1pg (n=11), respectively.

4. RESULTS: MAJOR, TRACE ELEMENTS AND ND-HF ISOTOPIC COMPOSITIONS

Selected Lanzo North pyroxenites show rough correlations in bulk MgO vs Al_2O_3, CaO and Ni. The MgO, Al_2O_3, CaO and Ni contents in (Grt)-Spl pyroxenites cluster around rather uniform values at relatively high MgO (~20 wt%) (**Fig. 3**). One sample (PY5) shows lower MgO (15 wt%) at higher Al_2O_3, CaO and low Ni (13.5 and 14 wt%, 400 ppm, respectively). On the other hand, Pl-Spl pyroxenites have higher MgO (up to 23 wt%) and Ni (up to 1100 ppm) and lower Al_2O_3 and

CaO contents (7.5 and 8 wt%, respectively). As a whole, the Lanzo N Pl-Spl pyroxenites plots in the field of the Pl-Spl pyroxenites from Beni Bousera and Ronda SCLM, and from the Ligurian ophiolites, whereas the (Grt)-Spl pyroxenites plot within the field of Beni Bousera and Ronda Grt pyroxenites, at generally higher MgO and Ni and lower CaO and Al_2O_3. Notably, PY5 (Grt)-Spl pyroxenite having low MgO and Ni, and high CaO, content is nearly undistinguishable from the Grt-pyroxenites reported in literature (**Fig. 3**).

The CI-normalized REE patterns of the cluster-bearing (Grt)-Spl pyroxenites reveal variable depletion in LREE (La_N/Sm_N = 0.12-0.32) coupled with selective enrichments in HREE over the MREE (Sm_N/Yb_N = 0.31-0.60) (**Fig. 3d; 4a**). These chemical characteristics agree with the local preservation of abundant Spl-Opx clusters and are similar to those of the External Ligurian Grt-pyroxenites, but at comparatively higher LREE (**Fig. 4a**). The high HREE abundances are also comparable with those observed in some garnet-bearing pyroxenites from orogenic ultramafic massifs of the Mediterranean area (Bodinier et al., 1987; Pearson et al., 1991, 1993; Garrido and Bodinier, 1999; Gysi et al., 2011; Montanini et al., 2012; Borghini et al., 2016). The REE patterns of the Pl-Spl pyroxenites are subparallel to those of (Grt)-Spl pyroxenites although they have relatively high and constant LREE (La_N/Sm_N =0.22-0.24) and nearly flat M-HREE patterns (Sm_N/Yb_N =0.62-0.68) (**Fig. 4a**). Overall, the CI-normalized patterns show an increase in LREE at decreasing HREE from the (Grt)-Spl pyroxenites towards the Pl-Spl pyroxenites (**Fig. 3d**). Similar chemical features are shown by the Cpx, which in the cluster-bearing (Grt)-Spl pyroxenites are characterized by high HREE, V and Sc contents and generally lower LREE compared to those in Pl-Spl peridotites (**Fig. 4b**; Table S3 in supplements). The compositions of Cpx presumably acquired most of the trace element signature from the whole-rock after equilibration at Spl-facies conditions (Vannucci et al., 1993; Rampone and Borghini, 2008; Borghini et al., 2013, 2016), indicating that garnet was at least locally abundant in the precursor mineral assemblages of some (Grt)-Spl pyroxenites.

Neodynium isotopic ratios were determined for Cpx, Pl and WR. Pyroxenites Cpx and WR reveal

299 a narrow isotopic variability, with present day $^{143}Nd/^{144}Nd$ ranging from 0.5131 to 0.5134 and
300 $^{147}Sm/^{144}Nd$ from 0.22 to 0.35 (**Fig. 5a**). On a closer inspection, Cpx and WR of 5 of the 7 samples
301 define an errorchron at 410 ± 17 Ma. The two Grt-Spl pyroxenites preserving Spl-Px clusters do not
302 plot along this array, retaining highly radiogenic $^{143}Nd/^{144}Nd$, but relatively low $^{147}Sm/^{144}Nd$ (**Fig.**
303 **5a**). Nd isotopes of Pl separates were also obtained from two Pl-Spl-pyroxenites. They provide Pl-
304 Cpx-WR internal isochrones at 152 ± 30 Ma and 149 ± 13 Ma. These ages are in good agreement
305 with the emplacement of Lanzo N massif at crustal depth as also indicated by the ages of the
306 MORB-type intrusions in Lanzo (Kaczmarek et al., 2008), and rather coeval with intrusive oceanic
307 crustal rocks of Jurassic Tethys (Rampone et al., 2014; Tribuzio et al., 2016 and references therein).
308 Whole-rock Hf isotopes of all pyroxenites define an errorchrone at 396 ± 27 Ma (**Fig. 5b**), notably
309 consistent with the Cpx-WR errorchrone yielded by Nd isotopes, if the (Grt)-Spl pyroxenites
310 preserving Spl-Px clusters are excluded. These cluster bearing (Grt)-Spl pyroxenites have the
311 highest $^{187}Lu/^{188}Hf$ and $^{187}Hf/^{188}Hf$ ratios, in agreement with a strong Grt signature. When
312 calculated at the time of emplacement of the Lanzo section at shallow depths (160 Ma), the initial
313 εNd-εHf values of all samples plot along the Nd-Hf terrestrial array. This suggests that at the time
314 of emplacement on the Jurassic seafloor, these pyroxenites were characterized by a wide isotopic
315 heterogeneity, varying from depleted to enriched Nd-Hf isotopic compositions and encompassing a
316 large portion of the present-day MORB field (**Fig. 6**).
317
318 **5. DISCUSSION**
319 **5.1 Exhumation at plagioclase-facies conditions**
320 The Spl-Pl pyroxenites in this study were sampled within the Pl-impregnated peridotites.
321 Hence, one can argue that these pyroxenites underwent chemical changes related to impregnation
322 of the host rocks, and that this process might have perturbed their geochemical and isotopic
323 compositions. Guarnieri et al. (2012) showed that Pl-facies impregnation of the Lanzo N
324 peridotites was related to the diffuse percolation of silica-saturated melts that crystallized gabbro-

noritic material within a former Spl-peridotite assemblage. This refertilization process caused the preferential addition of Pl+Opx with a consequent increase in SiO_2, Al_2O_3 and CaO at decreasing MgO and NiO contents (Rampone et al., 1996, 2008; Piccardo and Vissers, 2007) also coupled with the chemical equilibration of the original mantle phases with the infiltrating MORB-type melt (Piccardo et al., 2004; 2007b; Müntener et al., 2005; 2010). These are exactly the opposite chemical changes we envisage in the Spl-Pl pyroxenites, which are markedly enriched in MgO and NiO and depleted in Al_2O_3 and CaO compared to the (Grt)-Spl counterparts (**Fig. 3**). This suggests that the gabbroic pockets (plagioclase + olivine + neoblastic pyroxenes) grown between pyroxene and spinel porphyroclasts are likely the result of subsolidus recrystallization rather than the addition of infiltrating basaltic melts, as previously suggested by Piccardo et al. (2007b). Moreover, the Spl-Pl pyroxenite samples selected in this study do not show diffuse Pl-bearing veinlets crosscutting mantle minerals as typically described for impregnated peridotites (e.g. Rampone et al., 1997, 2008; Piccardo et al., 2007a). On the other hand, as observed in other pyroxenite occurrences from External Ligurides (Montanini et al., 2006, 2012; Borghini et al., 2016; Basch et al., 2020) and Erro-Tobbio massif (Rampone and Borghini, 2008), Pl in these samples appears as neoblasts together with new fine- and medium-grained pyroxenes or in association with olivine partly replacing large Spl porphyroclasts, thus suggesting that it mainly represents product of subsolidus recrystallization. Impregnation textures are nonetheless present at the vicinity of the contacts with the host Pl-peridotites, where the pyroxenites show Pl-bearing microveins crosscutting pyroxene porphyroclasts. It is thereby plausible that the infiltration of melts precipitating plagioclase in the host peridotites (Piccardo et al., 2007b; Guarnieri et al., 2012) was not able to modify the most internal portion of the studied pyroxenite layers, which thus preserved their isotopic compositions. Most likely, the volume of infiltrating melt was thereby small enough to be buffered by the pyroxene-rich matrix, determining the isotopic composition of the segregated plagioclase to be in close equilibrium with the bulk-rock composition.

The hypothesis that Pl in the pyroxenites formed as subsolidus equilibration is in agreement with the isotopic record of the Spl-Pl pyroxenites. Linear correlations in $^{147}Sm/^{144}Nd$-$^{143}Nd/^{144}Nd$ and $^{187}Lu/^{188}Hf$ -$^{177}Hf/^{178}Hf$ characterize the WR and Cpx from all lithologies, including those pyroxenites located within peridotites untouched by melt impregnation in the Jurassic. These linear correlations connect all samples and form two distinct errorchrones yielding ages of ~400 Ma for both Nd and Hf isotopes, which must represent the age of isotopic equilibration at Spl-facies (**Fig. 5**). For Nd isotopes, the WR-Cpx errorchron at ~400 Ma coexists with Pl-Cpx-WR internal isochrones of Jurassic age. The internal isochrones based on Nd isotopes of by two Spl-Pl pyroxenites have ages of 152 ± 30 Ma and 149 ± 13 Ma and indicate that the Pl-bearing assemblage formed in Mid-Jurassic (**Fig. 5**), nearly coeval with the intrusion of MORB-type gabbros within the Lanzo sequence (160 ± 4 Ma) (Kaczmarek et al., 2008). Although the plagioclase-facies recrystallization cannot be undoubtedly related to the process of Pl-facies impregnation in the host peridotite, it is plausible that the temperature increase due to melt migration in the host peridotite triggered subsolidus recrystallization, likely enhanced by the fertile bulk compositions of the pyroxenite assemblage (Hidas et al., 2021). Accordingly, (Grt)-Spl pyroxenites show only incipient plagioclase-bearing recrystallization because they escaped the heating related to melt impregnation of host peridotite.

If we assume that the two events were coeval, then our study furnishes the age of the impregnation of the host mantle peridotite, which is slightly younger than the timing proposed for the equilibration at Pl-facies conditions of the External Liguride ophiolites (186 ± 1.8 Ma, Montanini et al., 2012; 178 ± 8 Ma, Borghini et al., 2016). The isotopic evolution of two selected Spl-Pl and Grt-Spl samples is modeled in **Fig. 7.** The plot shows two samples having different WR compositions, here indicated in different Sm/Nd ratios, that suffered a first event of isotopic equilibration at Spl-facies conditions at 400 Ma, thereof followed by a closed-system WR isotopic evolution until present. At 160 Ma, one sample experienced an event of equilibration at Pl-facies conditions, evidenced by the formation of Pl in isotopic equilibrium with the WR and, as

response, a small shift in the Cpx Sm/Nd ratios. The following evolution led to further radiogenic Nd in-growth in Pl, WR and Cpx, aligned along a Jurassic errorchron. Cpx in pyroxenite incorporates most of the Sm and Nd of the WR, and the Pl-equilibration has a minor effect on the isotopic evolution of the Cpx in this sample. This allows the preservation of WR-Cpx errorchrons at ~400 Ma for both samples, coexisting with Pl-Cpx-WR internal isochrones having Jurassic ages (**Fig. 7**).

5.2 Early perturbation of the Nd-Hf isotope systematics

In the previous section, we showed that the major, trace elements and the Nd-Hf isotopes of the Lanzo North pyroxenites did not suffer significant chemical perturbations during the process of melt migration and impregnation experienced by the host peridotite during the Jurassic exhumation at rather shallow mantle level. Instead, the errorchrons defined by WR and Cpx in the Sm-Nd and Lu-Hf isotopic space for most samples indicate that their isotopic equilibration was attained during a 400 Ma-old event, which was likely related to their complete re-equilibration at spinel-facies mantle conditions (**Fig. 5**). The only exception is represented by two cluster-bearing (Grt)-Spl pyroxenites, which preserve large quantities of subrounded Spl-Px clusters and have very high HREE contents, both indicative of a precursor garnet. These samples do not plot on the 400 Ma errorchron for the Sm-Nd isotopes, having lower Sm/Nd ratios compared to the other (Grt)-Spl samples. Hence, if the initial εNd-εHf values are calculated at 400 Ma (provided by the Nd-Hf errorchrons, **Fig. 5**), most pyroxenites have Nd-Hf compositions clustering in the enriched portion of MORB (εNd 6-7; εHf 8-9; **Fig. 6**), whereas the cluster-bearing (Grt)-Spl pyroxenites plot below the mantle array, showing a distinctive decoupling at higher εNd (12-13) for comparatively low εHf (8-9), (**Fig. 6**).

One possibility to explain the anomalous isotopic compositions is that the two cluster-bearing samples suffered some recent process of interactions with melts that decreased the original Sm/Nd ratios, thus shifting the samples on the left of the errorchron in **Fig. 5a**. Following

this scenario, this process must have preserved the original Lu/Hf ratios, according to the occurrence of a Lu-Hf errorchron at 400 Ma (**Fig. 5**). The cluster-bearing (Grt)-Spl pyroxenites, however, are located within spinel lherzolites that escaped the melt impregnation in the Jurassic and are considered the oldest rock-type less-modified during the long-lasting history of melt-rock reaction processes affecting the mantle sequence (Guarnieri et al., 2012). Indeed, the preservation of Spl-Px clusters in both the peridotites and the pyroxenites and the evident Grt-signature observed in WR and Cpx of the pyroxenites indicate that these rocks were nearly preserved after their complete equilibration at Spl-facies conditions. In addition, the LREE in WR and Cpx from these samples are in the same range of those in the Pl-Spl pyroxenites, whereas a late metasomatic would have produced selective enrichments in these highly incompatible compared to the least compatible elements (e.g., Stracke, 2012). On this basis, the field data, the texture and the geochemical composition of the cluster-bearing (Grt)-Spl pyroxenites are strongly against the possibility that they were modified by a recent metasomatic event.

As alternative hypothesis, the anomalous signature of the cluster-bearing (Grt)-Spl pyroxenites was a consequence of a process of interaction with melts via reactive porous flow envisaged in the host peridotites (Guarnieri et al., 2012). This hypothesis can be evaluated considering the evolution of the studied pyroxenites in response to the melt migration processes. The Lanzo N pyroxenites form correlations in MgO vs. Al_2O_3, CaO and NiO contents, suggesting that they were presumably characterized by different modal amounts of Ol, Px and Grt (**Fig. 3; 4**). This is further supported by the projection of our samples into the pseudoternary system forsterite (Fo)/Ca-Tschermak molecule (CaTs)/quartz (Qz) projected from diopside [Di] (see **Fig. 8**) (O'Hara, 1972). Overall, the Lanzo N pyroxenites are silica-deficient and plot on the left side of the thermal divide (CaTs-En) (**Fig. 8**). In detail, the (Grt)-Spl pyroxenites, including those having Spl-Pyx clusters, are slightly shifted towards the Fo apex compared to the Grt-pyroxenites from External Liguride ophiolites, and from Beni Bousera, Ronda and Horoman peridotitic massifs (Bodinier et al., 1987; Pearson et al., 1991, 1993; Garrido and Bodinier, 1999; Gysi et al., 2011;

Montanini et al., 2012; Borghini et al., 2016), indicating higher modal amounts of modal Ol. Even higher amounts of Ol is revealed by the Lanzo N Spl-Pl pyroxenites, which, similar to the Spl-websterites from Beni Bousera and Ronda massifs, plot closer to the Fo apex. The overall increase in Ol modes from the (Grt)-Spl pyroxenite to the Spl-Pl pyroxenite may suggest that these rocks are remnants of Grt-pyroxenites consumed at various extents by interaction with basaltic melts (e.g., group B pyroxenites in Garrido & Bodinier, 1999). The REE WR compositions of the Lanzo N pyroxenites agree with this hypothesis. All the samples display rather similar LREE/MREE ratios (La/Sm=0.3-0.5), but display a gradual decreases in HREE from the cluster-bearing (Grt)-Spl pyroxenites towards the Spl-Pl pyroxenites (see **Fig. 3d,4**). This suggests that the overall increase in Ol mode revealed by the Spl-Pl pyroxenites was coupled with the addition of a melt phase that decreased their WR HREE contents, causing a gradual increase in Ce/Yb ratios at increasing MgO contents (**Fig. 3d**). As analogy, most of the host Spl-peridotites are modally rich in Ol, and show nearly flat M-HREE WR patterns (**Fig.4**). Based on major and trace element decoupling, these rocks have been interpreted as product of interaction between a former lherzolite and basaltic melt having an enriched MORB signature (Guarnieri et al., 2012). A gradual interaction with basaltic melts is further consistent with the REE compositions of the Cpxs, which also show large variations in HREE, with Cpx from the two cluster-bearing samples still preserving extremely high HREE contents. The WR and mineral compositions of the Lanzo N pyroxenites can be thereby indicative of progressive reaction with a melt that percolated a former Grt-pyroxenite and smoothed out at various extents the original Grt-signature. Under this light, we infer that both pyroxenites and host Spl-peridotite were diffusively percolated by the same basaltic melt.

The local preservation of strongly radiogenic Nd and Hf isotopic ratios of the Spl-harzburgites (**Fig. 6**), along with variable Sm/Nd and Lu/Hf ratios (**Fig. 5**) led Guarnieri et al. (2012) to suggest that the melt migration producing modally depleted harzburgites largely anticipated the Jurassic impregnation, and must have occurred in Paleozoic times. Based on the

455 preservation of Nd-Hf errorchrons in the pyroxenites, we can now constrain the age of this
456 process at ~400 Ma. This age may reflect the time of a Paleozoic extension and associated E-
457 MORB magmatism also documented in the External Liguride mantle (~430 Ma) (Borghini et al.,
458 2013), and can be possibly related to an extensional phase related to the opening of the
459 Paleotethys at the onset of the Varisican orogenic cycle (von Raumer et al., 2013 and references
460 therein).
461
462 **5.3 Inference on the origin of the pristine garnet-pyroxenites and development of decoupled**
463 **Nd-Hf isotopic signature: a geochemical model**
464 We previously inferred that the pyroxenites considered in this study were partly, and in
465 different extent, modified by migration of melt having a E-MORB geochemical signature. The
466 process of diffuse melt percolation combined to the complete recrystallization at spinel-facies
467 mantle conditions occurred at 400 Ma and profoundly overprinted the original textural, modal and
468 chemical features of the precursor garnet pyroxenites. However, some inferences on the origin of
469 the pristine pyroxenites can be gained by the composition of the least reacted samples, namely
470 those preserving Spl-Px clusters as evidence of former Grt. These samples show a marked Grt-
471 signature as for trace elements (i.e., high Sc, V and HREE and high Lu/Hf in WR and Cpx), high
472 εNd_{400}, but initial εHf_{400} similar to those of the other samples, thus showing Nd-Hf decoupling
473 below the mantle array (**Fig. 6**). Nd-Hf compositions below the mantle array are not uncommon
474 amongst Grt-pyroxenites worldwide and documented in External Ligurian ophiolites, Beni
475 Bussera and Ronda Massifs (see **Fig. 9**). According to their major and trace element chemistry,
476 these Grt-pyroxenites are generally interpreted as high pressure segregates of melts carrying the
477 isotopic signature of recycled oceanic crustal components (Pearson et al., 1991, 1993; Morishita
478 et al., 2003; Montanini et al., 2012; Marchesi et al., 2013; Montanini & Tribuzio, 2015; Varas-
479 Reus et al., 2018). In fact, the high mobility of Hf, Nd and Sm (22, 20 and 13%) (Stracke et al.,
480 2003; Niu, 2004) compared to Lu (immobile) produce a dehydrated oceanic crust with twice

481 higher Lu/Hf ratios (0.4) compared to average MORB (0.2), while leaving almost identical
482 Sm/Nd ratios (~0.3). Over time, this dehydrated crustal component would develop lower
483 $^{187}Hf/^{188}Hf$ at a given $^{143}Nd/^{144}Nd$, gradually diverging at lower εHf and slightly higher εNd
484 compared to the present-day values (Stracke et al., 2003). Marine sediments, on the other hand,
485 have much lower Sm/Nd and Lu/Hf than igneous ocean crust, and the addition of this component
486 to a dehydrated oceanic crust would produce gradual shifts in Nd-Hf towards less radiogenic
487 values (Kogiso et al., 1997). **Figure 9** shows that the isotopic field of recycled MORB (ranging
488 from 0.5 to 3.5 Ga) plus additions of minor marine sediments (Stracke et al., 2003; Varas-Reus et
489 al., 2018) can indeed explain most of the Nd-Hf isotopic decoupling seen in the Grt-pyroxenites
490 from Beni Bousera, Ronda and External Liguride ophiolites (grey starts in **Fig. 9**).
491 The cluster-bearing (Grt)-Spl pyroxenites from Lanzo N, however, do no plot within this
492 field, having even lower εHf for comparatively high εNd. The persistence of an errorchron at
493 ~400 Ma only in $^{187}Lu/^{188}Hf$ versus $^{177}Hf/^{178}Hf$ indicates that Hf isotopes in these rocks
494 equilibrated together with those of the other samples, whereas Nd isotopes of the two cluster-
495 bearing (Grt)-Spl pyroxenites experienced some incomplete equilibration with the reacting melt
496 and were partly inherited from that of the original Grt-pyroxenite. Hence, we argue that the melt-
497 pyroxenite interaction at 400 Ma caused the isotopic decoupling in the cluster-bearing (Grt)-Spl
498 pyroxenites. Due to the different affinities of Nd and Hf in the melt phase, and depending on the
499 Nd/Hf ratios of the two components, isotopic decoupling can occur during interaction between
500 depleted mantle peridotites and melts (Chauvel et al., 2008; Stracke et al., 2011; Guarnieri et al.,
501 2012). For a depleted peridotite interacting with a MORB melt, the lower Nd/Hf ratios of the
502 depleted end-member produces mixing lines plotting above the Nd-Hf mantle array; as a result,
503 reacted peridotites generally preserve high Hf isotopic values, while their original Nd signature is
504 easily concealed by equilibration with the migrating melt (Sanfilippo et al., 2019). On the other
505 hand, if at the time of melt-rock interaction the isotopically depleted end-member has high Nd/Hf,
506 Hf isotopes would more easily equilibrate with those of the melts, while radiogenic Nd is

507 preserved. As a consequence, interaction between melt and a precursor Grt-pyroxenite having
508 higher Nd/Hf ratios compared to a depleted peridotite, might have produced the Nd-Hf isotopic
509 decoupling below the mantle array revealed by the Lanzo N cluster-bearing (Grt)-Spl pyroxenites.
510 To test this hypothesis, we modeled a melt-rock reaction process between a precursor Grt-
511 pyroxenite and a MORB melt having Nd and Hf compositions in equilibrium with the Cpx of the
512 most enriched Lanzo N harzburgite. Despite the composition of the initial Grt-pyroxenite is
513 unknown, the REE pattern of the least modified samples recall those of Grt-pyroxenites from
514 External Ligurian ophiolites. Hence, we selected three end-members having different initial Nd-
515 Hf isotopes and whole rock geochemical compositions of Grt-pyroxenites from other sections of
516 External Ligurian ophiolites. The initial Grt-pyroxenite represents segregate from melts having a
517 geochemical signature akin a recycled MORB (i.e., long the "0 sediments line"), at ages of
518 recycling from 3.5 to 0.5 Ga (Varas-Reus et al., 2018) (see **Fig. 9**). In addition, we assumed for
519 the initial pyroxenite variable Sm/Nd and Lu/Hf ratios, to account for the expected compositional
520 variability of pyroxenites formed by deep segregation of melt in the mantle (Pearson et al., 1991,
521 1993; Morishita et al., 2003; Montanini et al., 2012; Marchesi et al., 2013; Montanini & Tribuzio,
522 2015; Varas-Reus et al., 2018). These parameters are arbitrary chosen and cannot take into
523 account the entire range of chemical variability of pyroxenites in the mantle, but are hereafter
524 used to test at what conditions the decoupling seen in the Grt-bearing samples can be
525 mathematically reproduced during a process of interaction with a melts.
526 We opted for the assimilation-fractional-crystallization (AFC) model of De Paolo (1981)
527 that has been successfully used to reproduce the Nd-Hf decoupling in mantle peridotites (Bizimis
528 et al., 2003; Chauvel et al., 2008; Stracke et al., 2011; Guarnieri et al., 2012; Sanfilippo et al.,
529 2019). Further details of the model are reported in the appendix. The results are plotted at steps of
530 F=0.02 (that is the melt mass during the AFC process) in **Figure 9** where the Nd-Hf isotopic
531 composition of the reaction products is compared to that of our samples. As a whole, the model is
532 able to reproduce the composition of the cluster-bearing (Grt)-Spl pyroxenites only if a

geochemically enriched pyroxenite, i.e., having high Nd/Hf ratios, is assimilated. This is in agreement with the lower Sm/Nd and higher L/MREE ratios of these samples compared to the other pyroxenites. On the contrary, the Nd-Hf isotopes of sample Py5 will be reproduced by interaction with a Grt-pyroxenite having low Nd/Hf ratios, in agreement with the low LREE of this sample. Independently on the initial composition, the isotopic composition of cluster-bearing samples equals that of a Grt-pyroxenite produced after ~70-80% of assimilation and recrystallization of its initial mass into a melt having an E-MORB signature. On the other hand, the compositions of the Pl-Spl pyroxenites samples having high MgO contents require high degrees of assimilation of the pre-existing pyroxenite, and recrystallization of an assemblage with a geochemical composition similar that of the migrating melt (F >90%). This is well supported by the generally higher Fo mode and higher bulk MgO and NiO contents in these samples, which indicate addition of olivine and consumption of pyroxene starting from the pristine pyroxenite assemblage.

6. CONCLUSIONS

This study places new temporal constraints to the long history of exhumation and melt-rock reaction of the Lanzo North peridotite massif, through chemical and Nd-Hf isotopes investigations on pyroxenite layers embedded within spinel and plagioclase peridotites, i.e. (Grt)-Spl pyroxenites and Pl-Spl pyroxenites, respectively. Spl-Pl pyroxenites preserve Pl-Cpx-WR Sm-Nd internal isochrons that indicate a closed-system event of Pl-facies equilibration in the Jurassic (152 ± 30 Ma and 149 ± 13 Ma). The intense plagioclase-facie recrystallization of Spl-Pl pyroxenites was likely triggered by the migration of MORB-type melts generating the host Pl-peridotites. Field and textural observations coupled to chemical compositions indicate that this melt migration process did not significantly perturb the bulk isotopic composition of the internal portions of the pyroxenites. On the other hand, at the time of their exhumation at the seafloor (160 Ma), these pyroxenites still revealed a large isotopic variability, inherited from more ancient events of melt

559 migration and melt-pyroxenite interaction. Textural features along with major and trace element
560 compositions, suggest that the studied pyroxenites represent former Grt-pyroxenites, and that the
561 early isotopic equilibration occurred in response to an event of reactive percolation of basaltic
562 melts concomitant to the complete re-equilibration at spinel-facies mantle conditions. The
563 preservation of Nd-Hf errorchrons in Cpx and WR suggest that this event of melt migration and
564 isotopic equilibration likely occurred at ~400 Ma.

565 The (Grt)-Spl pyroxenites preserving widespread textural and chemical evidence of former
566 Grt do not plot on the 400 errorchron for the Sm-Nd isotopes, resulting in high ε_{Nd} (~12) for
567 comparatively low ε_{Hf} (~10), when recalculated at 400 Ma (**Fig. 6**). Based on field and
568 geochemical evidence, we exclude the possibility that these samples experienced a late process of
569 metasomatism. Instead, we believe that these samples were the least affected by the basaltic melt
570 percolation. Geochemical models corroborate this idea, showing that variable degrees of
571 interaction between a former Grt-pyroxenite with melts having a E-MORB geochemical signature
572 might have shifted the original Nd-Hf isotopes below the mantle array (**Fig. 8**). The elemental
573 fractionation caused by this process resulted in a different isotopic evolution over time and by the
574 time of emplacement of the sequence on the Jurassic seafloor, caused the cluster-bearing (Grt)-Spl
575 pyroxenites to experienced a stronger radiogenic Hf ingrowth compared to the other samples. As a
576 result, by the time of emplacement of this mantle section at crustal depths, the samples were "re-
577 coupled" along the terrestrial array. In conclusion, changes in elemental ratios and a long-time
578 evolution preceding the emplacement of the Lanzo N mantle sequence at crustal depth partly
579 obscured the perturbation caused by this old event of melt migration event. This study underlines
580 the importance of using Nd and Hf isotope systematics to give time constraints to ancient process
581 of reactive melt migrations that can potentially modify the lithological and chemical heterogeneity
582 of the subcontinental mantle.
583

584 **Acknowledgments**

N. Rizzo and A. Mosconi are acknowledged for preliminary work on the chemical data. A. Risplendente is thanked for assistance with the WDS adata. This study is partly supported by the Italian Programma di Rilevante Interesse Nazionale to A. Sanfilippo (PRIN_2017KY5ZX8). Analyses carried out at the Pheasant Memorial Laboratory were supported by PML members, especially Chie Sakaguchi at Misasa. This project was partially supported by 21 COE Program of MEXT Japan represented by EN. RICORDA DI RINGRAZIARE REVIEWER AND EDITOR!!

APPENDIX

Geochemical model (Table S5): the melt-rock interaction model used to reproduce the Nd-Hf isotope ratios of the pyroxenites from Lanzo N is calculated using an AFC-type model based on equations 6a and 15a from DePaolo (1981), as similarly used in previous studies reproducing melt-rock reactions in the oceanic mantle (Kelemen et al., 1992; Stracke et al., 2011; Guarnieri et al., 2012; Sanfilippo et al., 2019). A melt having an E-MORB isotopic signature reacts with initial Grt-pyroxenites having initial Nd/Hf ratios of 1.5, 2.5 and 3.5. In analogy with some Grt-pyroxenites from the External Ligurian ophiolites (Montanini et al., 2015; Borghini et al., 2016), Beni-Bousera and Ronda mantle sequences (see Varas-Reus et al., 2018 and references therein), the starting Grt-pyroxenites are considered to be high-pressure cumulates or products of melt-rock reaction (see for instance discussion in Gysi et al., 2011; Montanini et al., 2012; Borghini et al., 2016). We assume constant magma mass during reaction and mass assimilated to mass crystallized ratio ~0.9. The interaction of the starting Grt-pyroxenite (0.4 grt + 0.6 cpx; form Gysi et al., 2011) with the E-MORB melt produces a progressive changes in the resulting pyroxenite compositions by dissolution of the primary mineralogical assemblage and crystallization of new phases concomitant with phase transition from garnet to spinel peridotite field. Based on the reaction for the Grt-Spl phase transition defined by Vannucci et al. (1993) and on petrographic evidence in the host peridotites, we here assume that this process resulted in the transformation of the original Grt-pyroxenite into a (Grt)Spl-peridotite following the reaction

0.4 grt + 0.6 cpx1 + melt 1 = 0.3 opx + 0.4 cpx2 + 0.3spl + melt 2 (1)

The Nd-Hf isotope ratios of the melts produced by this AFC process is depicted in **Fig. 5** and details are reported in supplementary Table S5. Parameters, partition coefficients and results of the model are reported in Table S5. Note that the proportions of crystallizing phases has a minor effect on the isotopic composition of the results of the reaction, as the latter are mostly dependent on the initial Nd/Hf ratios of the assimilant compared to that of the interacting melt (see text for further discussion).

References

Ackerman, L., Bizimis, M., Haluzová, E., Sláma, J., Svojtka, M., Hirajima, T., Erban, V., 2016. Re–Os and Lu–Hf isotopic constraints on the formation and age of mantle pyroxenites from the Bohemian Massif. Lithos 256–257, 197–210.

625 Anders, E., Ebihara, M., 1982. Solar system abundances of the elements. Geochim. Cosmochim.
626 Acta 46, 2363–2380.
627 Basch, V., Borghini, G., Fumagalli, P., Rampone, E., Ferrando, C., Gandolfo, A., 2020.
628 Plagioclase-facies thermobarometric evolution of the External Liguride pyroxenite-bearing
629 mantle (Suvero, Italy). Ofioliti 45, 1–11.
630 Becker, H., Horan, M.F., Walker, R.J., Gao, S., Lorand, J.P., Rudnick, R.L., 2006. Highly
631 siderophile element composition of the Earth's primitive upper mantle: constraints from new
632 data on peridotite massifs and xenoliths. Geochim. Cosmochim. Acta 70, 4528-4550.
633 Bizimis, M., Sen, G., Salters, V.J.M., 2003. Hf–Nd isotope decoupling in the oceanic lithosphere.
634 Constraints from spinel peridotites from Oahu, Hawaii. Earth Planet. Sci. Lett. 217, 43–58.
635 Blichert-Toft, J., Albarede, F., Kornprobst, J., 1999. Lu–Hf isotope systematics of garnet
636 pyroxenites from Beni Bousera, Morocco: implications for basalt origin. Science 283, 1303–
637 1306 (1999).
638 Byerly, B.L., Lassiter, J.C., 2014. Isotopically ultradepleted domains in the convecting upper
639 mantle: implications for MORB petrogenesis. Geology 42, 203–206.
640 Bodinier, J.-L., Guiraud, M., Fabries, J., Dostal, J., Dupuy, C., 1987. Petrogenesis of layered
641 pyroxenites from the Lherz, Freychinede and Prades ultramafic bodies (Ariege, French
642 Pyrenees). Geochim. Cosmochim. Acta 51, 279-290.
643 Bodinier J. L., 1988. Geochemistry and petrogenesis of the Lanzo peridotite body, Western Alps.
644 Tectonophysics 149, 67–88.
645 Bodinier, J.L., Menzies, M.A., Thirlwall, M.F., 1991. Continental to oceanic mantle transition: REE
646 and Sr–Nd isotopic geochemistry of the Lanzo Lherzolite Massif. J. Petrol. 191–210. Special
647 Lherzolite Issue.
648 Bodinier, J.-L., Godard, M., 2014. Orogenic, ophiolitic and abyssal peridotites. in "Treatise on
649 Geochemistry", vol. 2, 2nd Edition, H.D. Holland & K.K. Turekian, eds. Elsevier Science,
650 Oxford, UK.

651 Borghini, G., Rampone, E., Zanetti, A., Class, C., Cipriani, A., Hofmann, A.W., Goldstein, S.,
652 2013. Meter-scale Nd isotopic heterogeneity in pyroxenite-bearing Ligurian peridotites
653 encompasses global-scale upper mantle variability. Geology 41, 1055-1058.
654 Borghini, G., Rampone, E., Zanetti, A., Class, C., Cipriani, A., Hofmann, A.W., Goldstein, S.,
655 2016. Pyroxenite layersin the Northern Apennines upper mantle (Italy) – Generation by
656 pyroxenite melting and melt infiltration. J. Petrol. 57, 625–653.
657 Borghini, G., Fumagalli, P., 2018. Subsolidus phase relations in a mantle pyroxenite: an
658 experimental study from 0.7 to 1.5 GPa. Eur. J. Mineral. 30, 333–348.
659 Boudier F., 1978. Structure and petrology of the Lanzo peridotite massif (Piedmont Alps). Geol.
660 Soc. Am. Bull. 89, 1574–1591.
661 Cipriani, A., Brueckner, H.K., Bonatti, E., Brunelli, D., 2004. Oceanic crust generated by elusive
662 parents: Sr and Nd isotopes in basalt-peridotite pairs from the Mid-Atlantic Ridge. Geology 32,
663 657–660.
664 Chauvel, C., Lewin, E., Carpentier, M., Arndt, N.T., Marini, J.-C., 2008. Role of recycled oceanic
665 basalt and sediment in generating the Hf–Nd mantle array. Nature Geoscience 1, 64–67.
666 DePaolo, D.J., 1981. Trace element and isotopic effects of combined wall-rock assimilation and
667 fractional crystallization. Earth Planet. Sci. Lett. 53, 189–202.
668 Downes, H., 2007. Origin and significance of spinel and garnet pyroxenites in the shallow
669 lithospheric mantle: Ultramafic massifs in orogenic belts in Western Europe and NW Africa.
670 Lithos 99, 1-24.
671 Garrido, C.J., Bodinier, J.L., 1999. Diversity of mafic rocks in the Ronda peridotite: evidence for
672 pervasive melt–rock reaction during heating of subcontinental lithosphere by upwelling
673 asthenosphere. J. Petrol. 40, 729–754.
674 Guarnieri, L., Piccardo, G. B., Nakamura, E., Shimizu, N., Vannucci, R. & Zanetti, A. (2009).
675 Pyroxenites in the North Lanzo Peridotite Massif: Insights into deep lithospheric processes.
676 Plinius 35, CD-ROM.

677 Guarnieri, L., Nakamura, E., Piccardo, G.B., Sakaguchi, C., Shimizu, N., Vannucci, R., Zanetti, A.,
678 2012. Petrology, trace element and Sr, Nd, Hf isotope geochemistry of the North Lanzo
679 Peridotite Massif (Western Alps, Italy). J. Petrol. 53, 2259–2306.
680 Gysi, A.P., Jagoutz, O., Schmidt, M.W., Targuisti, K., 2011. Petrogenesis of pyroxenites and melt
681 infiltrations in the ultramafic complex of Beni Boussera, Northern Morocco. J. Petrol. 52,
682 1676-1735.
683 Hidas, K., Borghini, G., Tommasi, A., Zanetti, A., Rampone, E., 2021. Interplay between melt
684 infiltration and deformation in the deep lithospheric mantle (External Liguride ophiolite, North
685 Italy), Lithos, 380–381, 105855.
686 Higgie, K., Tommasi, A., 2014. Deformation in a partially molten mantle: Constraints from
687 plagioclase lherzolites from Lanzo, western Alps. Tectonophysics 615, 167-181.
688 Hirschmann, M.M., Stolper, E.M., 1996. A possible role for garnet pyroxenite in the origin of the
689 'garnet signature' in MORB. Contrib. Mineral. Petrol. 124, 185–208.
690 Hoogerduijn Strating, E.H., Rampone, E., Piccardo, G.B., Drury, M.R., Vissers, R.L.M., 1993.
691 Subsolidus emplacement of mantle peridotites during incipient oceanic rifting and opening of
692 the Mesozoic Tethys (Voltri Massif, NW, Italy). J. Petrol. 34, 901-927.
693 Imai, N., Terashima, S., Itoh, S., & Ando, A. (1995). 1994 compilation values for GSJ reference
694 samples,"Igneous rock series". Geochemical Journal, 29(1), 91–95.
695 Imai, N., Terashima, S., Itoh, S., & Ando, A. (1999). 1998 compilation of analytical data for five
696 GSJ geochemical reference samples: The "Instrumental analysis series". Geostandards
697 Newsletter, 23(2), 223-250.
698 Kaczmarek, M.A., Muntener, O., Rubatto, D., 2008. Trace element chemistry and U–Pb dating of
699 zircons from oceanic gabbros and their relationship with whole rock composition (Lanzo,
700 Italian Alps). Contrib. Mineral. Petrol. 155, 295–312.
701 Kelemen, P.B., Dick, H.J.B., Quick, J.E., 1992. Formation of harzburgite by pervasive melt/rock
702 reaction in the upper mantle. Nature 358, 635–641.

703 Kogiso, T., Tatsumi, Y., Nakano, S., 1997. Trace element transport during dehydration processes in
704 the subducted oceanic crust: 1. Experiments and implications for the origin of ocean island
705 basalts. Earth Planet. Sci. Lett. 148, 193-205.
706 Kumar, N., Reisberg, L., Zindler, A., 1996. A major and trace element and strontium, neodymium,
707 and osmium isotopic study of a thick pyroxenite layer from the Beni Bousera ultramafic
708 complex of northern Morocco. Geochim. Cosmochim. Acta 60, 1429-1444.
709 Lagabrielle, Y., Fudral, S., Kienast, J.R., 1989. The oceanic cover of the Lanzo peridotite body
710 (Western Italian Alps): lithostratigraphic and petrological evidences. Geodin. Acta 3, 43–55.
711 Lambart, S., Baker, M.B., Stolper, E.M., 2016. The role of pyroxenite in basalt genesis: Melt-PX, a
712 melting parameterization for mantle pyroxenites between 0.9 and 5 GPa. J. Geophys. Res. 121,
713 5708–5735.
714 Le Roux, V., Bodinier, J-L., Alard, O., O'Reilly, S.J., Griffin, W.L., 2009. Isotopic decoupling
715 during porous melt flow: A case-study in the Lherz peridotite. Earth Planet. Sci. Lett. 279, 76–
716 85.
717 Lu, Y., Makishima, A., Nakamura, E., 2007. Purification of Hf in silicate materials using extraction
718 chromatographic resin, and its application to precise determination of 176Hf/177Hf by MC-
719 ICP-MS with 179Hf spike, J. Anal. At. Spectrom. 22, 69-76.
720 Makishima, A., Nakamura, E., 1997. Suppression of matrix effect in ICP-MS by high power
721 operaton of ICP: Application to precise determination of Rb, Sr, Y, Cs, Ba, REE, Pb, Th and U
722 at ng /g level in a few milligram silicate sample. Geostand. Newslett. 21, 307-319.
723 Makishima, A., Nakamura, E., 2006. Determination of major, minor and trace elements in silicate
724 samples by ICP-QMS and ICP-SFMS applying isotope dilution-internal standardization (ID-IS)
725 and multi-stage internal standardization. Geostandards and Geoanalytical Research 30, 245-
726 271.

727 Makishima A., Nakamura, E., 2008. New preconcentration technique of Zr, Nb, Mo, Hf, Ta and W
728 employing coprecipitation with Ti compounds: Its application to Lu-Hf system and sequential
729 Pb-Sr-Nd-Sm separation, Geochem. J. 42,199-206.
730 Marchesi, C., Garrido, C.J., Bosch, D., Bodinier, J-L., Gervilla, F., Hidas, K., 2013. Mantle
731 refertilization by melts of crustal-derived garnet pyroxenite: Evidence from the Ronda
732 peridotite massif, southern Spain. Earth Planet. Sci. Lett. 362, 66-75.
733 McCarthy, A., Müntener, O., 2015. Ancient depletion and mantle heterogeneity: revisiting the
734 Permian-Jurassic paradox of Alpine peridotites. Geology 43, 255–258.
735 Montanini, A., Tribuzio, R., Anczkiewicz, R., 2006. Exhumation history of a garnet pyroxenite-
736 bearing mantle section from a continent-ocean transition (Northern Apennine ophiolites, Italy).
737 J. Petrol. 47, 1943-1971.
738 Montanini, A., Tribuzio, R., Thirlwall, M., 2012. Garnet clinopyroxenite layers from the mantle
739 sequences of the Northern Apennine ophiolites (Italy): Evidence for recycling of crustal
740 material. Earth Planet. Sci. Lett.351-352, 171-181.
741 Montanini, A., Tribuzio, R., 2015. Evolution of recycled crust within the mantle: constraints from
742 the garnet pyroxenites of the External Ligurian ophiolites (northern Apennines, Italy). Geology
743 43, 911-914.
744 Morishita, T., Arai, S., 2001. Petrogenesis of corundum-bearing mafic rock in the Horoman
745 Peridotite Complex, Japan. J. Petrol. 42, 1279-1299.
746 Morishita, T., Arai, S., Gervilla, F., Green, D.H., 2003. Closed-system geochemical recycling of
747 crustal materials in the upper mantle. Geochim. Cosmochim. Acta 67, 303–310.
748 Müntener, O., Piccardo, G.B., Polino, R., Zanetti, A., 2004. Revisiting the Lanzo peridotite (NW-
749 Italy):'Asthenospherization'of ancient mantle lithosphere. Ofioliti 30 (2), 111-124
750 Müntener O., Manatschal G., Desmurs L., Pettke T., 2010. Plagioclase peridotites in ocean–
751 continent transitions: refertilized mantle domains generated by melt stagnation in the shallow
752 mantle lithosphere. J. Petrol. 51, 255–294.

753 Nakamura, E., Makishima, A., Moriguti, T., Kobayashi, K., Sakaguchi, C., Yokoyama, T., Tanaka,
754 R., Kuritani, T., Takei, H., 2003. Comprehensive geochemical analyses of small amounts (<
755 100mg) of extraterrestrial samples for the analytical competition related to the sample return
756 mission MUSES-C. Inst. Space Astronaut. Sci. Rep. SP. 16, 49-101.
757 Niu, Y., 2004. Bulk-rock major and trace element compositions of abyssal peridotites: Implications
758 for mantle melting, melt extraction and post-melting processes beneath ocean ridges. J. Petrol.
759 45, 2423–2458.
760 Norrish, K., and Chappell, B. W., 1967. X-ray fluorescence spectrography, *In* Physical Methods in
761 Determinative Mineralogy, J. Zussman, ed., pp. 161–214, Academic Press, London.
762 O'Hara, M.J., 1972. Data reduction and projection schemes for complex compositions. In: EaM, U.
763 (Ed.), Progress in Experimental Petrology. NERC, Manchester, Edinburgh 103–126.
764 Pearson, D.G., Davies, G.R., Nixon, P.H., Greenwood, P.B., Mattey, D.P., 1991. Oxygen isotope
765 evidence for the origin of pyroxenites in the Beni Boussera peridotite massif, North Morocco:
766 derivation from subducted oceanic lithosphere. Earth Planet. Sci. Lett. 102, 289–301.
767 Pearson, D.G., Davies, G.R., Nixon, P.H., 1993. Geochemical constraints on the petrogenesis of
768 diamond facies pyroxenites from the Beni Bousera peridotite massif, North Morocco. J. Petrol.
769 34, 125-172.
770 Pearson, D.G., Nowell, G.M., 2004. Re-Os and Lu-Hf isotope constraints on the origin and age of
771 pyroxenites from the Beni Bousera peridotite massif: implications for mixed peridotite-
772 pyroxenite mantle source. J. Petrol. 45, 439-455.
773 Piccardo, G.B., Müntener, O., Zanetti A., 2007. Alpine-Apennine ophiolitic peridotites: new
774 concepts on their composition and evolution, Ofioliti 29 (1), 63-74.
775 Piccardo, G.B., Zanetti, A., Poggi, E., Spagnolo, G., Müntener, O., 2007. Melt/peridotite interaction
776 in the Lanzo South peridotite: field, textural and geochemical evidence. Lithos 94, 181–209.
777 Piccardo, G.B., 2010. The Lanzo peridotite massif, Italian wester Alps: Jurassic rifting of the
778 Ligurian Tethys. In: Coltorti, M., Downes, H., Gregoire, M. & O'Reilly, S. Y. (eds)

779 Petrological evolution of the European lithospheric mantle. Geological Society, London,
780 Special Publications 337, 47-69.
781 Piccardo, G.B., 2016. Evolution of the lithospheric mantle during passive rifting: Inferences from
782 the Alpine–Apennine orogenic peridotites. Gondwana Research 39, 230-249.
783 Pognante, U., Rosli, U., Toscani, L., 1985. Petrology of ultramafic and mafic rocks from the Lanzo
784 peridotite body (Western Alps). Lithos 18, 201-214.
785 Rampone, E., Hofmann, A.W., Piccardo, G. B., Vannucci, R., Bottazzi, P., Ottolini, L., 1996. Trace
786 element and isotope geochemistry of depleted peridotites from an N-MORB type ophiolite
787 (Internal Liguride, N. Italy). Contrib. Mineral. Petrol. 123, 61-76.
788 Rampone, E., Piccardo, G.B., Vannucci, R., Bottazzi, P., 1997. Chemistry and origin of ted melts in
789 ophiolitic peridotites. Geochim. Cosmochim. Acta 61, 4557-4569.
790 Rampone, E., Borghini, G., 2008. Melt migration and intrusion in the Erro-Tobbio peridotites
791 (Ligurian Alps, Italy): insights on magmatic processes in extending lithospheric mantle. Eur. J.
792 Mineral. 20, 573–585.
793 Rampone, E., Piccardo, G.B., Hofmann, A.W., 2008. Multi-stage melt-rock interaction in the Mt.
794 Maggiore (Corsica, France) ophiolitic peridotites: microstructural and geochemical records.
795 Contrib. Mineral. Petrol. 156, 453-475.
796 Rampone, E., Borghini, G., Romairone, A., Abouchami, W., Class, C., Goldstein, S.L., 2014. Sm-
797 Nd geochronology of the Erro-Tobbio gabbros (Ligurian Alps, Italy): insights on the evolution
798 of the Alpine Tethys. Lithos 205, 236-246.
799 Rampone, E., Borghini, G., Basch, V., 2020. Melt migration and melt-rock reaction in the Alpine-
800 Apennine peridotites: insights on mantle dynamics in extending lithosphere. Geoscience
801 Frontiers Special Issue: Ophiolites, 11, 151-166.
802 Rampone, E., & Sanfilippo, A., 2021. The heterogeneous Tethyan oceanic lithosphere of the Alpine
803 ophiolites. Elements: An International Magazine of Mineralogy, Geochemistry, and Petrology,
804 17(1), 23-28.

805 Reisberg L., Lorand J.-P., 1995. Longevity of sub-continental mantle lithosphere from osmium
806 isotope systematics in orogenic peridotite massifs. Nature 376, 159-162.
807 Salters, V.J.M., Dick, H.J.B., 2002. Mineralogy of the mid-ocean-ridge basalt source from
808 neodymium isotopic composition of abyssal peridotites. Nature 418, 68–72.
809 Sanfilippo, A., Tribuzio, R., Tiepolo, M., 2014. Mantle–crust interaction in the oceanic lithosphere:
810 constraints from minor and trace elements in olivine. Geochim. Cosmochim. Acta 141, 423–
811 439.
812 Sanfilippo, A., Salters,V., Tribuzio, R., Zanetti, A., 2019. Role of ancient, ultra-depleted mantle in
813 Mid-Ocean-Ridge magmatism. Earth Planet. Sci. Lett. 511, 89–98.
814 Stracke, A., Salters, V.J.M., Sims, K.W.W., 1999. Assessing the presence of garnet–pyroxenite in
815 the mantle sources of basalts through combined hafnium–neodymium–thorium isotope
816 systematics. Geochem. Geophys. Geosyst. 1.
817 Stracke, A., Bizimis, M., Salters, V.J.M., 2003. Recycling of oceanic crust: quantita- tive
818 constraints. Geochem. Geophys. Geosyst. 4, 8003. https://doi.org/10.1029/ 2001GC000223.
819 Stracke, A., Snow, J.E., Hellebrand, E., von der Handt, A., Bourdon, B., Birbaum, K., Gunther, D.,
820 2011. Abyssal peridotite Hf isotopes identify extreme mantle depletion. Earth Planet. Sci. Lett.
821 308, 359–368.
822 Stracke, A., 2012. Earth's heterogeneous mantle: a product of convection-driven interaction
823 between crust and mantle. Chem. Geol. 330–331, 274–299.
824 Takei, H., 2002. Development of precise analytical techniques for major and trace element
825 concentrations in rock samples and their applications to the Hishikari gold mine, southern
826 Kyushu, Japan, PhD thesis, Graduate School of Natural Science and Technology, Okayama
827 University, Tottori.
828 Tanaka, R., Makishima, A., Kitagawa, H., Nakamura, E., 2003. Suppression of Zr, Nb, Hf and Ta
829 coprecipitation in fluoride compounds for determination in Ca-rich materials. J. Anal. At.
830 Spectrom. 18, 1458-1463.

831 Terashima, S., Taniguchi, M., Mikoshiba, M., & Imai, N. (1998). Preparation of two new GSJ
832 geochemical reference materials: Basalt JB‐1b and coal fly ash JCFA‐1. Geostandards
833 Newsletter, 22(1), 113-117.
834 Tilhac, R., Gregoire, M., W.L., O'Reilly, Griffin, S.Y., Henry, H., Ceuleneer, G., 2017. Sources and
835 timing of pyroxenite formation in the sub-arc mantle: case study of the Cabo Ortegal Complex,
836 Spain. Earth Planet. Sci. Lett. 474, 490–4502.
837 Tilhac, R., Oliveira, B., Griffin, W.L., O'Reilly, S.Y., Schaefer, B.F., Alard, O., Ceuleneer, G.,
838 Afonso, J.C., Grégoire, M., 2020. Reworking of old continental lithosphere: unradiogenic Os
839 and decoupled Hf-Nd isotopes in sub-arc mantle pyroxenites. Lithos 354-355, 105346.
840 Tribuzio, R., Garzetti, F., Corfu, F., Tiepolo, M., Renna, MR., 2016. U–Pb zircon geochronology of
841 the Ligurian ophiolites (Northern Apennine, Italy): Implications for continental breakup to
842 slow seafloor spreading. Tectonophysics 666, 220-243.
843 Vannucci, R., Shimizu, N., Piccardo, G. B., Ottolini, L., Bottazzi, P., 1993. Distribution of trace-
844 elements during breakdown of mantle garnet: an example from Zabargad. Contrib. Mineral.
845 Petrol. 113, 437–449.
846 Varas-Reus, M.I., Garrido, C.J., Marchesi, C., Bosch, D., Hidas, K., 2018. Genesis of ultra-high
847 pressure garnet pyroxenites in orogenic peridotites and its bearing on the compositional
848 heterogeneity of the Earth's mantle. Geochim. Cosmochim. Acta, 232, 303–328.
849 Von Raumer, J., Bussy, F., Schaltegger, U., Schulz, B., Stampfli, G.M., 2013. Pre-Mesozoic Alpine
850 basements--Their place in the European Paleozoic framework. Geological Society of America
851 Bulletin 125, 89-108.
852 Warren, J.M., 2016. Global variations in abyssal peridotite compositions. Lithos 248–251, 193–
853 219.
854 Willis, J. (2010). Glass beads by borate fusions (1st ed.). Almelo, Netherlands: PANalytical B.V.
855 https://www.malvernpanalytical.com/en/assets/Glass%20beads%20by%20borate%20fusion
856 _tcm50-54735.pdf

857 Yokoyama, T., & Nakamura, E. (2002). Precise determination of ferrous iron in silicate rocks.
858 Geochimica et Cosmochimica Acta, 66(6), 1085‐1093. https://doi.org/10.1016/S0016-
859 7037(01)00809-2

860 **FIGURE CAPTIONS**
861

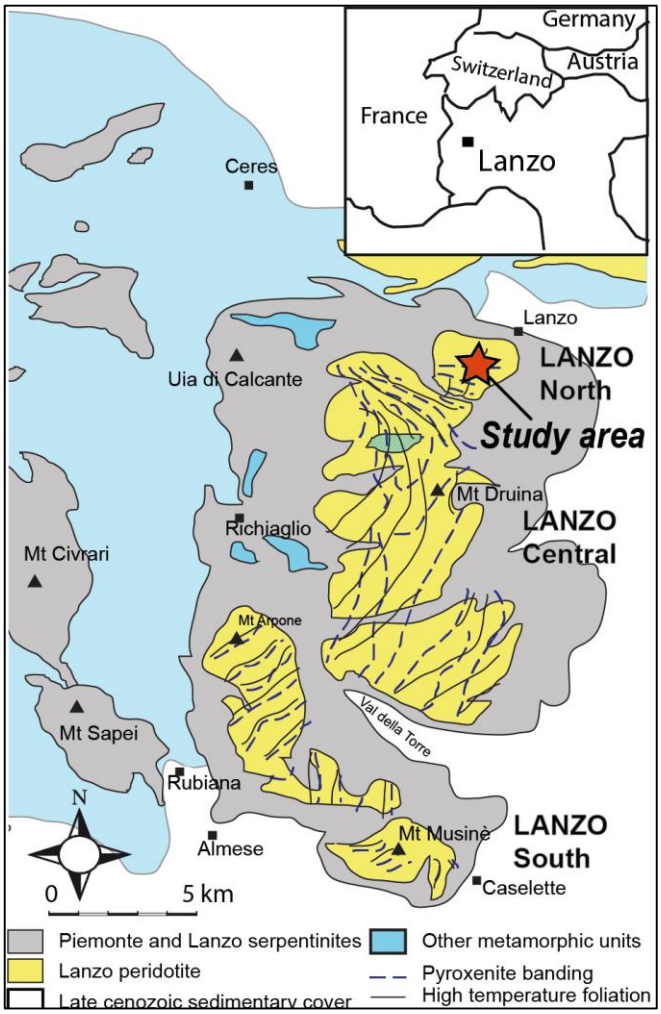

862
863

864 **Figure 1.** Geographical location (inset) and simplified geological map of the Lanzo peridotite
865 massif and surrounding rocks. Also shown are the foliation in the peridotites and the orientation of
866 the pyroxenite banding (redrawn after Boudier, 1978).
867

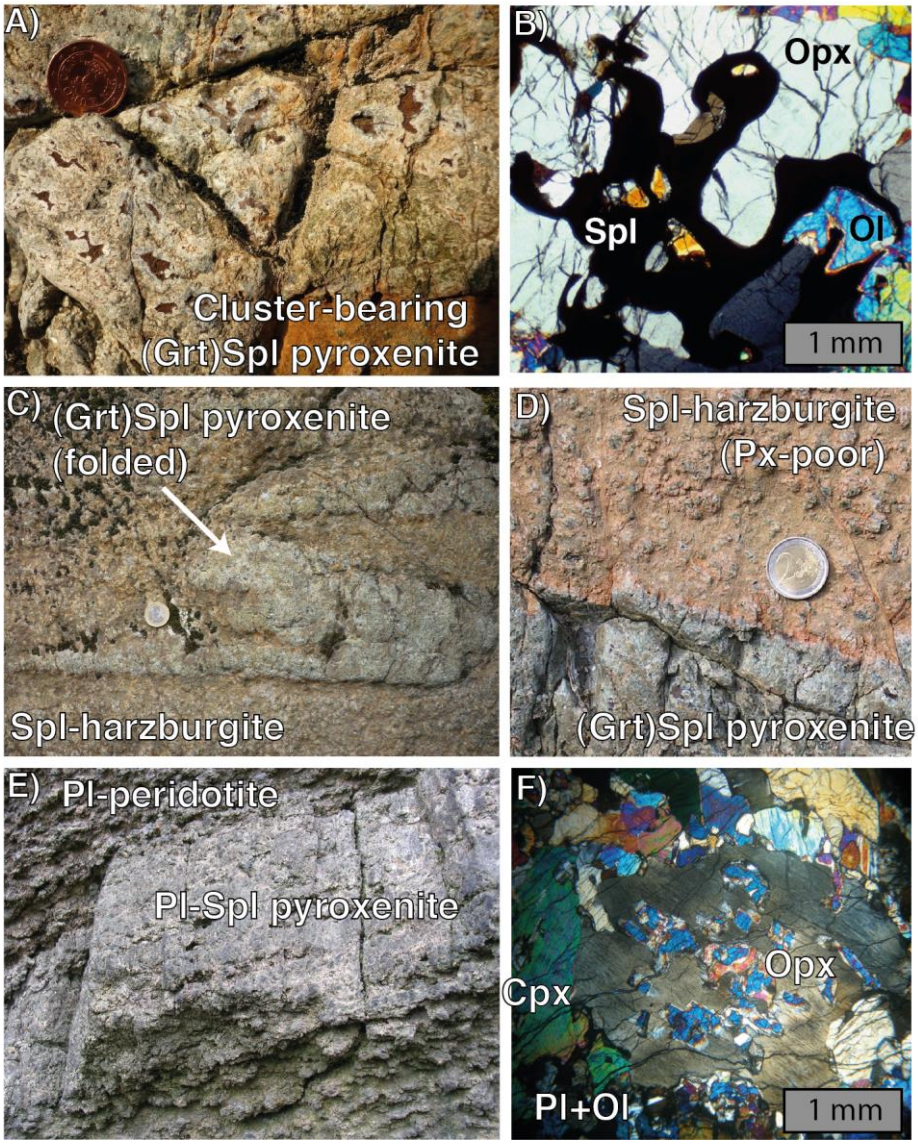

Figure 2. Representative field and textural features of the Lanzo N pyroxenites. A) Field occurrence of a (Grt)-Spl pyroxenite embedded in spinel lherzolites; they show millimetric symplectitic spl + opx + cpx clusters evidence of a former garnet (B). C) Plastically folded (Grt)-Spl pyroxenite included within a pyroxene-poor lherzolite. (D) Sharp contact between a (Grt)-Spl pyroxenite and the host Spl-harzburgite. (E) Spl-Pl pyroxenite included within a Pl-impregated peridotite. (F) Cross-polarized microphotograph of a Spl-Pl pyroxenite showing an orthopyroxene (Opx) porhyroclast containing exsolutions of plagioclase + secondary pyroxene, and partially replaced by Pl-bearing fine-grained neoblastic assemblage.

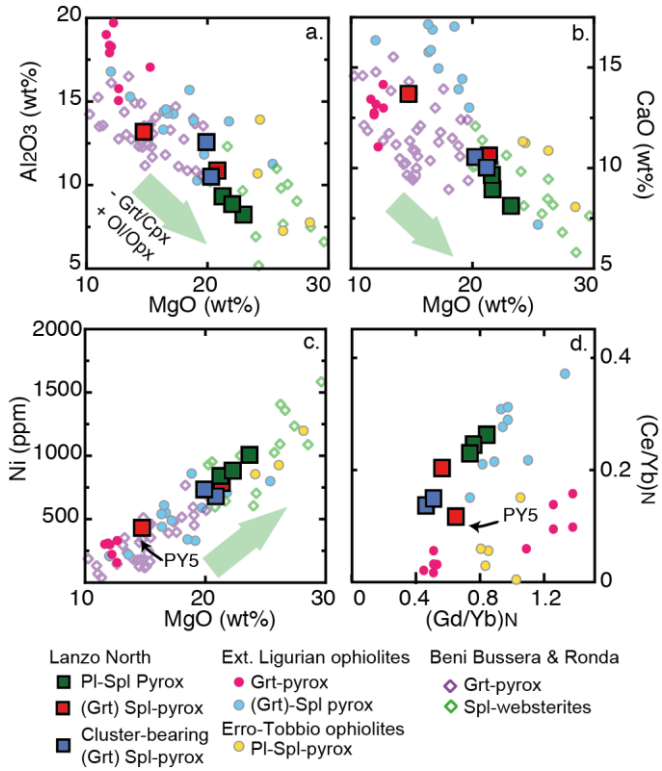

Figure 3. Bulk rock MgO (wt%) versus Al_2O_3 (wt%), CaO (wt%), Ni (ppm) contents and Gd/Yb versus Ce/Yb (N, normalized to CI values from Anders & Ebihara, 1982) of the Lanzo N pyroxenites. Grt-pyroxenites and Spl-websterites from Ronda and Beni Bousera massifs (Pearson et al., 1993; Garrido and Bodinieir, 1999; Gysi et al. 2011; Varas-Reus et al., 2018) are reported for comparison. For the External Liguride ophiolites we distinguished Grt-pyroxenites (Montanini et al., 2012), pyroxenites having garnet-like signature, i.e. (Grt)-Spl pyrox (Borghini et al., 2016). Pl-Spl pyroxenites from Erro-Tobbio ophiolite (Rampone and Borghini 2008) are also shown. The arrows indicate the overall increase in modal amount of olivine (Ol) and orthopyroxene (Opx) at decreasing garnet (Grt) and clinopyroxene (Cpx) as discussed in the text.

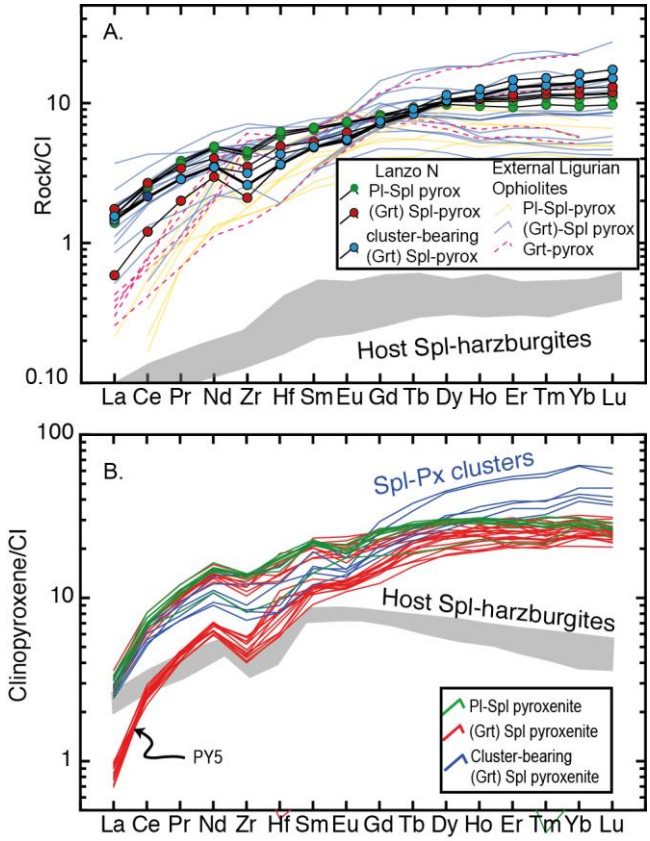

Figure 4. CI (Anders & Ebihara, 1982) normalized REE + Zr, Hf abundance patterns of whole rock compositions (a) and single clinopyroxene analyses (b) from Lanzo N pyroxenites; N, normalized to CI. In (a), the compositions of External Liguride pyroxenites (Montanini et al., 2012; Borghini et al., 2016) are also reported. The WR and Cpx compositions of host Spl-harzburgites are also reported (Guarnieri et al., 2012).

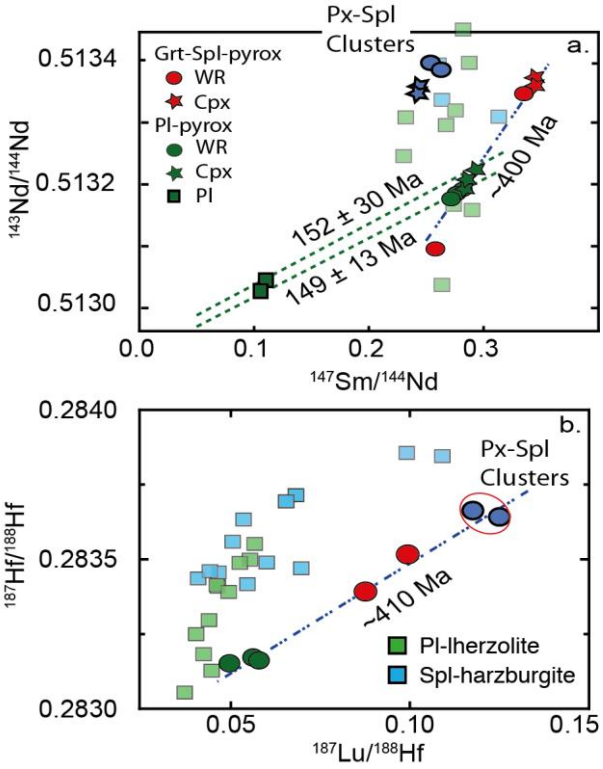

Figure 5. Bulk rock, clinopyroxene and plagioclase $^{147}Sm/^{144}Nd$ versus $^{143}Nd/^{144}Nd$ (a) and bulk-rock $^{187}Lu/^{188}Hf$ versus $^{17}Hf/^{188}Hf$ (b) of Lanzo N pyroxenites. Bulk-rock Nd and Hf isotopes data of the associated peridotites (Guarnieri et al., 2012) are also reported. Pl-Cpx-WR internal isochrones are defined for two Pl-Spl pyroxenites in (a). Errorchrones at 400 Ma based on both Nd and Hf isotopes data are defined by most samples, excluding cluster-bearing (Grt)-Spl pyroxenites that preserve high $^{143}Nd/^{144}Nd$ at comparatively low $^{147}Sm/^{144}Nd$ (see text).

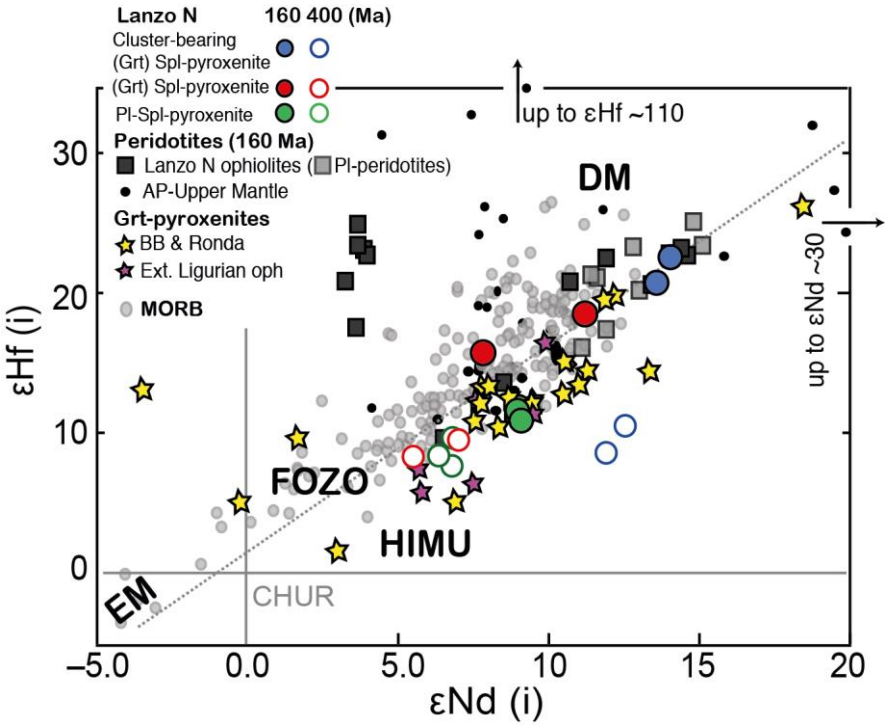

Figure 6. Initial Nd-Hf isotopic variations of Lanzo N pyroxenites and host peridotites calculated at the time of emplacement at Jurassic seafloor (160 Ma). Initial compositions of Lanzo N pyroxenites calculated at 400 Ma (empty red and green symbols) are also indicated (see text). The initial whole-rock compositions of Grt-pyroxenites from External Liguride ophiolites (Montanini et al., 2012), Ronda and Beni Bousera (Blichert-Toft et al., 1999; Pearson and Nowell, 2004; Varas-Reus et al., 2018) are calculated at time of exhumation as indicated in literature. The present-day compositions of clinopyroxenes from abyssal peridotites (Stracke et al., 2011), mantle xenoliths (Bizimis et al., 2003; Byerly and Lassitier, 2014) and MORB (after Stracke 2012) are also shown for comparison. Representative compositions of mantle end-members DM, EM, FOZO and HIMU are from Stracke (2012).

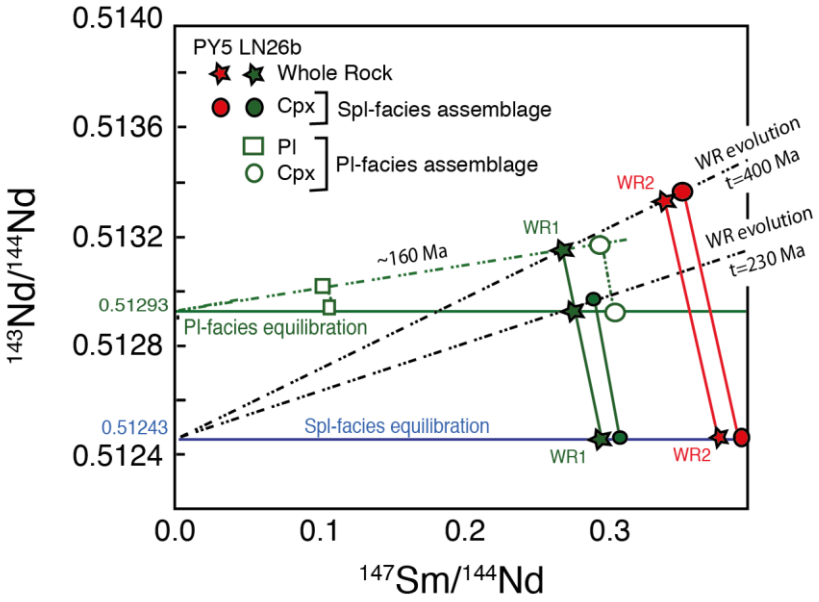

Figure 7. Nd-isotopic evolution of Spl-Pl pyroxenites. $^{147}Sm/^{144}Nd$ versus $^{143}Nd/^{144}Nd$ isotope ratios of whole rock, clinopyroxene and plagioclase in two representative samples of Spl-Pl pyroxenite (LN26b) (WR1) and (Grt)-Spl pyroxenite (Py5) (WR2). Both rocks initially equilibrated at spinel facies conditions at t=400 Ma, at different Sm/Nd ratios. At ~160 Ma, WR1 equilibrated at plagioclase facies conditions, resetting the Cpx $^{143}Nd/^{144}Nd$ ratios to the WR ratios, and forming plagioclase with the same $^{143}Nd/^{144}Nd$ isotope ratio. Because Cpx incorporates most of the Sm and Nd of the WR, this late equilibration event has a minor effect on the isotopic evolution allowing the preservation of a WR-Cpx errorchron defined for both samples, coexisting with a Pl-Cpx-WR internal isochron giving Jurassic ages.

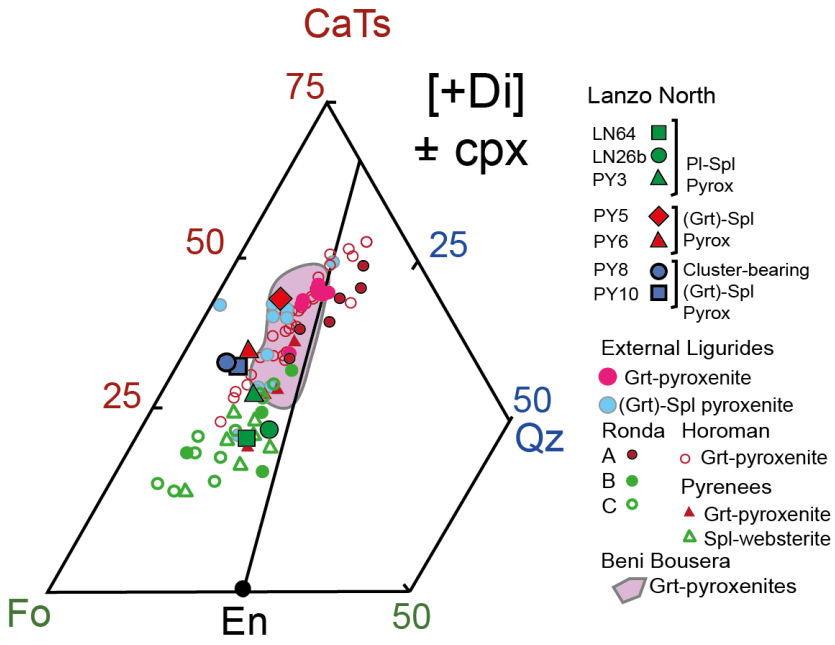

Figure 8. Molar projections from diospide [Di] into the pseudoternary diagram forsterite-Ca-Tschermak-quartz (Fo-CaTs-Qz) (O'Hara, 1972) of Lanzo North pyroxenites. The pyroxenite in this study are compared to garnet- and spinel-bearing pyroxenites from External Liguride ophiolites (Montanini et al., 2012, Borghini et al., 2016), Ronda (Garrido & Bodinier, 1999; Bodinier et al., 2008; Varas et al., 2018), Pyrenees (Bodinier et al., 1987), Horoman (Takazawa et al., 1999; Morishita & Arai, 2001), and Beni Bousera (Pearson et al., 1993; Kumar et al., 1996; Gysi et al., 2011; Varas et al., 2018).

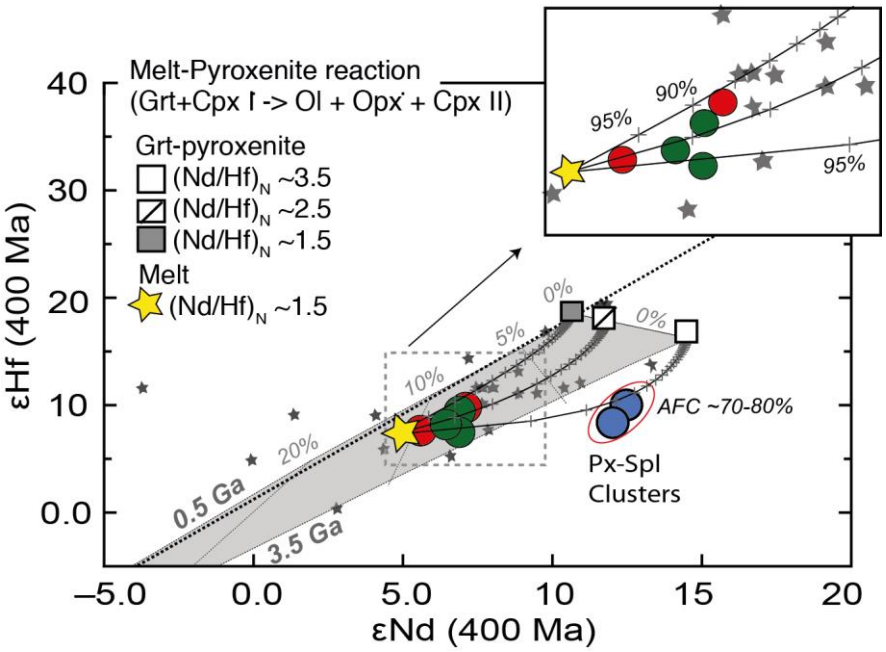

941

942 **Figure 9.** Nd-Hf isotopic variations of Lanzo N pyroxenites calculated at 400 Ma are
943 compared to the whole-rock compositions of Grt-pyroxenites from External Liguride ophiolites,
944 Ronda and Beni Boussera (grey stars; see **Fig. 6**). The grey field represents the compositions of
945 recycled altered MORB at ages of 0.5 and 3.5 Ga and at various proportions of marine sediments as
946 indicated by italic numbers (0-5-10-20%) (from Varas-Reus et al., 2018). The results of the AFC
947 models are reported at steps of F=0.05 starting from three end-member Grt-pyroxenite
948 compositions (see text for further explanation).

949

A 400 Ma-long Nd-Hf isotopic evolution of melt-modified garnet-pyroxenites in an ancient subcontinental lithosphere (Lanzo North ophiolite, Western Alps)

Alessio Sanfilippo*[1,2], Giulio Borghini[3], Luisa Guarnieri[4], Eizo Nakamura[5], Giovanni B. Piccardo[4], Riccardo Vannucci[1,2], Alberto Zanetti[2]

[1]Università degli Studi di Pavia, Via Ferrata 1, 27100 Pavia, Italy.
[2]Istituto Geoscienze e Georisorse, CNR, Via Ferrata 1, 27100, Italy.
[3]Dipartimento di Scienze della Terra, Università degli Studi di Milano, via Botticelli 23, 20133 Milano, Italy
[4]Accademia delle Scienze di Torino, Via Accademia delle Scienze, 6, 10123 Torino, Italy
[5]The Pheasant Memorial Laboratory for Geochemistry and Cosmochemistry, Institute for Planetary Materials, Okayama University, Misasa, Tottori 682-0193, Japan
*correspondence to *alessio.sanfilippo@unipv.it*

ABSTRACT

Pyroxenite veining is widely preserved in peridotite massifs, and used to derive information on the origin and evolution of upper mantle domains. These lithospheric mantle sections can be isolated from the convecting mantle for > 1 Ga or more, suffering a long history of melting and/or melt-rock reaction processes, which modify their original chemical and isotopic compositions. Here, we show the effect of ancient process of melt-rock reaction in the chemistry of garnet pyroxenites from Lanzo North Massif, an iconic lithospheric mantle section exhumed during the opening of the Jurassic Alpine Tethys. Selected pyroxenites are more than 10 cm thick, and embedded within peridotites that have textures and chemical compositions indicative of a complex history of interaction with migrating melts. Whole rock and clinopyroxene Nd-Hf isotopes of the pyroxenites consistently indicate that the first melt-rock reaction event occurred at ~400 Ma, likely in combination with exhumation from the garnet to the spinel-facies mantle conditions. Two samples still retain textural relicts and chemical evidence of precursor garnet and have high ε_{Nd} (~12) for comparatively low ε_{Hf} (~10), when recalculated at 400 Ma, which suggest that they were less affected by this ancient percolation process. The chemical evidence of such a long history of melt-rock reactions was preserved from 400 Ma until present. Finally, two pyroxenites located within plagioclase peridotites show evidence for an event of re-equilibration at plagioclase-facies conditions, likely triggered by infiltration of melt in the host rock. These samples reveal the coexistence of two internal Sm-Nd isochrones at 152 ± 30 Ma and 149 ± 13 Ma, thereby providing temporal constraints to the event of melt impregnation of the host peridotites as consequence of the opening of the Ligurian Tethys ocean.

Keywords: pyroxenite; Nd-Hf isotopes; Lanzo ophiolite; melt-rock reaction; subcontinental lithospheric mantle

40

41 **1. INTRODUCTION**

42 The upper mantle is a heterogeneous mixture of domains having different geochemical signatures
43 inherited from a long-history of melting, recycling and re-fertilization processes (e.g. Stracke,
44 2012). Due to their fertile character, geochemically enriched domains are preferentially melted and
45 thereby rarely recovered amongst abyssal peridotites (Salters and Dick, 2002; Warren, 2016).
46 Geochemically enriched lithologies, mainly represented by pyroxenite veining, are nonetheless
47 preserved in subcontinental peridotite massifs (Garrido and Bodinier, 1999; Downes, 2007;
48 Bodinier and Godard, 2014) and, locally, in ophiolites formed at slow spreading environments (e.g.,
49 Montanini et al., 2012; Borghini et al., 2016). Indeed, most orogenic peridotites contain a great
50 variety of pyroxenites and some of them, called "garnet pyroxenites", are mostly constituted by
51 pyroxene and garnet, proving to be equilibrated at high pressure (e.g. Bodinier et al., 1987; Pearson
52 et al., 1991; Morishita et al., 2003; Montanini et al. 2012). Contrary to what observed for abyssal
53 peridotites (Cipriani et al., 2004; Stracke et al., 2011), which on average retain isotopic
54 compositions more depleted than the associated MORB, the isotopic ratios of garnet pyroxenites
55 extends towards enriched values (that is low $^{143}Nd/^{144}Nd$ and $^{176}Hf/^{177}Hf$, and high $^{87}Sr/^{86}Sr$ isotopic
56 ratios), covering the entire variability of melts erupted at ocean ridges. The variability of Sr-Nd-Hf
57 isotopic compositions related to pyroxenites is often coupled with very old Re-Os model ages (>1
58 Ga), thus consistent with the expected isotopic variability and timescale for crustal recycling in the
59 mantle (Blichert-Toft et al., 1999; Pearson and Nowell, 2004; Ackerman et al., 2016; Varas-Reus et
60 al., 2018; Tilhac et al., 2020). These data support the hypothesis that enriched domains in the upper
61 mantle mostly derive from recycled portions of oceanic or continental lithosphere, including
62 igneous crust, lithospheric mantle and associated sediments (e.g. Stracke et al., 2003; Lambart et al.,
63 2016).

64 Most peridotite massifs represent ancient lithospheric portions emplaced at crustal depths
65 after being isolated form the convecting mantle for hundreds of millions of years, or more (Reisberg

and Lorand, 1995). During their exhumation, these mantle sequences commonly experience events of partial melting or interaction with migrating melts leading to changes in their original mineralogy, texture and composition (Le Roux et al., 2009; McCarthy and Müntener, 2015; Rampone et al., 2020; Rampone and Sanfilippo, 2021). While fast exhumation rates prevent any substantial perturbations in the long-lived radiogenic isotope systematics (such as Rb-Sr; Sm-Nd; Lu-Hf; U-Th-Pb) (Blichert-Toft et al., 1999; Pearson and Nowell, 2004; Varas-Reus et al., 2018), a long-lasting history of exhumation associated with melting and/or interactions with migrating melts may result in significant variation in parent/daughter isotope ratios, causing deviations from the original isotopic signature (Pearson et al., 1991; Tilhac et al., 2017).

Here, we focus on garnet-pyroxenites within melt-modified peridotites from a subcontinental mantle to discuss the chemical changes imposed by old melt migration and their effect on the long-term Nd-Hf isotopic evolution of pyroxenites. We use major-trace elements and Nd-Hf isotope compositions of decimetre-thick pyroxenites from the Lanzo North massif (Western Italian Alps), a well-studied lithospheric sub-continental mantle section exhumed at the ocean seafloor during the opening of the Ligurian Tethys, in the Middle Jurassic (Boudier, 1978; Lagabrielle et al., 1989). Previous studies on the host peridotites indicate that this mantle sequence suffered a multistage history of interaction with melts having an enriched (E)-MORB signature (Guarnieri et al., 2012). New chemical/isotopic compositions of the pyroxenites are here used to constrain an older event of migration and spinel-facies equilibration at 400 Ma. Geochemical modelling suggests that this event caused a shift towards low Hf isotope ratios for comparatively high Nd isotope ratios, producing unusual Nd-Hf isotope decoupling below the mantle array. We infer that the chemical response to this ancient history of melt-rock reaction is preserved until present. Moreover, two samples collected within plagioclase-bearing peridotites preserve Sm-Nd internal isochrones indicating that the equilibration at plagioclase-facies mantle conditions occurred at closed system, likely triggered by increase in temperature due to the infiltration of melts into the

host peridotite during the emplacement of the Lanzo North mantle sequence on the Jurassic seafloor.

2. LANZO NORTH PERIDOTITE MASSIF: PETROLOGICAL BACKGROUND

2.1 Peridotites

The Lanzo peridotite massif is part of the Sesia-Lanzo Zone, an accretionary prism of the Alpine orogeny formed by continental crustal rocks and subordinate subcontinental mantle slivers from the Adriatic plate (Fig. 1). The Sesia-Lanzo Zone represents the thinned and partially exhumed ocean-continent transition (OCT) along the Adriatic margin of the Alpine Tethys, and is bound to the east to the lower continental crustal rocks of the Adriatic plate (i.e., Ivrea-Verbano Zone, Southern Alps) by the Insubric line (the Peri-Adriatic lineament) and to west to meta-ophiolitic units of the Jurassic Piedmontese basin (i.e. Pennidic units; Fig. 1). The Lanzo ultramafic massif constitutes the southernmost portion of the Sesia-Lanzo Zone, and it has been subdivided in three domains, namely South, Central and North, on the basis of distinct geochemical characteristics (after Boudier, 1978; Bodinier et al., 1991). The Lanzo North massif exposes exceptionally well-preserved subcontinental mantle peridotites, locally intruded by ~160 Ma-old MORB-type gabbros (Piccardo et al., 2007a;b; Kaczmarek et al., 2008) and basalt dykes (**Fig. 1**). Primary contacts with a Jurassic sedimentary cover indicate the exhumation of the mantle section on the Alpine Tethys seafloor (Lagabrielle et al., 1989).

Several contributions described the overall characteristics of the different rock types in the Lanzo North (Boudier, 1978; Pognante et al., 1985; Bodinier, 1988; Bodinier et al., 1991; Piccardo et al., 2007a; Piccardo, 2010; Guarnieri et al., 2012); the main results are hereafter summarised. The older rock type is spinel lherzolite tectonite, which locally exceeds 10 vol% of porphyroclastic clinopyroxene (Cpx) and, in place, contain centimeter-size symplectitic clusters of spinel + orthopyroxene and minor clinopyroene (Spl+Px). Similar to other peridotite occurrences (e.g., Hoogerduijn Strating et al., 1993; Vannucci et al., 1993), these textures were considered products of

117 garnet breakdown after transition to spinel-facies mantle conditions, thus suggesting an early
118 equilibration at garnet facies conditions. These spinel lherzolites retain PM-like PGE patterns and
119 up to 1 Ga-old Re depletion ages (calculated after Becker et al., 2006) that are coupled with
120 relatively fertile major and incompatible trace element compositions. They yielded Sm-Nd and Lu-
121 Hf model ages up to 2.1 Ga (Bodinier et al., 1991; Guarnieri et al., 2012). Chemical and isotopic
122 data, thus, indicate a geochemical affinity acquired after a long-time isolation from the convective
123 mantle in a subcontinental lithosphere, and an early process of re-equilibration at garnet-facies
124 conditions (Boudier, 1978; Bodinier et al., 1991; Guarnieri et al., 2012).
125 The Spl-Px cluster-bearing spinel lherzolite tectonite is partially replaced by pyroxene-poor
126 spinel harzburgites, also called reactive harzburgite (Guarnieri et al., 2012). Indeed, microtextural
127 and geochemical evidence indicate that these modally depleted rocks formed by reactive
128 percolation of silica-undersaturated melts with a E-type MORB geochemical signature (Guarnieri et
129 al., 2012). The high LREE contents and variable Nd-Hf isotopes are the distinctive signatures of
130 these melt-modified rocks. Symplectitic Spl+Px clusters rarely occur in the harzburgites, suggesting
131 that they were consumed during the melt-rock reaction process. The preservation of radiogenic Nd
132 and Hf isotopic ratios at variable Sm/Nd and Lu/Hf in these Spl-harzburgites led Guarnieri et al.
133 (2012) to suggest that the event of migration of olivine-saturated melts occurred in Paleozoic times.
134 Locally, both lherzolites and modally depleted harzburgites show plagioclase-orthopyroxene
135 micro-veins that crosscut the spinel-facies mineral assemblage, associated with a consequent
136 increase in bulk rock SiO_2, Al_2O_3 and CaO at decreasing MgO and NiO contents (Guarnieri et al.,
137 2012). These plagioclase-bearing peridotites form hectometric-scale domains that suggest a
138 localized event of migration of silica-saturated MORB-like melts uprising in response to the passive
139 upwelling of the asthenospheric mantle and continental extension that led to the opening of the
140 Ligurian Tethys ocean in Jurassic times (Piccardo et al., 2003; Muntener et al., 2004; Piccardo and
141 Vissers, 2007; Piccardo et al., 2007a; b; Piccardo, 2010; Higgie and Tommasi, 2014; Piccardo,
142 2016). This process is common in the ophiolitic mantle sequences of the Alpine-Appenine

143 ophiolites and is referred to as “plagioclase-impregnation” (see Rampone and Sanfilippo, 2021 for a
144 review).
145
146 **2.2 Pyroxenites**
147 Pyroxenites are widespread in the Lanzo North mantle sequence where they occur as
148 centimeter- to decimeter-thick layers within the different rock types (**Fig. 2**). The pyroxenites are
149 often parallel or sub-parallel to tectonic foliation of host peridotite (**Fig. 2d,e**), although they
150 locally are intensely folded and boudinated (Boudier, 1978; Piccardo et al., 2007b, Piccardo, 2010)
151 (**Fig. 2c**). This is in agreement with the idea that thick pyroxenites represent long-lived
152 heterogeneities deformed at deep lithospheric conditions (Bodinier and Godard, 2014). Thick
153 pyroxenite layers occur within spinel lherzolites, spinel harzburgites and plagioclase(Pl)-
154 peridotites, as previously described by Boudier (1978), Piccardo et al. (2007b) and Guarnieri et al.
155 (2012).
156 In this study, we focused on samples from the inner portions of thick (>10 cm) pyroxenite
157 layers. Samples were distinguished in three types of pyroxenites, based on their host rock. (i)
158 cluster-bearing (Grt)-Spl pyroxenites were collected within spinel lherzolites (**Fig. 2a,b**), which
159 represent the oldest rock-type in Lanzo North massif (Guarnieri et al., 2012). These pyroxenites
160 contain exceptionally diffuse Spl-Px clusters (**Fig. 2a,b**), similar to those locally found in the host
161 fertile lherzolites (Guarnieri et al., 2012). These microstructures coupled with geochemical
162 characteristics of the pyroxenes, such as very high Sc and V contents and HREE (Yb at 40-60 x CI)
163 in spinel-bearing clinopyroxene porphyroclasts, indicate that they are the sub-solidus product of
164 spinel-facies recrystallization of precursor garnet pyroxenites (see also Piccardo et al., 2007b;
165 Guarnieri et al., 2009; 2012), suggesting that they originated at least at $P > 1.5$ GPa (Piccardo,
166 2010; Borghini and Fumagalli, 2018). (ii) (Grt)-Spl pyroxenites occur within modally depleted
167 spinel harzburgites, which formed by olivine-forming and pyroxene-dissolving reactions induced
168 by percolating melts (Guarnieri et al., 2012). They rarely show Spl-Px clusters and commonly have

169 porphyroclastic textures made by coarse clinopyroxene and orthopyroxene and sporadic large
170 green spinel. Large olivine porphyroclasts are also locally present although commonly replaced by
171 serpentine. In pyroxenite groups "i" and "ii", rare exsolutions of secondary pyroxene plus
172 plagioclase into coarse-grained pyroxene porphyroclasts and thin plagioclase + olivine coronas
173 around Spl indicate the incipient recrystallization at plagioclase-facies conditions ($P < 1.0$ GPa,
174 Piccardo et al., 2007b). (iii) Spl-Pl pyroxenites occur within plagioclase-impregnated peridotites
175 (**Fig. 2e**). They have websteritic composition and compared to the Grt-Spl pyroxenites contains
176 higher amounts of serpentinized olivine. Spl-Px clusters are absent in the Spl-Pl pyroxenites that
177 instead show much larger extent of plagioclase-bearing recrystallization. This latter is testified by
178 large domains of plagioclase + olivine + pyroxene neoblasts and diffuse occurrence of pyroxene +
179 plagioclase exolutions partially replacing the coarse pyroxene and spinel porphyroclasts (**Fig. 2f**).
180 In place, one Spl-Pl pyroxenite sample also shows thin plagioclase + orthopyroxene coronas
181 surrounding clinopyroxene porphyroclasts (Piccardo et al., 2007b). These textures testify an event
182 of equilibration at Pl-facies conditions likely triggered by the melt impregnation of the host
183 peridotite (Piccardo et al., 2007b). As noted in previous studies, the field and microstructural
184 features of the Lanzo N pyroxenites provide evidence that these rocks experienced multiple stages
185 of equilibration, ranging from garnet- to spinel- to plagioclase-facies, as response of the
186 progressive exhumation of the Lanzo North peridotite massif on the Jurassic seafloor (see Piccardo
187 et al. 2007b; Guarnieri et al., 2012 and references therein).
188
189 **3. ANALITICAL METHODOLOGY**
190 Samples for this study were selected from the innermost portions of thick (>10 cm)
191 pyroxenite layers. Analytical methodologies are identical to those reported in Guarnieri et al.
192 (2012) for the host peridotites from Lanzo North. Hereafter, we include a brief description of each
193 method, the reader is referred to Guarnieri et al. (2012) for further details. Major and trace elements
194 whole-rock analyses were performed at the Pheasant Memorial Laboratory for Geochemistry and

195 Cosmochemistry (PML), Institute for Study of the Earth's Interior (ISEI, reorganized into the
196 current Institute for Planetary Materials, IPM, in 2016), Okayama University at Misasa, Japan.
197 Whole-rock major element compositions were determined by X-ray fluorescence spectrometry
198 (XRF) with a Phillips PW 2400, using lithium tetraborate glass beads (1:10 ratio of sample and
199 flux; Takei, 2002). Fusion temperature for bead preparation was set at 1,050 ˚C to avoid loss of
200 alkali metals (Willis, 2010). The LOI (loss on ignition) was obtained by gravimetric method, and
201 FeO content was determined by titration (Yokoyama & Nakamura, 2002). Matrix correction
202 follows Norrish & Chappell (1977). Instrumental calibration was performed using the reference
203 igneous rocks (n = 13) provided from Geological Survey of Japan (GSJ); those include andesites
204 (JA-2 and JA-3), basalts (JB-1b, JB-2 and JB-3), rhyolites (JR-1, JR-2 and JR-3), granites (JG-1a
205 and JG-2), gabbros (JGb-1 and JGb-2), peridotite (JP-1), and hornblendite (JH-1). Major-element
206 compositions of these reference rocks are from Imai et al. (1995, 1999) and Terashima et al.
207 (1998). Accuracy of calibration is better than 1%, estimated from root mean square of residues.
208 Trace elements were analyzed by inductively coupled plasma-quadrupole mass
209 spectrometry (Agilent 7500CS) using the techniques of Makishima and Nakamura (2006). For Rb,
210 Sr, Y, Cs, Ba, REE, Pb, Th, and U analysis, samples were spiked with ^{149}Sm and dissolved
211 following the method of Makishima and Nakamura (1997). For the HFSE (Zr, Nb, Hf, and Ta)
212 analysis, a mixed ^{91}Zr-^{179}Hf spike was added to the samples. Samples were dissolved following the
213 Teflon bomb method of Tanaka et al. (2003). The 2sigma reproducibility of the rock standard JB-2
214 is less than 7% (n=3), and procedural blanks were less than 13 pg (n=2) for Rb, Sr, Y, Cs, Ba,
215 REE, Pb, Th, and U analysis. For the HFSE analysis, the 2sigma reproducibility of the rock
216 standard JB-3 is less than 5% (n=3), procedural blanks were less than 150pg for Nb, Hf and Ta,
217 5.7ng for Zr. Blank correction was applied to all the obtained elemental concentrations, and was
218 less than 1% for Rb, Sr, Y, Cs, Ba, REE, Pb, Th, and U. Since the aluminum addition method
219 (Tanaka et al, 2003) was applied to the HFSE analysis, the high blank value in the analysis is
220 attributed to the added Al solution corresponding to the decomposed sample amount (~50 mg).

Except for Nb in PY5 (9% correction), the blank corrections for Zr, Nb, and Hf were less than 4%; however, Ta resulted in corrections from 60 to 150%, and nearly 400% in PY5. Typical detection limits (3sigma) in the analyses are sub-ppt up to 30ppt, which corresponds to sub-ppb to 30ppb of elemental concentration in the sample.

Major elements compositions of clinopyroxene and plagioclase (Tables S2, S3): were determined using a JEOL 8200 SuperProbe at the Dipartimento di Scienze della Terra, Università degli Studi di Milano. Accelerating voltage was 15 kV, beam current 15 nA. Natural and synthetic minerals and glasses were used as standards. In-situ trace element analysis of clinopyroxenes and plagioclase was carried out by laser ablation inductively coupled plasma mass spectrometry (LA-ICP-MS) at the IGG-CNR of Pavia, Italy. The laser probe consisted of a Q-switched Nd:YAG laser, model Quantel (Brilliant); the spot diameter was typically of 50 um. The ablated material was analyzed using an Elan DRC-e quadrupole mass spectrometer. NIST SRM 610 synthetic glass was used as an external standard. The CaO content determined by electron microprobe analysis (EMPA) was used as an internal standard. Precision and accuracy were assessed from repeated analyses of the BCR-2 g standard and were usually better than ±10%.

Neodymium-Hf isotope determinations for whole-rock, clinopyroxene (Cpx) and plagioclase (Pl) were performed at the PML as described above (Table S4). Neodymium isotopic composition and Nd and Sm abundances were analyzed on whole-rock, clinopyroxenes and plagioclase, whereas Hf isotopes and Lu and Hf concentrations were obtained for whole rocks exclusively. Clinopyroxene and plagioclase separates were handpicked under a binocular microscope. Although the isotopic exchange between seawater and the original mineral assemblage during late-stage alteration is negligible for Nd and Hf, to minimize the possible effects of seawater alteration, clinopyroxenes and whole-rocks were leached following a multi-day and multi-stage procedure. Analyses of Sm-Nd isotope ratios and concentrations were performed by thermal ionization mass spectrometry (TIMS) following the techniques of Nakamura et al. (2003). Sample powders (100-130mg of whole rock, 10-60mg of Cpx, 80mg of Pl) were spiked with ^{150}Nd and

247 ^{149}Sm prior to dissolution and Nd isotope ratios and abundances by isotope dilution were
248 determined simultaneously on a Thermo Fisher Scientific Triton TIMS equipped with nine Faraday
249 cups. Samarium abundances were determined by isotope dilution procedures using a Finnigan-
250 MAT262 solid-source TIMS equipped with five Faraday cups following Nakamura et al. (2003).
251 Mean value of ^{143}Nd/^{144}Nd and reproducibility obtained by analyses of the in-house standard PML-
252 Nd was 0.511737 +/- 0.000013 (2sigma, n=15), and corresponded value of the La Jolla standard
253 was 0.511872 +/- 0.000013 (2sigma). The result of the reference rock standards JB2 and JB3 were
254 0.513114+/- 0.000029 (2sigma, n=4) and 0.513078+/- 0.000013 (2sigma, n=5), respectively. Total
255 procedural blanks of Nd and Sm were 0.7pg (n=5) and 0.1pg (n=5) for Cpx and Pl, 2pg (n=5) and
256 0.2 pg (n=5) for whole-rock, respectively.

257 For Lu and Hf abundance and Hf isotope ratio determination, MC-ICP-MS (Thermo Fisher
258 Scientific Neptune) was used. Whole -rock powders (100-130mg) were spiked with ^{176}Lu and ^{179}Hf
259 prior to decomposition and Hf isotope ratios and abundances by isotope dilution were determined
260 simultaneously applying the techniques of Lu et al. (2007) and Makishima and Nakamura (2008).
261 Lu contents were also measured following the procedures of Makishima and Nakamura (2008).
262 Hafnium isotopic data were normalized to ^{176}Hf/^{177}Hf = 0.282192 for JMC 14374, which
263 corresponds to ^{176}Hf/^{177}Hf = 0.282160 for JMC 475. The ^{176}Hf/^{177}Hf result of the reference rock
264 standards JB3 was 0.283224+/- 0.000011 (2sigma, n=5). Total procedural blanks of Hf and Lu were
265 154pg (n=11) and 0.1pg (n=11), respectively.
266

267 **4. RESULTS: MAJOR, TRACE ELEMENTS AND ND-HF ISOTOPIC COMPOSITIONS**

268 Selected Lanzo North pyroxenites show rough correlations in bulk MgO vs Al_2O_3, CaO and Ni.
269 The MgO, Al_2O_3, CaO and Ni contents in (Grt)-Spl pyroxenites cluster around rather uniform
270 values at relatively high MgO (~20 wt%) (**Fig. 3**). One sample (PY5) shows lower MgO (15 wt%)
271 at higher Al_2O_3, CaO and low Ni (13.5 and 14 wt%, 400 ppm, respectively). On the other hand, Pl-
272 Spl pyroxenites have higher MgO (up to 23 wt%) and Ni (up to 1100 ppm) and lower Al_2O_3 and

CaO contents (7.5 and 8 wt%, respectively). As a whole, the Lanzo N Pl-Spl pyroxenites plots in the field of the Pl-Spl pyroxenites from Beni Bousera and Ronda SCLM, and from the Ligurian ophiolites, whereas the (Grt)-Spl pyroxenites plot within the field of Beni Bousera and Ronda Grt pyroxenites, at generally higher MgO and Ni and lower CaO and Al_2O_3. Notably, PY5 (Grt)-Spl pyroxenite having low MgO and Ni, and high CaO, content is nearly undistinguishable from the Grt-pyroxenites reported in literature (**Fig. 3**).

The CI-normalized REE patterns of the cluster-bearing (Grt)-Spl pyroxenites reveal variable depletion in LREE (La_N/Sm_N = 0.12-0.32) coupled with selective enrichments in HREE over the MREE (Sm_N/Yb_N = 0.31-0.60) (**Fig. 3d; 4a**). These chemical characteristics agree with the local preservation of abundant Spl-Opx clusters and are similar to those of the External Ligurian Grt-pyroxenites, but at comparatively higher LREE (**Fig. 4a**). The high HREE abundances are also comparable with those observed in some garnet-bearing pyroxenites from orogenic ultramafic massifs of the Mediterranean area (Bodinier et al., 1987; Pearson et al., 1991, 1993; Garrido and Bodinier, 1999; Gysi et al., 2011; Montanini et al., 2012; Borghini et al., 2016). The REE patterns of the Pl-Spl pyroxenites are subparallel to those of (Grt)-Spl pyroxenites although they have relatively high and constant LREE (La_N/Sm_N =0.22-0.24) and nearly flat M-HREE patterns (Sm_N/Yb_N =0.62-0.68) (**Fig. 4a**). Overall, the CI-normalized patterns show an increase in LREE at decreasing HREE from the (Grt)-Spl pyroxenites towards the Pl-Spl pyroxenites (**Fig. 3d**). Similar chemical features are shown by the Cpx, which in the cluster-bearing (Grt)-Spl pyroxenites are characterized by high HREE, V and Sc contents and generally lower LREE compared to those in Pl-Spl peridotites (**Fig. 4b**; Table S3 in supplements). The compositions of Cpx presumably acquired most of the trace element signature from the whole-rock after equilibration at Spl-facies conditions (Vannucci et al., 1993; Rampone and Borghini, 2008; Borghini et al., 2013, 2016), indicating that garnet was at least locally abundant in the precursor mineral assemblages of some (Grt)-Spl pyroxenites.

Neodynium isotopic ratios were determined for Cpx, Pl and WR. Pyroxenites Cpx and WR reveal

299 a narrow isotopic variability, with present day $^{143}Nd/^{144}Nd$ ranging from 0.5131 to 0.5134 and
300 $^{147}Sm/^{144}Nd$ from 0.22 to 0.35 (**Fig. 5a**). On a closer inspection, Cpx and WR of 5 of the 7 samples
301 define an errorchron at 410 ± 17 Ma. The two Grt-Spl pyroxenites preserving Spl-Px clusters do not
302 plot along this array, retaining highly radiogenic $^{143}Nd/^{144}Nd$, but relatively low $^{147}Sm/^{144}Nd$ (**Fig.**
303 **5a**). Nd isotopes of Pl separates were also obtained from two Pl-Spl-pyroxenites. They provide Pl-
304 Cpx-WR internal isochrones at 152 ± 30 Ma and 149 ± 13 Ma. These ages are in good agreement
305 with the emplacement of Lanzo N massif at crustal depth as also indicated by the ages of the
306 MORB-type intrusions in Lanzo (Kaczmarek et al., 2008), and rather coeval with intrusive oceanic
307 crustal rocks of Jurassic Tethys (Rampone et al., 2014; Tribuzio et al., 2016 and references therein).
308 Whole-rock Hf isotopes of all pyroxenites define an errorchrone at 396 ± 27 Ma (**Fig. 5b**), notably
309 consistent with the Cpx-WR errorchrone yielded by Nd isotopes, if the (Grt)-Spl pyroxenites
310 preserving Spl-Px clusters are excluded. These cluster bearing (Grt)-Spl pyroxenites have the
311 highest $^{187}Lu/^{188}Hf$ and $^{187}Hf/^{188}Hf$ ratios, in agreement with a strong Grt signature. When
312 calculated at the time of emplacement of the Lanzo section at shallow depths (160 Ma), the initial
313 εNd-εHf values of all samples plot along the Nd-Hf terrestrial array. This suggests that at the time
314 of emplacement on the Jurassic seafloor, these pyroxenites were characterized by a wide isotopic
315 heterogeneity, varying from depleted to enriched Nd-Hf isotopic compositions and encompassing a
316 large portion of the present-day MORB field (**Fig. 6**).
317

318 **5. DISCUSSION**

319 **5.1 Exhumation at plagioclase-facies conditions**

320 The Spl-Pl pyroxenites in this study were sampled within the Pl-impregnated peridotites.
321 Hence, one can argue that these pyroxenites underwent chemical changes related to impregnation
322 of the host rocks, and that this process might have perturbed their geochemical and isotopic
323 compositions. Guarnieri et al. (2012) showed that Pl-facies impregnation of the Lanzo N
324 peridotites was related to the diffuse percolation of silica-saturated melts that crystallized gabbro-

noritic material within a former Spl-peridotite assemblage. This refertilization process caused the preferential addition of Pl+Opx with a consequent increase in SiO_2, Al_2O_3 and CaO at decreasing MgO and NiO contents (Rampone et al., 1996, 2008; Piccardo and Vissers, 2007) also coupled with the chemical equilibration of the original mantle phases with the infiltrating MORB-type melt (Piccardo et al., 2004; 2007b; Müntener et al., 2005; 2010). These are exactly the opposite chemical changes we envisage in the Spl-Pl pyroxenites, which are markedly enriched in MgO and NiO and depleted in Al_2O_3 and CaO compared to the (Grt)-Spl counterparts (**Fig. 3**). This suggests that the gabbroic pockets (plagioclase + olivine + neoblastic pyroxenes) grown between pyroxene and spinel porphyroclasts are likely the result of subsolidus recrystallization rather than the addition of infiltrating basaltic melts, as previously suggested by Piccardo et al. (2007b). Moreover, the Spl-Pl pyroxenite samples selected in this study do not show diffuse Pl-bearing veinlets crosscutting mantle minerals as typically described for impregnated peridotites (e.g. Rampone et al., 1997, 2008; Piccardo et al., 2007a). On the other hand, as observed in other pyroxenite occurrences from External Ligurides (Montanini et al., 2006, 2012; Borghini et al., 2016; Basch et al., 2020) and Erro-Tobbio massif (Rampone and Borghini, 2008), Pl in these samples appears as neoblasts together with new fine- and medium-grained pyroxenes or in association with olivine partly replacing large Spl porphyroclasts, thus suggesting that it mainly represents product of subsolidus recrystallization. Impregnation textures are nonetheless present at the vicinity of the contacts with the host Pl-peridotites, where the pyroxenites show Pl-bearing microveins crosscutting pyroxene porphyroclasts. It is thereby plausible that the infiltration of melts precipitating plagioclase in the host peridotites (Piccardo et al., 2007b; Guarnieri et al., 2012) was not able to modify the most internal portion of the studied pyroxenite layers, which thus preserved their isotopic compositions. Most likely, the volume of infiltrating melt was thereby small enough to be buffered by the pyroxene-rich matrix, determining the isotopic composition of the segregated plagioclase to be in close equilibrium with the bulk-rock composition.

351 The hypothesis that Pl in the pyroxenites formed as subsolidus equilibration is in agreement
352 with the isotopic record of the Spl-Pl pyroxenites. Linear correlations in $^{147}Sm/^{144}Nd$-$^{143}Nd/^{144}Nd$
353 and $^{187}Lu/^{188}Hf$ -$^{177}Hf/^{178}Hf$ characterize the WR and Cpx from all lithologies, including those
354 pyroxenites located within peridotites untouched by melt impregnation in the Jurassic. These
355 linear correlations connect all samples and form two distinct errorchrones yielding ages of ~400
356 Ma for both Nd and Hf isotopes, which must represent the age of isotopic equilibration at Spl-
357 facies (**Fig. 5**). For Nd isotopes, the WR-Cpx errorchron at ~400 Ma coexists with Pl-Cpx-WR
358 internal isochrones of Jurassic age. The internal isochrones based on Nd isotopes of by two Spl-Pl
359 pyroxenites have ages of 152 ± 30 Ma and 149 ± 13 Ma and indicate that the Pl-bearing
360 assemblage formed in Mid-Jurassic (**Fig. 5**), nearly coeval with the intrusion of MORB-type
361 gabbros within the Lanzo sequence (160 ± 4 Ma) (Kaczmarek et al., 2008). Although the
362 plagioclase-facies recrystallization cannot be undoubtedly related to the process of Pl-facies
363 impregnation in the host peridotite, it is plausible that the temperature increase due to melt
364 migration in the host peridotite triggered subsolidus recrystallization, likely enhanced by the
365 fertile bulk compositions of the pyroxenite assemblage (Hidas et al., 2021). Accordingly, (Grt)-
366 Spl pyroxenites show only incipient plagioclase-bearing recrystallization because they escaped
367 the heating related to melt impregnation of host peridotite.
368 If we assume that the two events were coeval, then our study furnishes the age of the
369 impregnation of the host mantle peridotite, which is slightly younger than the timing proposed for
370 the equilibration at Pl-facies conditions of the External Liguride ophiolites (186 ± 1.8 Ma,
371 Montanini et al., 2012; 178 ± 8 Ma, Borghini et al., 2016). The isotopic evolution of two selected
372 Spl-Pl and Grt-Spl samples is modeled in **Fig. 7.** The plot shows two samples having different
373 WR compositions, here indicated in different Sm/Nd ratios, that suffered a first event of isotopic
374 equilibration at Spl-facies conditions at 400 Ma, thereof followed by a closed-system WR isotopic
375 evolution until present. At 160 Ma, one sample experienced an event of equilibration at Pl-facies
376 conditions, evidenced by the formation of Pl in isotopic equilibrium with the WR and, as

response, a small shift in the Cpx Sm/Nd ratios. The following evolution led to further radiogenic Nd in-growth in Pl, WR and Cpx, aligned along a Jurassic errorchron. Cpx in pyroxenite incorporates most of the Sm and Nd of the WR, and the Pl-equilibration has a minor effect on the isotopic evolution of the Cpx in this sample. This allows the preservation of WR-Cpx errorchrons at ~400 Ma for both samples, coexisting with Pl-Cpx-WR internal isochrones having Jurassic ages (**Fig. 7)**.

5.2 Early perturbation of the Nd-Hf isotope systematics

In the previous section, we showed that the major, trace elements and the Nd-Hf isotopes of the Lanzo North pyroxenites did not suffer significant chemical perturbations during the process of melt migration and impregnation experienced by the host peridotite during the Jurassic exhumation at rather shallow mantle level. Instead, the errorchrons defined by WR and Cpx in the Sm-Nd and Lu-Hf isotopic space for most samples indicate that their isotopic equilibration was attained during a 400 Ma-old event, which was likely related to their complete re-equilibration at spinel-facies mantle conditions (**Fig. 5**). The only exception is represented by two cluster-bearing (Grt)-Spl pyroxenites, which preserve large quantities of subrounded Spl-Px clusters and have very high HREE contents, both indicative of a precursor garnet. These samples do not plot on the 400 Ma errorchron for the Sm-Nd isotopes, having lower Sm/Nd ratios compared to the other (Grt)-Spl samples. Hence, if the initial εNd-εHf values are calculated at 400 Ma (provided by the Nd-Hf errorchrons, **Fig. 5**), most pyroxenites have Nd-Hf compositions clustering in the enriched portion of MORB (εNd 6-7; εHf 8-9; **Fig. 6**), whereas the cluster-bearing (Grt)-Spl pyroxenites plot below the mantle array, showing a distinctive decoupling at higher εNd (12-13) for comparatively low εHf (8-9), (**Fig. 6**).

One possibility to explain the anomalous isotopic compositions is that the two cluster-bearing samples suffered some recent process of interactions with melts that decreased the original Sm/Nd ratios, thus shifting the samples on the left of the errorchron in **Fig. 5a**. Following

403 this scenario, this process must have preserved the original Lu/Hf ratios, according to the
404 occurrence of a Lu-Hf errorchron at 400 Ma (**Fig. 5**). The cluster-bearing (Grt)-Spl pyroxenites,
405 however, are located within spinel lherzolites that escaped the melt impregnation in the Jurassic
406 and are considered the oldest rock-type less-modified during the long-lasting history of melt-rock
407 reaction processes affecting the mantle sequence (Guarnieri et al., 2012). Indeed, the preservation
408 of Spl-Px clusters in both the peridotites and the pyroxenites and the evident Grt-signature
409 observed in WR and Cpx of the pyroxenites indicate that these rocks were nearly preserved after
410 their complete equilibration at Spl-facies conditions. In addition, the LREE in WR and Cpx from
411 these samples are in the same range of those in the Pl-Spl pyroxenites, whereas a late metasomatic
412 would have produced selective enrichments in these highly incompatible compared to the least
413 compatible elements (e.g., Stracke, 2012). On this basis, the field data, the texture and the
414 geochemical composition of the cluster-bearing (Grt)-Spl pyroxenites are strongly against the
415 possibility that they were modified by a recent metasomatic event.

416 As alternative hypothesis, the anomalous signature of the cluster-bearing (Grt)-Spl
417 pyroxenites was a consequence of a process of interaction with melts via reactive porous flow
418 envisaged in the host peridotites (Guarnieri et al., 2012). This hypothesis can be evaluated
419 considering the evolution of the studied pyroxenites in response to the melt migration processes.
420 The Lanzo N pyroxenites form correlations in MgO vs. Al_2O_3, CaO and NiO contents, suggesting
421 that they were presumably characterized by different modal amounts of Ol, Px and Grt (**Fig. 3; 4**).
422 This is further supported by the projection of our samples into the pseudoternary system forsterite
423 (Fo)/Ca-Tschermak molecule (CaTs)/quartz (Qz) projected from diopside [Di] (see **Fig. 8**)
424 (O'Hara, 1972). Overall, the Lanzo N pyroxenites are silica-deficient and plot on the left side of
425 the thermal divide (CaTs-En) (**Fig. 8**). In detail, the (Grt)-Spl pyroxenites, including those having
426 Spl-Pyx clusters, are slightly shifted towards the Fo apex compared to the Grt-pyroxenites from
427 External Liguride ophiolites, and from Beni Bousera, Ronda and Horoman peridotitic massifs
428 (Bodinier et al., 1987; Pearson et al., 1991, 1993; Garrido and Bodinier, 1999; Gysi et al., 2011;

Montanini et al., 2012; Borghini et al., 2016), indicating higher modal amounts of modal Ol. Even higher amounts of Ol is revealed by the Lanzo N Spl-Pl pyroxenites, which, similar to the Spl-websterites from Beni Bousera and Ronda massifs, plot closer to the Fo apex. The overall increase in Ol modes from the (Grt)-Spl pyroxenite to the Spl-Pl pyroxenite may suggest that these rocks are remnants of Grt-pyroxenites consumed at various extents by interaction with basaltic melts (e.g., group B pyroxenites in Garrido & Bodinier, 1999). The REE WR compositions of the Lanzo N pyroxenites agree with this hypothesis. All the samples display rather similar LREE/MREE ratios (La/Sm=0.3-0.5), but display a gradual decreases in HREE from the cluster-bearing (Grt)-Spl pyroxenites towards the Spl-Pl pyroxenites (see **Fig. 3d,4**). This suggests that the overall increase in Ol mode revealed by the Spl-Pl pyroxenites was coupled with the addition of a melt phase that decreased their WR HREE contents, causing a gradual increase in Ce/Yb ratios at increasing MgO contents (**Fig. 3d**). As analogy, most of the host Spl-peridotites are modally rich in Ol, and show nearly flat M-HREE WR patterns (**Fig.4**). Based on major and trace element decoupling, these rocks have been interpreted as product of interaction between a former lherzolite and basaltic melt having an enriched MORB signature (Guarnieri et al., 2012). A gradual interaction with basaltic melts is further consistent with the REE compositions of the Cpxs, which also show large variations in HREE, with Cpx from the two cluster-bearing samples still preserving extremely high HREE contents. The WR and mineral compositions of the Lanzo N pyroxenites can be thereby indicative of progressive reaction with a melt that percolated a former Grt-pyroxenite and smoothed out at various extents the original Grt-signature. Under this light, we infer that both pyroxenites and host Spl-peridotite were diffusively percolated by the same basaltic melt.

The local preservation of strongly radiogenic Nd and Hf isotopic ratios of the Spl-harzburgites (**Fig. 6**), along with variable Sm/Nd and Lu/Hf ratios (**Fig. 5**) led Guarnieri et al. (2012) to suggest that the melt migration producing modally depleted harzburgites largely anticipated the Jurassic impregnation, and must have occurred in Paleozoic times. Based on the

455 preservation of Nd-Hf errorchrons in the pyroxenites, we can now constrain the age of this
456 process at ~400 Ma. This age may reflect the time of a Paleozoic extension and associated E-
457 MORB magmatism also documented in the External Liguride mantle (~430 Ma) (Borghini et al.,
458 2013), and can be possibly related to an extensional phase related to the opening of the
459 Paleotethys at the onset of the Varisican orogenic cycle (von Raumer et al., 2013 and references
460 therein).
461
462 **5.3 Inference on the origin of the pristine garnet-pyroxenites and development of decoupled**
463 **Nd-Hf isotopic signature: a geochemical model**
464 We previously inferred that the pyroxenites considered in this study were partly, and in
465 different extent, modified by migration of melt having a E-MORB geochemical signature. The
466 process of diffuse melt percolation combined to the complete recrystallization at spinel-facies
467 mantle conditions occurred at 400 Ma and profoundly overprinted the original textural, modal and
468 chemical features of the precursor garnet pyroxenites. However, some inferences on the origin of
469 the pristine pyroxenites can be gained by the composition of the least reacted samples, namely
470 those preserving Spl-Px clusters as evidence of former Grt. These samples show a marked Grt-
471 signature as for trace elements (i.e., high Sc, V and HREE and high Lu/Hf in WR and Cpx), high
472 $\varepsilon Nd_{400,}$ but initial εHf_{400} similar to those of the other samples, thus showing Nd-Hf decoupling
473 below the mantle array (**Fig. 6**). Nd-Hf compositions below the mantle array are not uncommon
474 amongst Grt-pyroxenites worldwide and documented in External Ligurian ophiolites, Beni
475 Bussera and Ronda Massifs (see **Fig. 9**). According to their major and trace element chemistry,
476 these Grt-pyroxenites are generally interpreted as high pressure segregates of melts carrying the
477 isotopic signature of recycled oceanic crustal components (Pearson et al., 1991, 1993; Morishita
478 et al., 2003; Montanini et al., 2012; Marchesi et al., 2013; Montanini & Tribuzio, 2015; Varas-
479 Reus et al., 2018). In fact, the high mobility of Hf, Nd and Sm (22, 20 and 13%) (Stracke et al.,
480 2003; Niu, 2004) compared to Lu (immobile) produce a dehydrated oceanic crust with twice

481 higher Lu/Hf ratios (0.4) compared to average MORB (0.2), while leaving almost identical
482 Sm/Nd ratios (~0.3). Over time, this dehydrated crustal component would develop lower
483 $^{187}Hf/^{188}Hf$ at a given $^{143}Nd/^{144}Nd$, gradually diverging at lower εHf and slightly higher εNd
484 compared to the present-day values (Stracke et al., 2003). Marine sediments, on the other hand,
485 have much lower Sm/Nd and Lu/Hf than igneous ocean crust, and the addition of this component
486 to a dehydrated oceanic crust would produce gradual shifts in Nd-Hf towards less radiogenic
487 values (Kogiso et al., 1997). **Figure 9** shows that the isotopic field of recycled MORB (ranging
488 from 0.5 to 3.5 Ga) plus additions of minor marine sediments (Stracke et al., 2003; Varas-Reus et
489 al., 2018) can indeed explain most of the Nd-Hf isotopic decoupling seen in the Grt-pyroxenites
490 from Beni Bousera, Ronda and External Liguride ophiolites (grey starts in **Fig. 9**).
491 The cluster-bearing (Grt)-Spl pyroxenites from Lanzo N, however, do no plot within this
492 field, having even lower εHf for comparatively high εNd. The persistence of an errorchron at
493 ~400 Ma only in $^{187}Lu/^{188}Hf$ versus $^{177}Hf/^{178}Hf$ indicates that Hf isotopes in these rocks
494 equilibrated together with those of the other samples, whereas Nd isotopes of the two cluster-
495 bearing (Grt)-Spl pyroxenites experienced some incomplete equilibration with the reacting melt
496 and were partly inherited from that of the original Grt-pyroxenite. Hence, we argue that the melt-
497 pyroxenite interaction at 400 Ma caused the isotopic decoupling in the cluster-bearing (Grt)-Spl
498 pyroxenites. Due to the different affinities of Nd and Hf in the melt phase, and depending on the
499 Nd/Hf ratios of the two components, isotopic decoupling can occur during interaction between
500 depleted mantle peridotites and melts (Chauvel et al., 2008; Stracke et al., 2011; Guarnieri et al.,
501 2012). For a depleted peridotite interacting with a MORB melt, the lower Nd/Hf ratios of the
502 depleted end-member produces mixing lines plotting above the Nd-Hf mantle array; as a result,
503 reacted peridotites generally preserve high Hf isotopic values, while their original Nd signature is
504 easily concealed by equilibration with the migrating melt (Sanfilippo et al., 2019). On the other
505 hand, if at the time of melt-rock interaction the isotopically depleted end-member has high Nd/Hf,
506 Hf isotopes would more easily equilibrate with those of the melts, while radiogenic Nd is

507 preserved. As a consequence, interaction between melt and a precursor Grt-pyroxenite having
508 higher Nd/Hf ratios compared to a depleted peridotite, might have produced the Nd-Hf isotopic
509 decoupling below the mantle array revealed by the Lanzo N cluster-bearing (Grt)-Spl pyroxenites.
510 To test this hypothesis, we modeled a melt-rock reaction process between a precursor Grt-
511 pyroxenite and a MORB melt having Nd and Hf compositions in equilibrium with the Cpx of the
512 most enriched Lanzo N harzburgite. Despite the composition of the initial Grt-pyroxenite is
513 unknown, the REE pattern of the least modified samples recall those of Grt-pyroxenites from
514 External Ligurian ophiolites. Hence, we selected three end-members having different initial Nd-
515 Hf isotopes and whole rock geochemical compositions of Grt-pyroxenites from other sections of
516 External Ligurian ophiolites. The initial Grt-pyroxenite represents segregate from melts having a
517 geochemical signature akin a recycled MORB (i.e., long the "0 sediments line"), at ages of
518 recycling from 3.5 to 0.5 Ga (Varas-Reus et al., 2018) (see **Fig. 9**). In addition, we assumed for
519 the initial pyroxenite variable Sm/Nd and Lu/Hf ratios, to account for the expected compositional
520 variability of pyroxenites formed by deep segregation of melt in the mantle (Pearson et al., 1991,
521 1993; Morishita et al., 2003; Montanini et al., 2012; Marchesi et al., 2013; Montanini & Tribuzio,
522 2015; Varas-Reus et al., 2018). These parameters are arbitrary chosen and cannot take into
523 account the entire range of chemical variability of pyroxenites in the mantle, but are hereafter
524 used to test at what conditions the decoupling seen in the Grt-bearing samples can be
525 mathematically reproduced during a process of interaction with a melts.
526 We opted for the assimilation-fractional-crystallization (AFC) model of De Paolo (1981)
527 that has been successfully used to reproduce the Nd-Hf decoupling in mantle peridotites (Bizimis
528 et al., 2003; Chauvel et al., 2008; Stracke et al., 2011; Guarnieri et al., 2012; Sanfilippo et al.,
529 2019). Further details of the model are reported in the appendix. The results are plotted at steps of
530 F=0.02 (that is the melt mass during the AFC process) in **Figure 9** where the Nd-Hf isotopic
531 composition of the reaction products is compared to that of our samples. As a whole, the model is
532 able to reproduce the composition of the cluster-bearing (Grt)-Spl pyroxenites only if a

533 geochemically enriched pyroxenite, i.e., having high Nd/Hf ratios, is assimilated. This is in
534 agreement with the lower Sm/Nd and higher L/MREE ratios of these samples compared to the
535 other pyroxenites. On the contrary, the Nd-Hf isotopes of sample Py5 will be reproduced by
536 interaction with a Grt-pyroxenite having low Nd/Hf ratios, in agreement with the low LREE of
537 this sample. Independently on the initial composition, the isotopic composition of cluster-bearing
538 samples equals that of a Grt-pyroxenite produced after ~70-80% of assimilation and
539 recrystallization of its initial mass into a melt having an E-MORB signature. On the other hand,
540 the compositions of the Pl-Spl pyroxenites samples having high MgO contents require high
541 degrees of assimilation of the pre-existing pyroxenite, and recrystallization of an assemblage with
542 a geochemical composition similar that of the migrating melt (F >90%). This is well supported by
543 the generally higher Fo mode and higher bulk MgO and NiO contents in these samples, which
544 indicate addition of olivine and consumption of pyroxene starting from the pristine pyroxenite
545 assemblage.
546

547 **6. CONCLUSIONS**

548 This study places new temporal constraints to the long history of exhumation and melt-rock
549 reaction of the Lanzo North peridotite massif, through chemical and Nd-Hf isotopes investigations
550 on pyroxenite layers embedded within spinel and plagioclase peridotites, i.e. (Grt)-Spl pyroxenites
551 and Pl-Spl pyroxenites, respectively. Spl-Pl pyroxenites preserve Pl-Cpx-WR Sm-Nd internal
552 isochrons that indicate a closed-system event of Pl-facies equilibration in the Jurassic (152 ± 30
553 Ma and 149 ± 13 Ma). The intense plagioclase-facie recrystallization of Spl-Pl pyroxenites was
554 likely triggered by the migration of MORB-type melts generating the host Pl-peridotites. Field and
555 textural observations coupled to chemical compositions indicate that this melt migration process
556 did not significantly perturb the bulk isotopic composition of the internal portions of the
557 pyroxenites. On the other hand, at the time of their exhumation at the seafloor (160 Ma), these
558 pyroxenites still revealed a large isotopic variability, inherited from more ancient events of melt

559 migration and melt-pyroxenite interaction. Textural features along with major and trace element
560 compositions, suggest that the studied pyroxenites represent former Grt-pyroxenites, and that the
561 early isotopic equilibration occurred in response to an event of reactive percolation of basaltic
562 melts concomitant to the complete re-equilibration at spinel-facies mantle conditions. The
563 preservation of Nd-Hf errorchrons in Cpx and WR suggest that this event of melt migration and
564 isotopic equilibration likely occurred at ~400 Ma.

565 The (Grt)-Spl pyroxenites preserving widespread textural and chemical evidence of former
566 Grt do not plot on the 400 errorchron for the Sm-Nd isotopes, resulting in high ε_{Nd} (~12) for
567 comparatively low ε_{Hf} (~10), when recalculated at 400 Ma (**Fig. 6**). Based on field and
568 geochemical evidence, we exclude the possibility that these samples experienced a late process of
569 metasomatism. Instead, we believe that these samples were the least affected by the basaltic melt
570 percolation. Geochemical models corroborate this idea, showing that variable degrees of
571 interaction between a former Grt-pyroxenite with melts having a E-MORB geochemical signature
572 might have shifted the original Nd-Hf isotopes below the mantle array (**Fig. 8**). The elemental
573 fractionation caused by this process resulted in a different isotopic evolution over time and by the
574 time of emplacement of the sequence on the Jurassic seafloor, caused the cluster-bearing (Grt)-Spl
575 pyroxenites to experienced a stronger radiogenic Hf ingrowth compared to the other samples. As a
576 result, by the time of emplacement of this mantle section at crustal depths, the samples were "re-
577 coupled" along the terrestrial array. In conclusion, changes in elemental ratios and a long-time
578 evolution preceding the emplacement of the Lanzo N mantle sequence at crustal depth partly
579 obscured the perturbation caused by this old event of melt migration event. This study underlines
580 the importance of using Nd and Hf isotope systematics to give time constraints to ancient process
581 of reactive melt migrations that can potentially modify the lithological and chemical heterogeneity
582 of the subcontinental mantle.

583

584 **Acknowledgments**

N. Rizzo and A. Mosconi are acknowledged for preliminary work on the chemical data. A. Risplendente is thanked for assistance with the WDS adata. This study is partly supported by the Italian Programma di Rilevante Interesse Nazionale to A. Sanfilippo (PRIN_2017KY5ZX8). Analyses carried out at the Pheasant Memorial Laboratory were supported by PML members, especially Chie Sakaguchi at Misasa. This project was partially supported by 21 COE Program of MEXT Japan represented by EN. RICORDA DI RINGRAZIARE REVIEWER AND EDITOR!!

APPENDIX

Geochemical model (Table S5): the melt-rock interaction model used to reproduce the Nd-Hf isotope ratios of the pyroxenites from Lanzo N is calculated using an AFC-type model based on equations 6a and 15a from DePaolo (1981), as similarly used in previous studies reproducing melt-rock reactions in the oceanic mantle (Kelemen et al., 1992; Stracke et al., 2011; Guarnieri et al., 2012; Sanfilippo et al., 2019). A melt having an E-MORB isotopic signature reacts with initial Grt-pyroxenites having initial Nd/Hf ratios of 1.5, 2.5 and 3.5. In analogy with some Grt-pyroxenites from the External Ligurian ophiolites (Montanini et al., 2015; Borghini et al., 2016), Beni-Bousera and Ronda mantle sequences (see Varas-Reus et al., 2018 and references therein), the starting Grt-pyroxenites are considered to be high-pressure cumulates or products of melt-rock reaction (see for instance discussion in Gysi et al., 2011; Montanini et al., 2012; Borghini et al., 2016). We assume constant magma mass during reaction and mass assimilated to mass crystallized ratio ~0.9. The interaction of the starting Grt-pyroxenite (0.4 grt + 0.6 cpx; form Gysi et al., 2011) with the E-MORB melt produces a progressive changes in the resulting pyroxenite compositions by dissolution of the primary mineralogical assemblage and crystallization of new phases concomitant with phase transition from garnet to spinel peridotite field. Based on the reaction for the Grt-Spl phase transition defined by Vannucci et al. (1993) and on petrographic evidence in the host peridotites, we here assume that this process resulted in the transformation of the original Grt-pyroxenite into a (Grt)Spl-peridotite following the reaction

0.4 grt + 0.6 cpx1 + melt 1 = 0.3 opx + 0.4 cpx2 + 0.3spl + melt 2 (1)

The Nd-Hf isotope ratios of the melts produced by this AFC process is depicted in **Fig. 5** and details are reported in supplementary Table S5. Parameters, partition coefficients and results of the model are reported in Table S5. Note that the proportions of crystallizing phases has a minor effect on the isotopic composition of the results of the reaction, as the latter are mostly dependent on the initial Nd/Hf ratios of the assimilant compared to that of the interacting melt (see text for further discussion).

References

Ackerman, L., Bizimis, M., Haluzová, E., Sláma, J., Svojtka, M., Hirajima, T., Erban, V., 2016. Re–Os and Lu–Hf isotopic constraints on the formation and age of mantle pyroxenites from the Bohemian Massif. Lithos 256–257, 197–210.

625 Anders, E., Ebihara, M., 1982. Solar system abundances of the elements. Geochim. Cosmochim. Acta
626 46, 2363–2380.
627 Basch, V., Borghini, G., Fumagalli, P., Rampone, E., Ferrando, C., Gandolfo, A., 2020. Plagioclase-
628 facies thermobarometric evolution of the External Liguride pyroxenite-bearing mantle (Suvero,
629 Italy). Ofioliti 45, 1–11.
630 Becker, H., Horan, M.F., Walker, R.J., Gao, S., Lorand, J.P., Rudnick, R.L., 2006. Highly siderophile
631 element composition of the Earth's primitive upper mantle: constraints from new data on
632 peridotite massifs and xenoliths. Geochim. Cosmochim. Acta 70, 4528-4550.
633 Bizimis, M., Sen, G., Salters, V.J.M., 2003. Hf–Nd isotope decoupling in the oceanic lithosphere.
634 Constraints from spinel peridotites from Oahu, Hawaii. Earth Planet. Sci. Lett. 217, 43–58.
635 Blichert-Toft, J., Albarede, F., Kornprobst, J., 1999. Lu–Hf isotope systematics of garnet pyroxenites
636 from Beni Bousera, Morocco: implications for basalt origin. Science 283, 1303–1306 (1999).
637 Byerly, B.L., Lassiter, J.C., 2014. Isotopically ultradepleted domains in the convecting upper mantle:
638 implications for MORB petrogenesis. Geology 42, 203–206.
639 Bodinier, J.-L., Guiraud, M., Fabries, J., Dostal, J., Dupuy, C., 1987. Petrogenesis of layered
640 pyroxenites from the Lherz, Freychinede and Prades ultramafic bodies (Ariege, French
641 Pyrenees). Geochim. Cosmochim. Acta 51, 279-290.
642 Bodinier J. L., 1988. Geochemistry and petrogenesis of the Lanzo peridotite body, Western Alps.
643 Tectonophysics 149, 67–88.
644 Bodinier, J.L., Menzies, M.A., Thirlwall, M.F., 1991. Continental to oceanic mantle transition: REE
645 and Sr–Nd isotopic geochemistry of the Lanzo Lherzolite Massif. J. Petrol. 191–210. Special
646 Lherzolite Issue.
647 Bodinier, J.-L., Godard, M., 2014. Orogenic, ophiolitic and abyssal peridotites. in "Treatise on
648 Geochemistry", vol. 2, 2nd Edition, H.D. Holland & K.K. Turekian, eds. Elsevier Science,
649 Oxford, UK.
650 Borghini, G., Rampone, E., Zanetti, A., Class, C., Cipriani, A., Hofmann, A.W., Goldstein, S., 2013.

651 Meter-scale Nd isotopic heterogeneity in pyroxenite-bearing Ligurian peridotites encompasses
652 global-scale upper mantle variability. Geology 41, 1055-1058.
653 Borghini, G., Rampone, E., Zanetti, A., Class, C., Cipriani, A., Hofmann, A.W., Goldstein, S., 2016.
654 Pyroxenite layersin the Northern Apennines upper mantle (Italy) – Generation by pyroxenite
655 melting and melt infiltration. J. Petrol. 57, 625–653.
656 Borghini, G., Fumagalli, P., 2018. Subsolidus phase relations in a mantle pyroxenite: an experimental
657 study from 0.7 to 1.5 GPa. Eur. J. Mineral. 30, 333–348.
658 Boudier F., 1978. Structure and petrology of the Lanzo peridotite massif (Piedmont Alps). Geol. Soc.
659 Am. Bull. 89, 1574–1591.
660 Cipriani, A., Brueckner, H.K., Bonatti, E., Brunelli, D., 2004. Oceanic crust generated by elusive
661 parents: Sr and Nd isotopes in basalt-peridotite pairs from the Mid-Atlantic Ridge. Geology 32,
662 657–660.
663 Chauvel, C., Lewin, E., Carpentier, M., Arndt, N.T., Marini, J.-C., 2008. Role of recycled oceanic
664 basalt and sediment in generating the Hf–Nd mantle array. Nature Geoscience 1, 64–67.
665 DePaolo, D.J., 1981. Trace element and isotopic effects of combined wall-rock assimilation and
666 fractional crystallization. Earth Planet. Sci. Lett. 53, 189–202.
667 Downes, H., 2007. Origin and significance of spinel and garnet pyroxenites in the shallow
668 lithospheric mantle: Ultramafic massifs in orogenic belts in Western Europe and NW Africa.
669 Lithos 99, 1-24.
670 Garrido, C.J., Bodinier, J.L., 1999. Diversity of mafic rocks in the Ronda peridotite: evidence for
671 pervasive melt–rock reaction during heating of subcontinental lithosphere by upwelling
672 asthenosphere. J. Petrol. 40, 729–754.
673 Guarnieri, L., Piccardo, G. B., Nakamura, E., Shimizu, N., Vannucci, R. & Zanetti, A. (2009).
674 Pyroxenites in the North Lanzo Peridotite Massif: Insights into deep lithospheric processes.
675 Plinius 35, CD-ROM.
676 Guarnieri, L., Nakamura, E., Piccardo, G.B., Sakaguchi, C., Shimizu, N., Vannucci, R., Zanetti, A.,

677 2012. Petrology, trace element and Sr, Nd, Hf isotope geochemistry of the North Lanzo Peridotite
678 Massif (Western Alps, Italy). J. Petrol. 53, 2259–2306.
679 Gysi, A.P., Jagoutz, O., Schmidt, M.W., Targuisti, K., 2011. Petrogenesis of pyroxenites and melt
680 infiltrations in the ultramafic complex of Beni Boussera, Northern Morocco. J. Petrol. 52, 1676-
681 1735.
682 Hidas, K., Borghini, G., Tommasi, A., Zanetti, A., Rampone, E., 2021. Interplay between melt
683 infiltration and deformation in the deep lithospheric mantle (External Liguride ophiolite, North
684 Italy), Lithos, 380–381, 105855.
685 Higgie, K., Tommasi, A., 2014. Deformation in a partially molten mantle: Constraints from
686 plagioclase lherzolites from Lanzo, western Alps. Tectonophysics 615, 167-181.
687 Hirschmann, M.M., Stolper, E.M., 1996. A possible role for garnet pyroxenite in the origin of the
688 'garnet signature' in MORB. Contrib. Mineral. Petrol. 124, 185–208.
689 Hoogerduijn Strating, E.H., Rampone, E., Piccardo, G.B., Drury, M.R., Vissers, R.L.M., 1993.
690 Subsolidus emplacement of mantle peridotites during incipient oceanic rifting and opening of
691 the Mesozoic Tethys (Voltri Massif, NW, Italy). J. Petrol. 34, 901-927.
692 Imai, N., Terashima, S., Itoh, S., & Ando, A. (1995). 1994 compilation values for GSJ reference
693 samples,"Igneous rock series". Geochemical Journal, 29(1), 91–95.
694 Imai, N., Terashima, S., Itoh, S., & Ando, A. (1999). 1998 compilation of analytical data for five
695 GSJ geochemical reference samples: The "Instrumental analysis series". Geostandards
696 Newsletter, 23(2), 223-250.
697 Kaczmarek, M.A., Muntener, O., Rubatto, D., 2008. Trace element chemistry and U–Pb dating of
698 zircons from oceanic gabbros and their relationship with whole rock composition (Lanzo, Italian
699 Alps). Contrib. Mineral. Petrol. 155, 295–312.
700 Kelemen, P.B., Dick, H.J.B., Quick, J.E., 1992. Formation of harzburgite by pervasive melt/rock
701 reaction in the upper mantle. Nature 358, 635–641.
702 Kogiso, T., Tatsumi, Y., Nakano, S., 1997. Trace element transport during dehydration processes in

703 the subducted oceanic crust: 1. Experiments and implications for the origin of ocean island
704 basalts. Earth Planet. Sci. Lett. 148, 193-205.
705 Kumar, N., Reisberg, L., Zindler, A., 1996. A major and trace element and strontium, neodymium,
706 and osmium isotopic study of a thick pyroxenite layer from the Beni Bousera ultramafic complex
707 of northern Morocco. Geochim. Cosmochim. Acta 60, 1429-1444.
708 Lagabrielle, Y., Fudral, S., Kienast, J.R., 1989. The oceanic cover of the Lanzo peridotite body
709 (Western Italian Alps): lithostratigraphic and petrological evidences. Geodin. Acta 3, 43–55.
710 Lambart, S., Baker, M.B., Stolper, E.M., 2016. The role of pyroxenite in basalt genesis: Melt-PX, a
711 melting parameterization for mantle pyroxenites between 0.9 and 5 GPa. J. Geophys. Res. 121,
712 5708–5735.
713 Le Roux, V., Bodinier, J-L., Alard, O., O'Reilly, S.J., Griffin, W.L., 2009. Isotopic decoupling during
714 porous melt flow: A case-study in the Lherz peridotite. Earth Planet. Sci. Lett. 279, 76–85.
715 Lu, Y., Makishima, A., Nakamura, E., 2007. Purification of Hf in silicate materials using extraction
716 chromatographic resin, and its application to precise determination of 176Hf/177Hf by MC-
717 ICP-MS with 179Hf spike, J. Anal. At. Spectrom. 22, 69-76.
718 Makishima, A., Nakamura, E., 1997. Suppression of matrix effect in ICP-MS by high power
719 operaton of ICP: Application to precise determination of Rb, Sr, Y, Cs, Ba, REE, Pb, Th and U
720 at ng /g level in a few milligram silicate sample. Geostand. Newslett. 21, 307-319.
721 Makishima, A., Nakamura, E., 2006. Determination of major, minor and trace elements in silicate
722 samples by ICP-QMS and ICP-SFMS applying isotope dilution-internal standardization (ID-IS)
723 and multi-stage internal standardization. Geostandards and Geoanalytical Research 30, 245-
724 271.
725 Makishima A., Nakamura, E., 2008. New preconcentration technique of Zr, Nb, Mo, Hf, Ta and W
726 employing coprecipitation with Ti compounds: Its application to Lu-Hf system and sequential
727 Pb-Sr-Nd-Sm separation, Geochem. J. 42,199-206.
728 Marchesi, C., Garrido, C.J., Bosch, D., Bodinier, J-L., Gervilla, F., Hidas, K., 2013. Mantle

729 refertilization by melts of crustal-derived garnet pyroxenite: Evidence from the Ronda peridotite
730 massif, southern Spain. Earth Planet. Sci. Lett. 362, 66-75.
731 McCarthy, A., Müntener, O., 2015. Ancient depletion and mantle heterogeneity: revisiting the
732 Permian-Jurassic paradox of Alpine peridotites. Geology 43, 255–258.
733 Montanini, A., Tribuzio, R., Anczkiewicz, R., 2006. Exhumation history of a garnet pyroxenite-
734 bearing mantle section from a continent-ocean transition (Northern Apennine ophiolites, Italy).
735 J. Petrol. 47, 1943-1971.
736 Montanini, A., Tribuzio, R., Thirlwall, M., 2012. Garnet clinopyroxenite layers from the mantle
737 sequences of the Northern Apennine ophiolites (Italy): Evidence for recycling of crustal material.
738 Earth Planet. Sci. Lett.351-352, 171-181.
739 Montanini, A., Tribuzio, R., 2015. Evolution of recycled crust within the mantle: constraints from the
740 garnet pyroxenites of the External Ligurian ophiolites (northern Apennines, Italy). Geology 43,
741 911-914.
742 Morishita, T., Arai, S., 2001. Petrogenesis of corundum-bearing mafic rock in the Horoman Peridotite
743 Complex, Japan. J. Petrol. 42, 1279-1299.
744 Morishita, T., Arai, S., Gervilla, F., Green, D.H., 2003. Closed-system geochemical recycling of
745 crustal materials in the upper mantle. Geochim. Cosmochim. Acta 67, 303–310.
746 Müntener, O., Piccardo, G.B., Polino, R., Zanetti, A., 2004. Revisiting the Lanzo peridotite (NW-
747 Italy):'Asthenospherization'of ancient mantle lithosphere. Ofioliti 30 (2), 111-124
748 Müntener O., Manatschal G., Desmurs L., Pettke T., 2010. Plagioclase peridotites in ocean–continent
749 transitions: refertilized mantle domains generated by melt stagnation in the shallow mantle
750 lithosphere. J. Petrol. 51, 255–294.
751 Nakamura, E., Makishima, A., Moriguti, T., Kobayashi, K., Sakaguchi, C., Yokoyama, T., Tanaka,
752 R., Kuritani, T., Takei, H., 2003. Comprehensive geochemical analyses of small amounts (<
753 100mg) of extraterrestrial samples for the analytical competition related to the sample return
754 mission MUSES-C. Inst. Space Astronaut. Sci. Rep. SP. 16, 49-101.

755 Niu, Y., 2004. Bulk-rock major and trace element compositions of abyssal peridotites: Implications
756 for mantle melting, melt extraction and post-melting processes beneath ocean ridges. J. Petrol.
757 45, 2423–2458.
758 Norrish, K., and Chappell, B. W., 1967. X-ray fluorescence spectrography, *In* Physical Methods in
759 Determinative Mineralogy, J. Zussman, ed., pp. 161–214, Academic Press, London.
760 O'Hara, M.J., 1972. Data reduction and projection schemes for complex compositions. In: EaM, U.
761 (Ed.), Progress in Experimental Petrology. NERC, Manchester, Edinburgh 103–126.
762 Pearson, D.G., Davies, G.R., Nixon, P.H., Greenwood, P.B., Mattey, D.P., 1991. Oxygen isotope
763 evidence for the origin of pyroxenites in the Beni Boussera peridotite massif, North Morocco:
764 derivation from subducted oceanic lithosphere. Earth Planet. Sci. Lett. 102, 289–301.
765 Pearson, D.G., Davies, G.R., Nixon, P.H., 1993. Geochemical constraints on the petrogenesis of
766 diamond facies pyroxenites from the Beni Bousera peridotite massif, North Morocco. J. Petrol.
767 34, 125-172.
768 Pearson, D.G., Nowell, G.M., 2004. Re-Os and Lu-Hf isotope constraints on the origin and age of
769 pyroxenites from the Beni Bousera peridotite massif: implications for mixed peridotite-
770 pyroxenite mantle source. J. Petrol. 45, 439-455.
771 Piccardo, G.B., Müntener, O., Zanetti A., 2007. Alpine-Apennine ophiolitic peridotites: new concepts
772 on their composition and evolution, Ofioliti 29 (1), 63-74.
773 Piccardo, G.B., Zanetti, A., Poggi, E., Spagnolo, G., Müntener, O., 2007. Melt/peridotite interaction
774 in the Lanzo South peridotite: field, textural and geochemical evidence. Lithos 94, 181–209.
775 Piccardo, G.B., 2010. The Lanzo peridotite massif, Italian wester Alps: Jurassic rifting of the Ligurian
776 Tethys. In: Coltorti, M., Downes, H., Gregoire, M. & O'Reilly, S. Y. (eds) Petrological evolution
777 of the European lithospheric mantle. Geological Society, London, Special Publications 337, 47-
778 69.
779 Piccardo, G.B., 2016. Evolution of the lithospheric mantle during passive rifting: Inferences from the
780 Alpine–Apennine orogenic peridotites. Gondwana Research 39, 230-249.

781 Pognante, U., Rosli, U., Toscani, L., 1985. Petrology of ultramafic and mafic rocks from the Lanzo
782 peridotite body (Western Alps). Lithos 18, 201-214.
783 Rampone, E., Hofmann, A.W., Piccardo, G. B., Vannucci, R., Bottazzi, P., Ottolini, L., 1996. Trace
784 element and isotope geochemistry of depleted peridotites from an N-MORB type ophiolite
785 (Internal Liguride, N. Italy). Contrib. Mineral. Petrol. 123, 61-76.
786 Rampone, E., Piccardo, G.B., Vannucci, R., Bottazzi, P., 1997. Chemistry and origin of ted melts in
787 ophiolitic peridotites. Geochim. Cosmochim. Acta 61, 4557-4569.
788 Rampone, E., Borghini, G., 2008. Melt migration and intrusion in the Erro-Tobbio peridotites
789 (Ligurian Alps, Italy): insights on magmatic processes in extending lithospheric mantle. Eur. J.
790 Mineral. 20, 573–585.
791 Rampone, E., Piccardo, G.B., Hofmann, A.W., 2008. Multi-stage melt-rock interaction in the Mt.
792 Maggiore (Corsica, France) ophiolitic peridotites: microstructural and geochemical records.
793 Contrib. Mineral. Petrol. 156, 453-475.
794 Rampone, E., Borghini, G., Romairone, A., Abouchami, W., Class, C., Goldstein, S.L., 2014. Sm-Nd
795 geochronology of the Erro-Tobbio gabbros (Ligurian Alps, Italy): insights on the evolution of
796 the Alpine Tethys. Lithos 205, 236-246.
797 Rampone, E., Borghini, G., Basch, V., 2020. Melt migration and melt-rock reaction in the Alpine-
798 Apennine peridotites: insights on mantle dynamics in extending lithosphere. Geoscience
799 Frontiers Special Issue: Ophiolites, 11, 151-166.
800 Rampone, E., & Sanfilippo, A., 2021. The heterogeneous Tethyan oceanic lithosphere of the Alpine
801 ophiolites. Elements: An International Magazine of Mineralogy, Geochemistry, and Petrology,
802 17(1), 23-28.
803 Reisberg L., Lorand J.-P., 1995. Longevity of sub-continental mantle lithosphere from osmium
804 isotope systematics in orogenic peridotite massifs. Nature 376, 159-162.
805 Salters, V.J.M., Dick, H.J.B., 2002. Mineralogy of the mid-ocean-ridge basalt source from
806 neodymium isotopic composition of abyssal peridotites. Nature 418, 68–72.

807 Sanfilippo, A., Tribuzio, R., Tiepolo, M., 2014. Mantle–crust interaction in the oceanic lithosphere:
808 constraints from minor and trace elements in olivine. Geochim. Cosmochim. Acta 141, 423–439.
809 Sanfilippo, A., Salters,V., Tribuzio, R., Zanetti, A., 2019. Role of ancient, ultra-depleted mantle in
810 Mid-Ocean-Ridge magmatism. Earth Planet. Sci. Lett. 511, 89–98.
811 Stracke, A., Salters, V.J.M., Sims, K.W.W., 1999. Assessing the presence of garnet–pyroxenite in the
812 mantle sources of basalts through combined hafnium–neodymium–thorium isotope systematics.
813 Geochem. Geophys. Geosyst. 1.
814 Stracke, A., Bizimis, M., Salters, V.J.M., 2003. Recycling of oceanic crust: quantita- tive constraints.
815 Geochem. Geophys. Geosyst. 4, 8003. https://doi.org/10.1029/ 2001GC000223.
816 Stracke, A., Snow, J.E., Hellebrand, E., von der Handt, A., Bourdon, B., Birbaum, K., Gunther, D.,
817 2011. Abyssal peridotite Hf isotopes identify extreme mantle depletion. Earth Planet. Sci. Lett.
818 308, 359–368.
819 Stracke, A., 2012. Earth's heterogeneous mantle: a product of convection-driven interaction between
820 crust and mantle. Chem. Geol. 330–331, 274–299.
821 Takei, H., 2002. Development of precise analytical techniques for major and trace element
822 concentrations in rock samples and their applications to the Hishikari gold mine, southern
823 Kyushu, Japan, PhD thesis, Graduate School of Natural Science and Technology, Okayama
824 University, Tottori.
825 Tanaka, R., Makishima, A., Kitagawa, H., Nakamura, E., 2003. Suppression of Zr, Nb, Hf and Ta
826 coprecipitation in fluoride compounds for determination in Ca-rich materials. J. Anal. At.
827 Spectrom. 18, 1458-1463.
828 Terashima, S., Taniguchi, M., Mikoshiba, M., & Imai, N. (1998). Preparation of two new GSJ
829 geochemical reference materials: Basalt JB‐1b and coal fly ash JCFA‐1. Geostandards
830 Newsletter, 22(1), 113-117.
831 Tilhac, R., Gregoire, M., W.L., O'Reilly, Griffin, S.Y., Henry, H., Ceuleneer, G., 2017. Sources and
832 timing of pyroxenite formation in the sub-arc mantle: case study of the Cabo Ortegal Complex,

833 Spain. Earth Planet. Sci. Lett. 474, 490–4502.
834 Tilhac, R., Oliveira, B., Griffin, W.L., O'Reilly, S.Y., Schaefer, B.F., Alard, O., Ceuleneer, G.,
835 Afonso, J.C., Grégoire, M., 2020. Reworking of old continental lithosphere: unradiogenic Os and
836 decoupled Hf-Nd isotopes in sub-arc mantle pyroxenites. Lithos 354-355, 105346.
837 Tribuzio, R., Garzetti, F., Corfu, F., Tiepolo, M., Renna, MR., 2016. U–Pb zircon geochronology of
838 the Ligurian ophiolites (Northern Apennine, Italy): Implications for continental breakup to slow
839 seafloor spreading. Tectonophysics 666, 220-243.
840 Vannucci, R., Shimizu, N., Piccardo, G. B., Ottolini, L., Bottazzi, P., 1993. Distribution of trace-
841 elements during breakdown of mantle garnet: an example from Zabargad. Contrib. Mineral.
842 Petrol. 113, 437–449.
843 Varas-Reus, M.I., Garrido, C.J., Marchesi, C., Bosch, D., Hidas, K., 2018. Genesis of ultra-high
844 pressure garnet pyroxenites in orogenic peridotites and its bearing on the compositional
845 heterogeneity of the Earth's mantle. Geochim. Cosmochim. Acta, 232, 303–328.
846 Von Raumer, J., Bussy, F., Schaltegger, U., Schulz, B., Stampfli, G.M., 2013. Pre-Mesozoic Alpine
847 basements--Their place in the European Paleozoic framework. Geological Society of America
848 Bulletin 125, 89-108.
849 Warren, J.M., 2016. Global variations in abyssal peridotite compositions. Lithos 248–251, 193–219.
850 Willis, J. (2010). Glass beads by borate fusions (1st ed.). Almelo, Netherlands: PANalytical B.V.
851 https://www.malvernpanalytical.com/en/assets/Glass%20beads%20by%20borate%20fusion
852 _tcm50-54735.pdf
853 Yokoyama, T., & Nakamura, E. (2002). Precise determination of ferrous iron in silicate rocks.
854 Geochimica et Cosmochimica Acta, 66(6), 1085‑1093. https://doi.org/10.1016/S0016-
855 7037(01)00809-2

856 **FIGURE CAPTIONS**
857

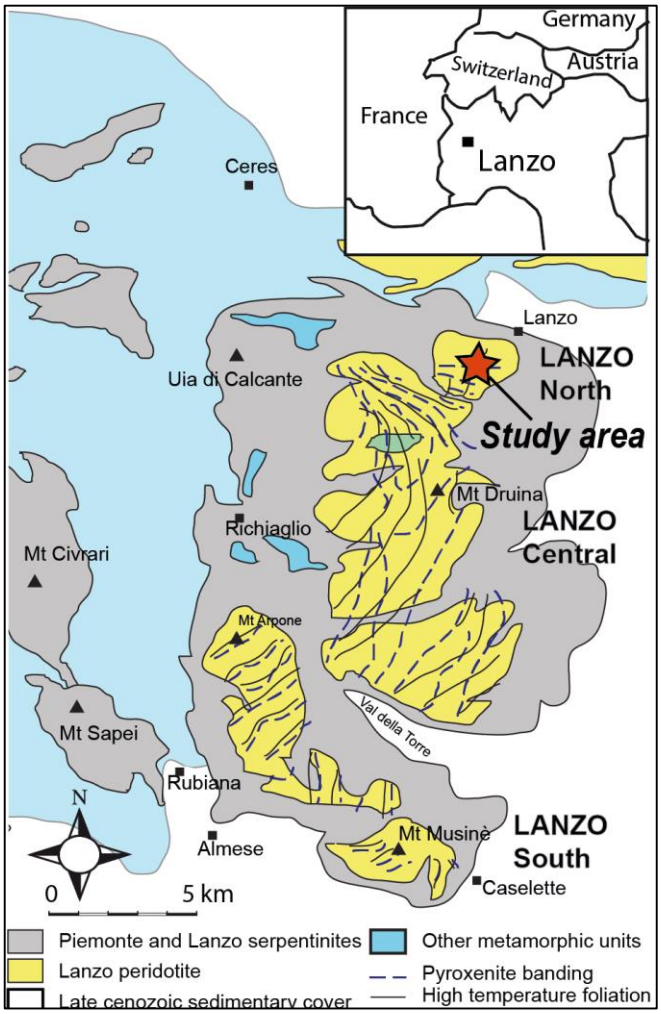

858
859

860 **Figure 1.** Geographical location (inset) and simplified geological map of the Lanzo peridotite
861 massif and surrounding rocks. Also shown are the foliation in the peridotites and the orientation of
862 the pyroxenite banding (redrawn after Boudier, 1978).
863

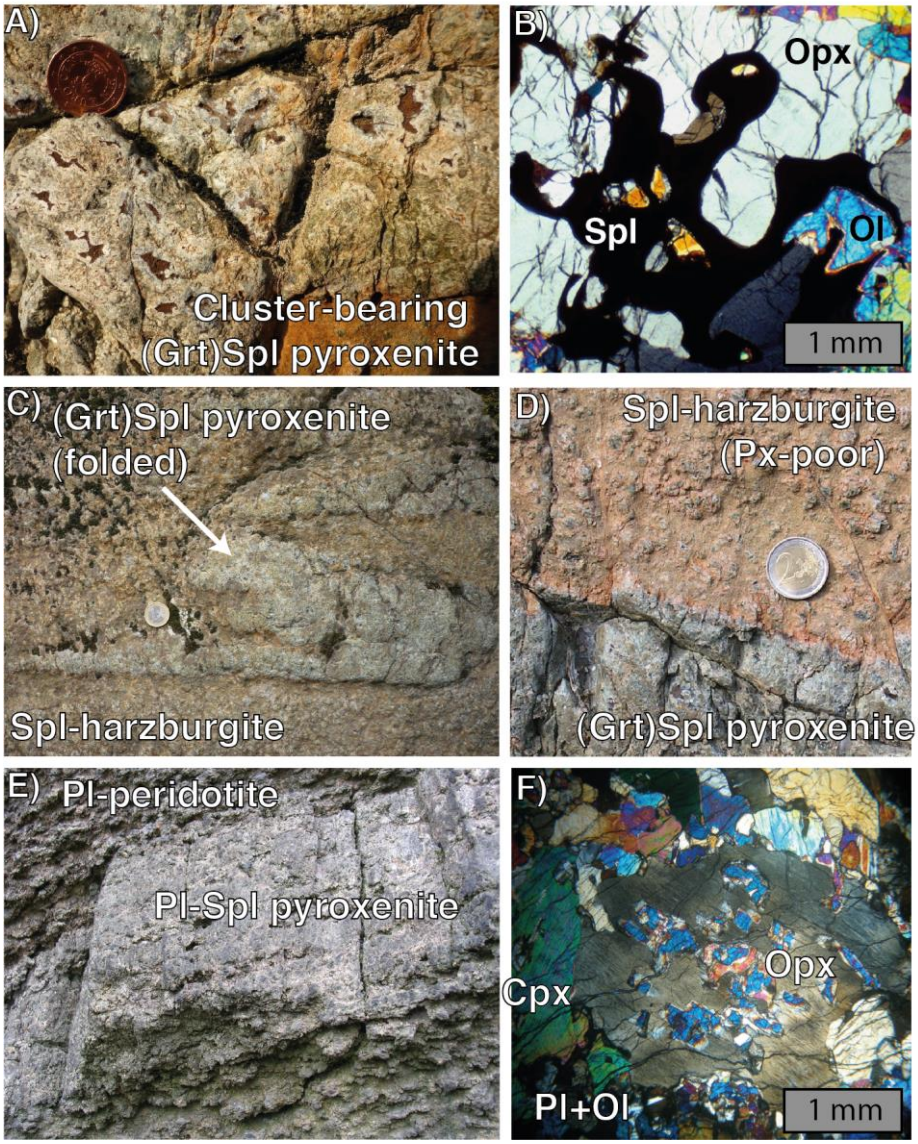

Figure 2. Representative field and textural features of the Lanzo N pyroxenites. A) Field occurrence of a (Grt)-Spl pyroxenite embedded in spinel lherzolites; they show millimetric symplectitic spl + opx + cpx clusters evidence of a former garnet (B). C) Plastically folded (Grt)-Spl pyroxenite included within a pyroxene-poor lherzolite. (D) Sharp contact between a (Grt)-Spl pyroxenite and the host Spl-harzburgite. (E) Spl-Pl pyroxenite included within a Pl-impregated peridotite. (F) Cross-polarized microphotograph of a Spl-Pl pyroxenite showing an orthopyroxene (Opx) porhyroclast containing exsolutions of plagioclase + secondary pyroxene, and partially replaced by Pl-bearing fine-grained neoblastic assemblage.

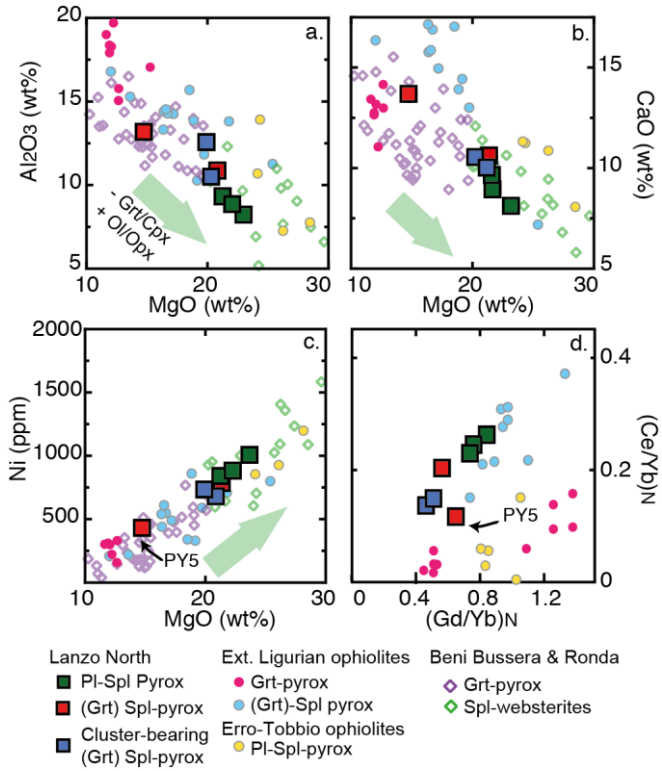

873

874 **Figure 3.** Bulk rock MgO (wt%) versus Al_2O_3 (wt%), CaO (wt%), Ni (ppm) contents and
875 Gd/Yb versus Ce/Yb (N, normalized to CI values from Anders & Ebihara, 1982) of the Lanzo N
876 pyroxenites. Grt-pyroxenites and Spl-websterites from Ronda and Beni Bousera massifs (Pearson et
877 al., 1993; Garrido and Bodinieir, 1999; Gysi et al. 2011; Varas-Reus et al., 2018) are reported for
878 comparison. For the External Liguride ophiolites we distinguished Grt-pyroxenites (Montanini et
879 al., 2012), pyroxenites having garnet-like signature, i.e. (Grt)-Spl pyrox (Borghini et al., 2016). Pl-
880 Spl pyroxenites from Erro-Tobbio ophiolite (Rampone and Borghini 2008) are also shown. The
881 arrows indicate the overall increase in modal amount of olivine (Ol) and orthopyroxene (Opx) at
882 decreasing garnet (Grt) and clinopyroxene (Cpx) as discussed in the text.

883

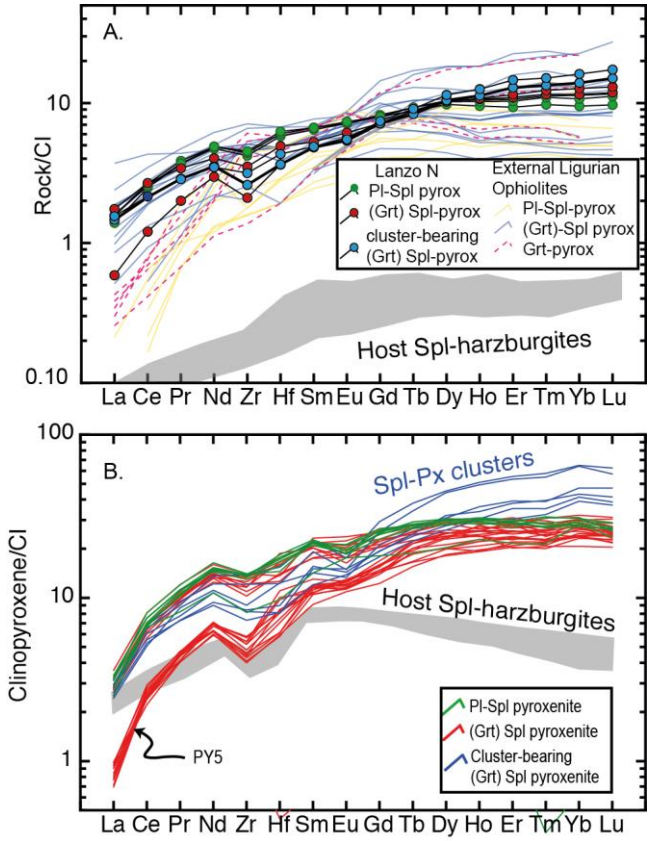

Figure 4. CI (Anders & Ebihara, 1982) normalized REE + Zr, Hf abundance patterns of whole rock compositions (a) and single clinopyroxene analyses (b) from Lanzo N pyroxenites; N, normalized to CI. In (a), the compositions of External Liguride pyroxenites (Montanini et al., 2012; Borghini et al., 2016) are also reported. The WR and Cpx compositions of host Spl-harzburgites are also reported (Guarnieri et al., 2012).

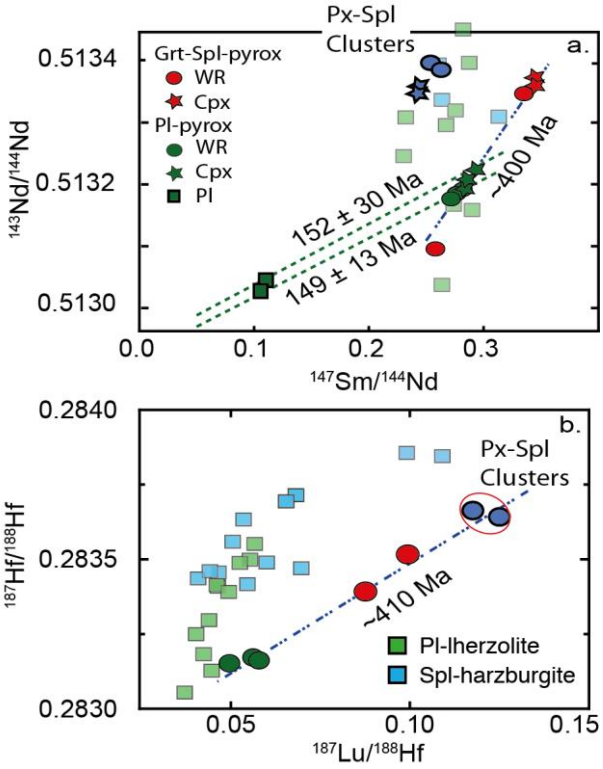

Figure 5. Bulk rock, clinopyroxene and plagioclase $^{147}Sm/^{144}Nd$ versus $^{143}Nd/^{144}Nd$ (a) and bulk-rock $^{187}Lu/^{188}Hf$ versus $^{17}Hf/^{188}Hf$ (b) of Lanzo N pyroxenites. Bulk-rock Nd and Hf isotopes data of the associated peridotites (Guarnieri et al., 2012) are also reported. Pl-Cpx-WR internal isochrones are defined for two Pl-Spl pyroxenites in (a). Errorchrones at 400 Ma based on both Nd and Hf isotopes data are defined by most samples, excluding cluster-bearing (Grt)-Spl pyroxenites that preserve high $^{143}Nd/^{144}Nd$ at comparatively low $^{147}Sm/^{144}Nd$ (see text).

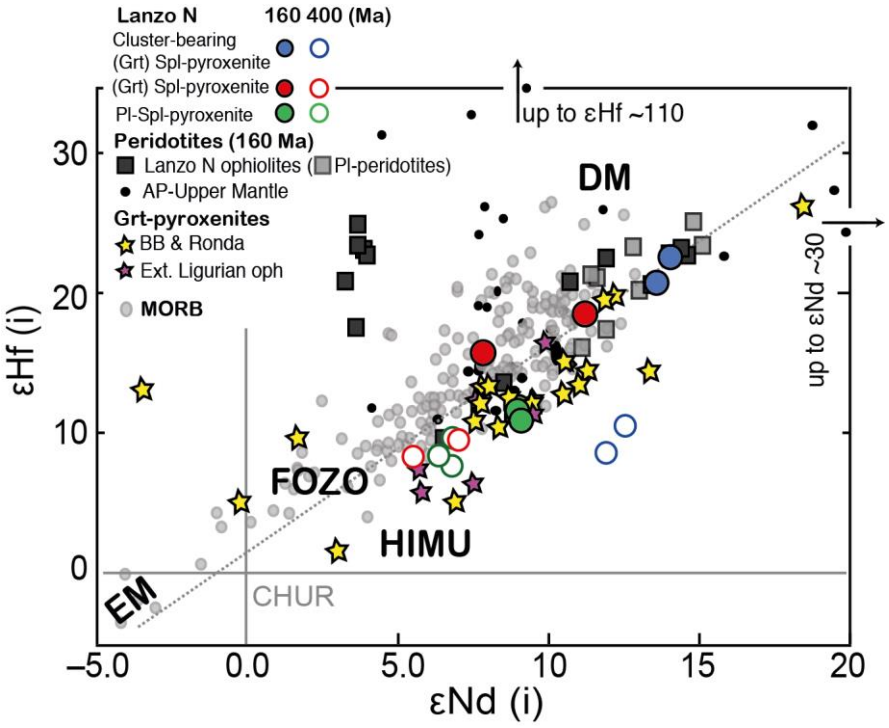

Figure 6. Initial Nd-Hf isotopic variations of Lanzo N pyroxenites and host peridotites calculated at the time of emplacement at Jurassic seafloor (160 Ma). Initial compositions of Lanzo N pyroxenites calculated at 400 Ma (empty red and green symbols) are also indicated (see text). The initial whole-rock compositions of Grt-pyroxenites from External Liguride ophiolites (Montanini et al., 2012), Ronda and Beni Bousera (Blichert-Toft et al., 1999; Pearson and Nowell, 2004; Varas-Reus et al., 2018) are calculated at time of exhumation as indicated in literature. The present-day compositions of clinopyroxenes from abyssal peridotites (Stracke et al., 2011), mantle xenoliths (Bizimis et al., 2003; Byerly and Lassitier, 2014) and MORB (after Stracke 2012) are also shown for comparison. Representative compositions of mantle end-members DM, EM, FOZO and HIMU are from Stracke (2012).

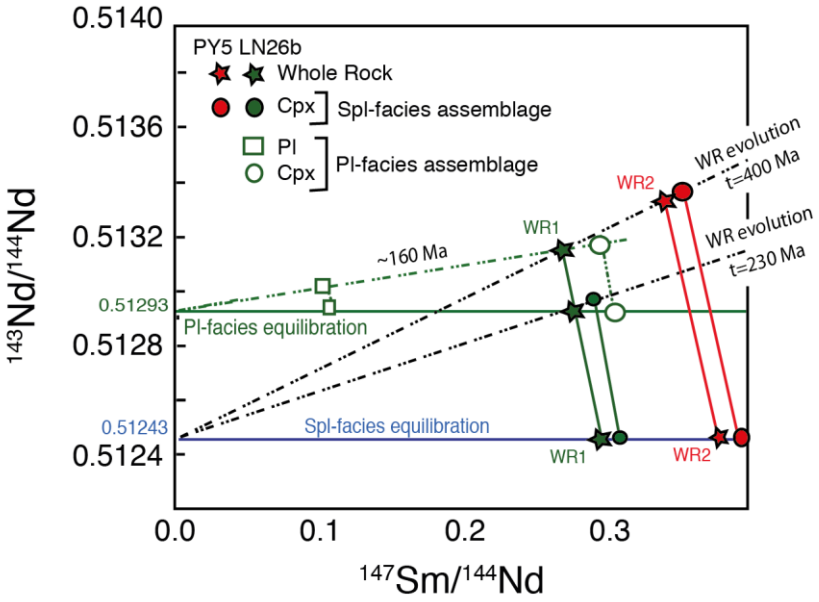

Figure 7. Nd-isotopic evolution of Spl-Pl pyroxenites. $^{147}Sm/^{144}Nd$ versus $^{143}Nd/^{144}Nd$ isotope ratios of whole rock, clinopyroxene and plagioclase in two representative samples of Spl-Pl pyroxenite (LN26b) (WR1) and (Grt)-Spl pyroxenite (Py5) (WR2). Both rocks initially equilibrated at spinel facies conditions at t=400 Ma, at different Sm/Nd ratios. At ~160 Ma, WR1 equilibrated at plagioclase facies conditions, resetting the Cpx $^{143}Nd/^{144}Nd$ ratios to the WR ratios, and forming plagioclase with the same $^{143}Nd/^{144}Nd$ isotope ratio. Because Cpx incorporates most of the Sm and Nd of the WR, this late equilibration event has a minor effect on the isotopic evolution allowing the preservation of a WR-Cpx errorchron defined for both samples, coexisting with a Pl-Cpx-WR internal isochron giving Jurassic ages.

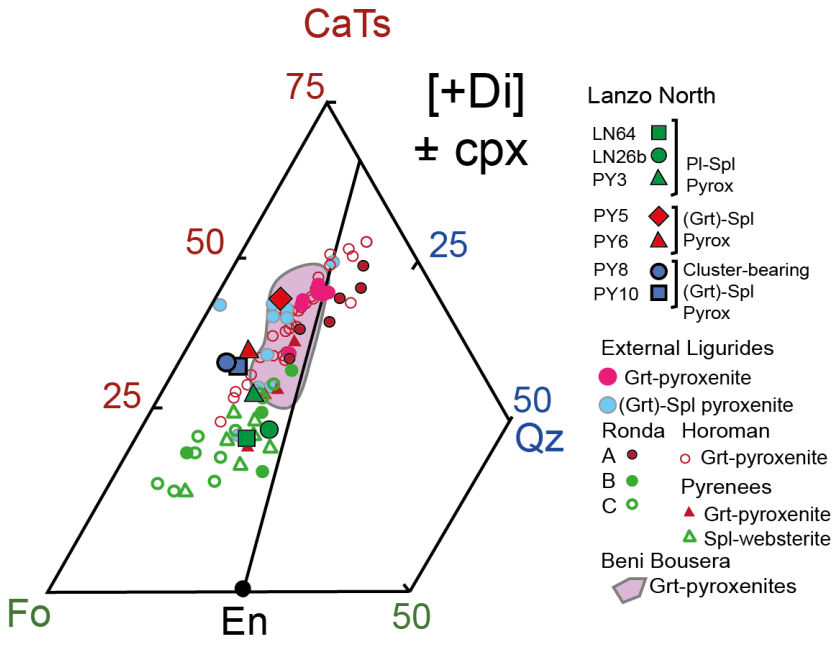

Figure 8. Molar projections from diospide [Di] into the pseudoternary diagram forsterite-Ca-Tschermak-quartz (Fo-CaTs-Qz) (O'Hara, 1972) of Lanzo North pyroxenites. The pyroxenite in this study are compared to garnet- and spinel-bearing pyroxenites from External Liguride ophiolites (Montanini et al., 2012, Borghini et al., 2016), Ronda (Garrido & Bodinier, 1999; Bodinier et al., 2008; Varas et al., 2018), Pyrenees (Bodinier et al., 1987), Horoman (Takazawa et al., 1999; Morishita & Arai, 2001), and Beni Bousera (Pearson et al., 1993; Kumar et al., 1996; Gysi et al., 2011; Varas et al., 2018).

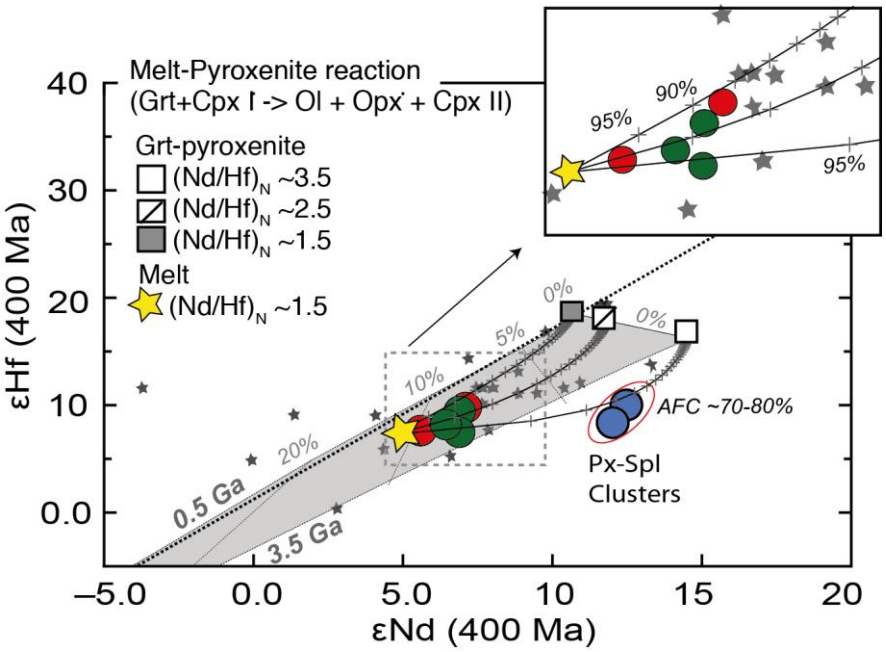

Figure 9. Nd-Hf isotopic variations of Lanzo N pyroxenites calculated at 400 Ma are compared to the whole-rock compositions of Grt-pyroxenites from External Liguride ophiolites, Ronda and Beni Boussera (grey stars; see **Fig. 6**). The grey field represents the compositions of recycled altered MORB at ages of 0.5 and 3.5 Ga and at various proportions of marine sediments as indicated by italic numbers (0-5-10-20%) (from Varas-Reus et al., 2018). The results of the AFC models are reported at steps of F=0.05 starting from three end-member Grt-pyroxenite compositions (see text for further explanation).

Figure 1

Click here to access/download;Figure;Fig1.png

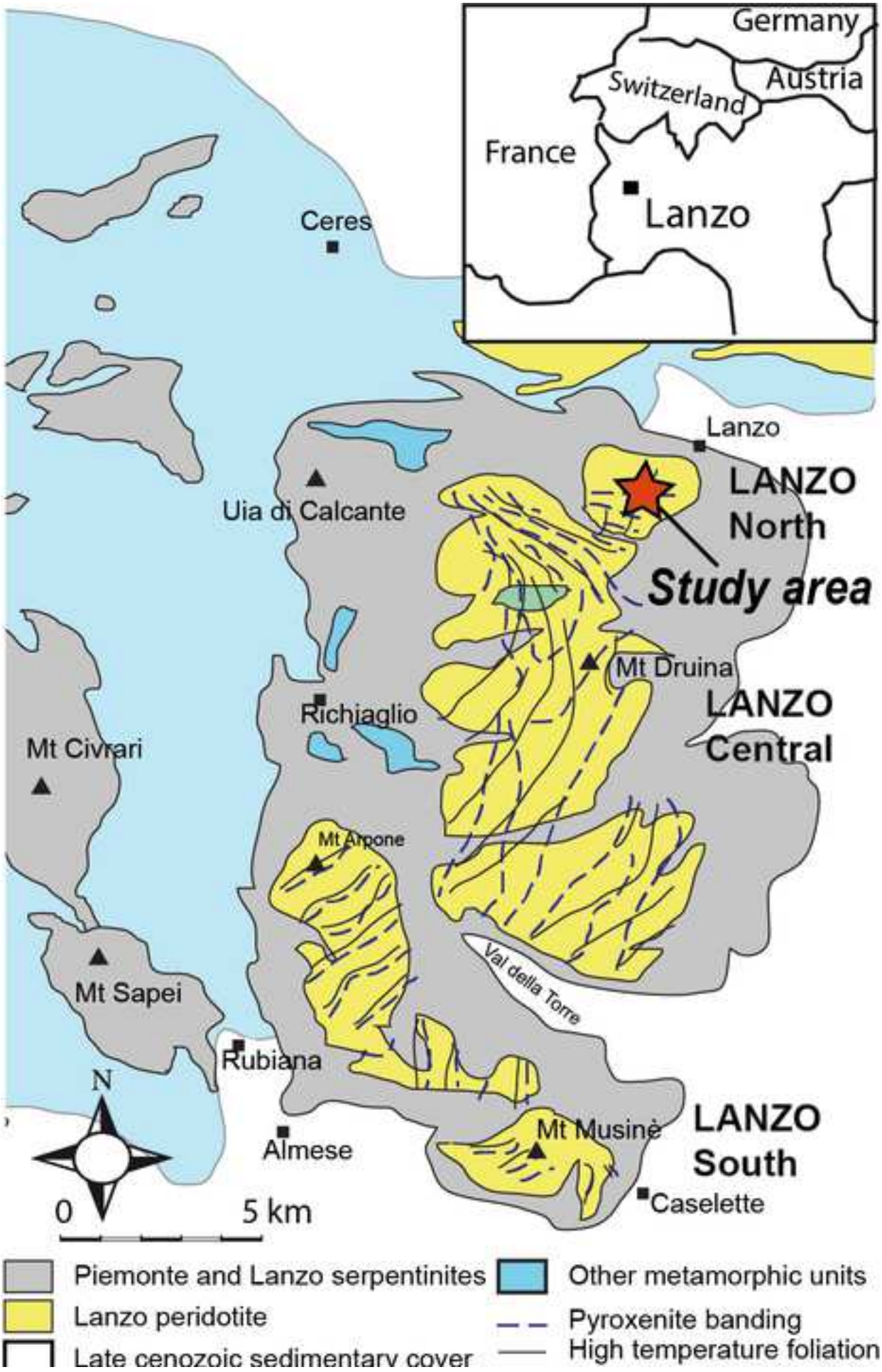

Figure 2

Click here to access/download;Figure;Fig2.png

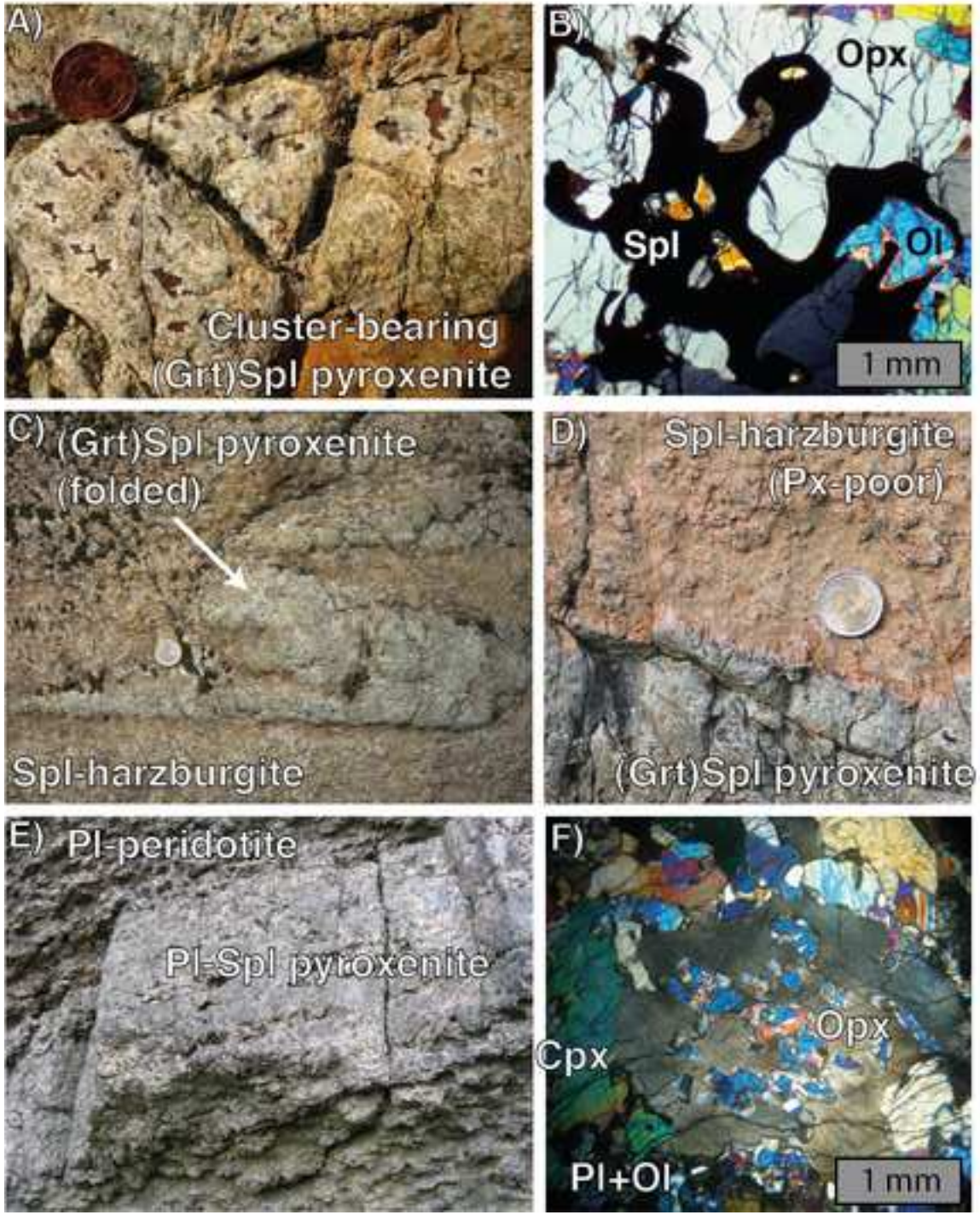

Figure 3

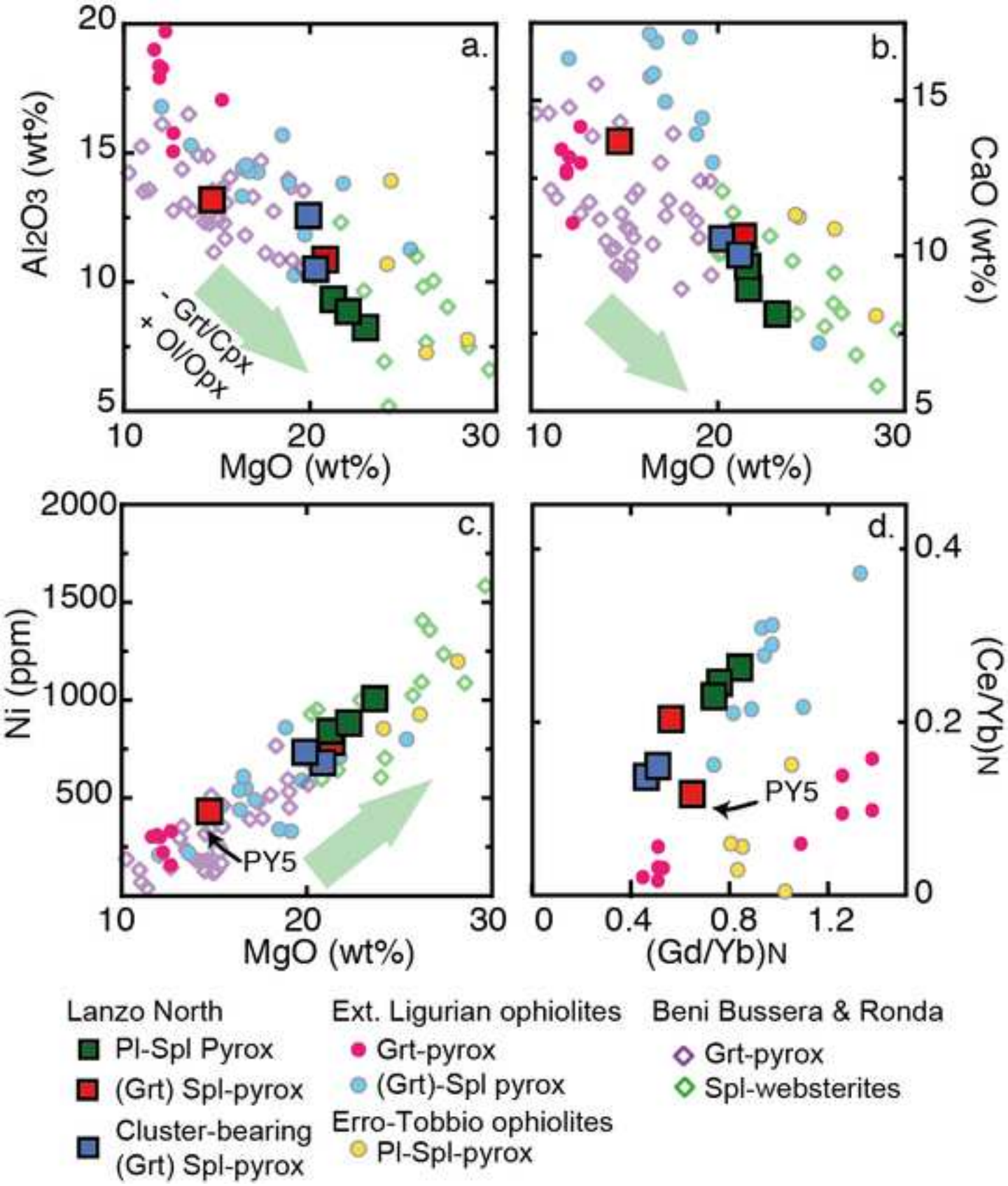

Figure 4

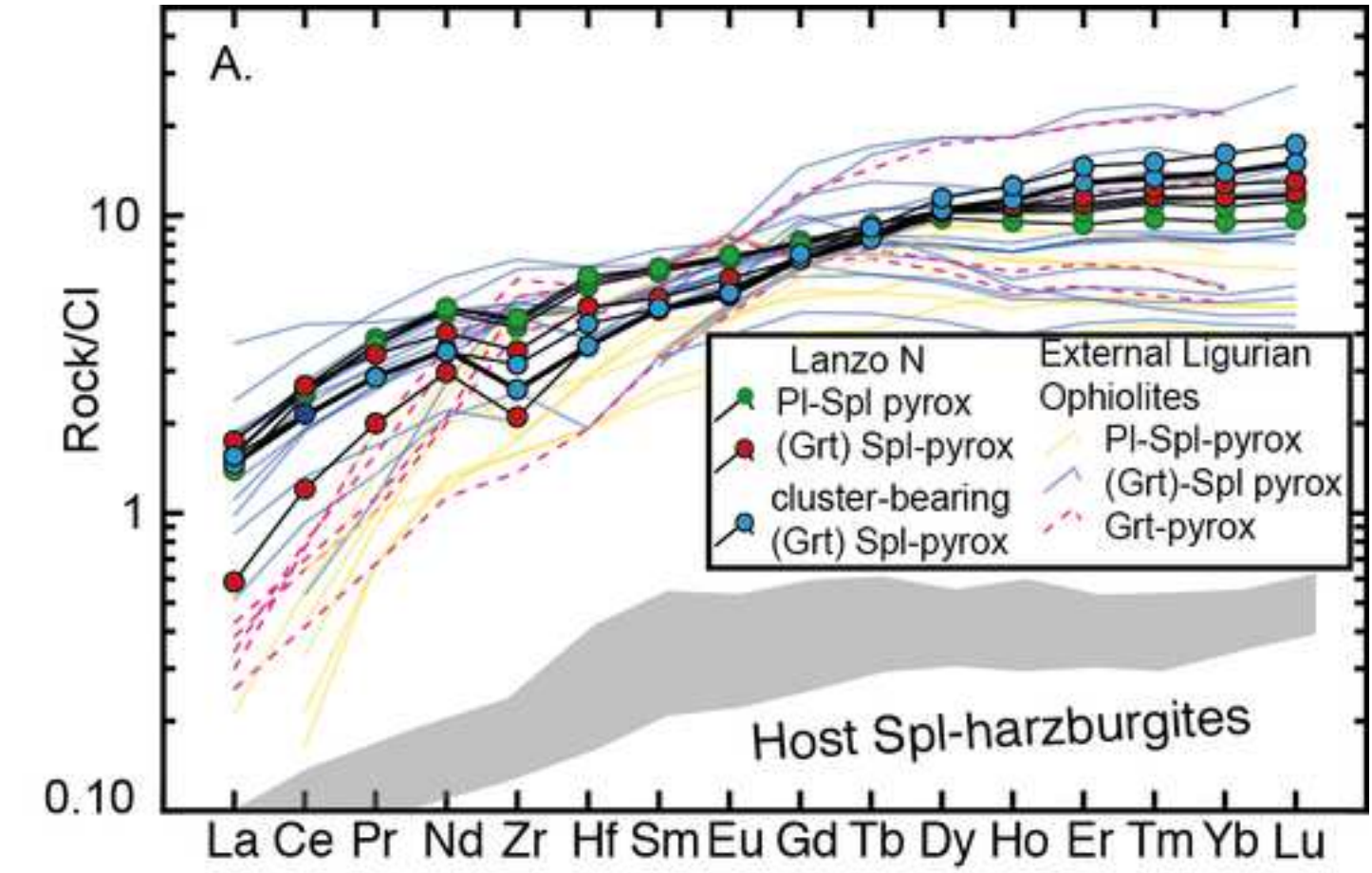

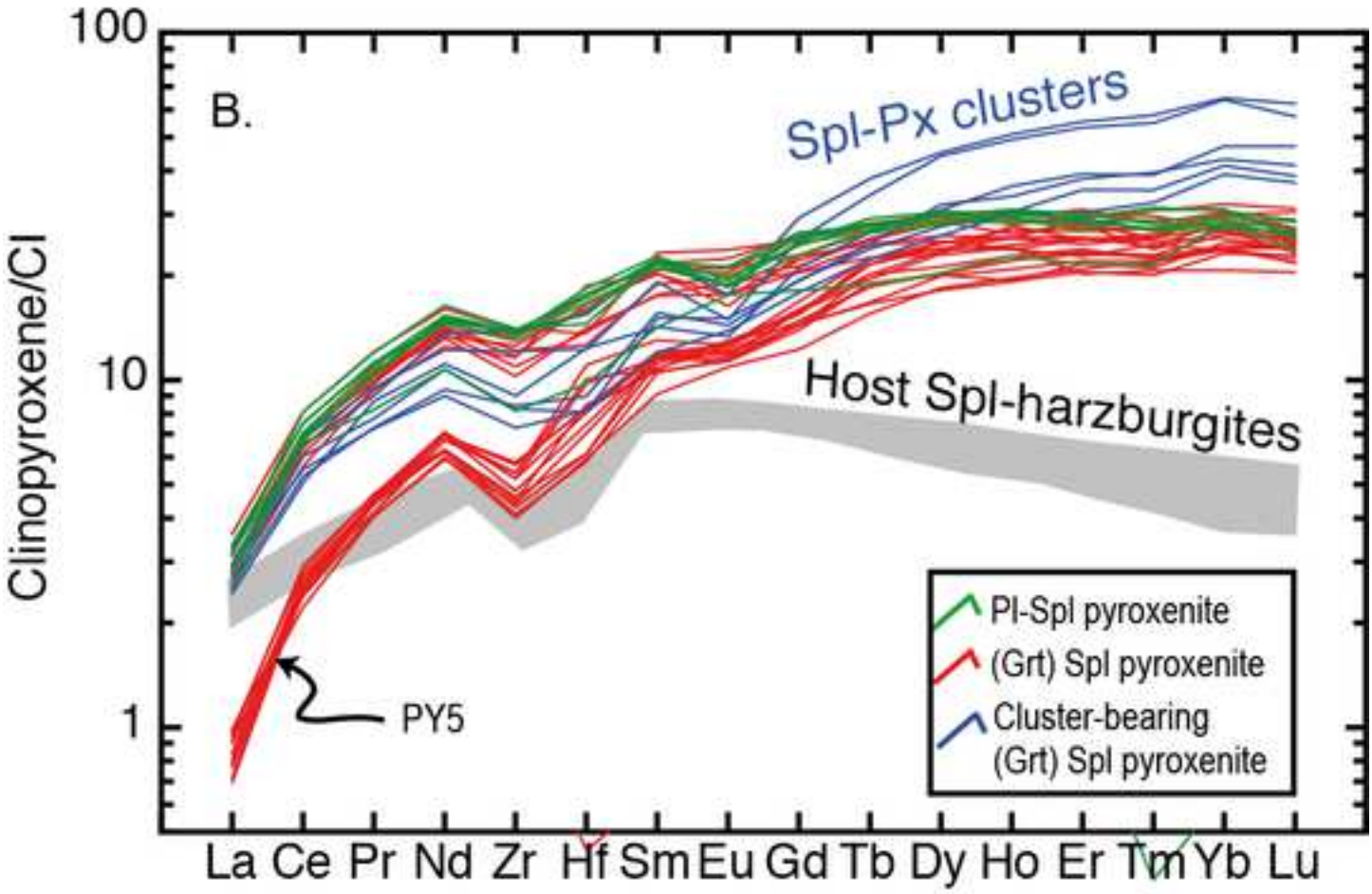

Figure 5

Click here to access/download;Figure;fig5.png

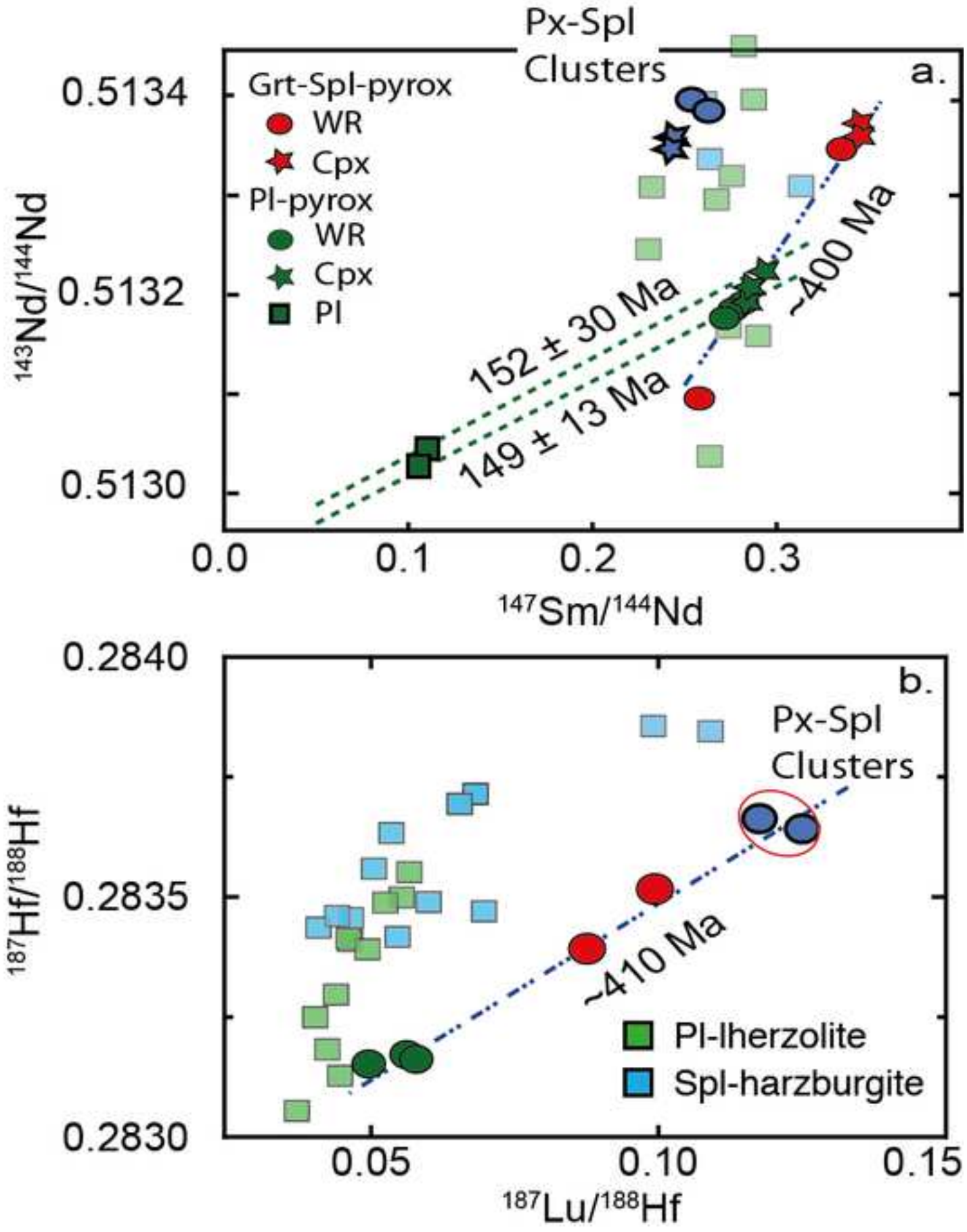

Figure 6

Click here to access/download;Figure;fig6.png

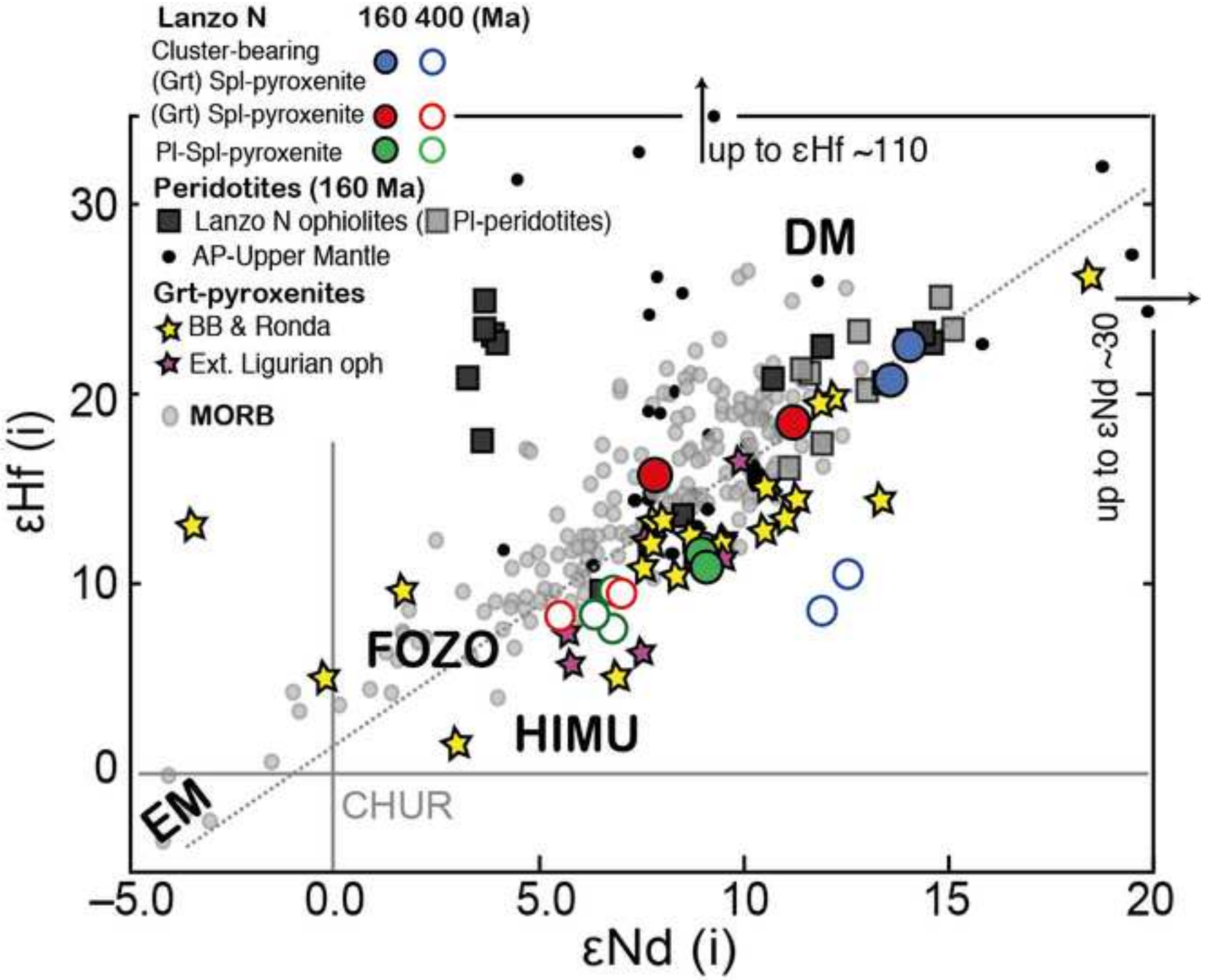

Figure 7

Click here to access/download;Figure;fig7.png

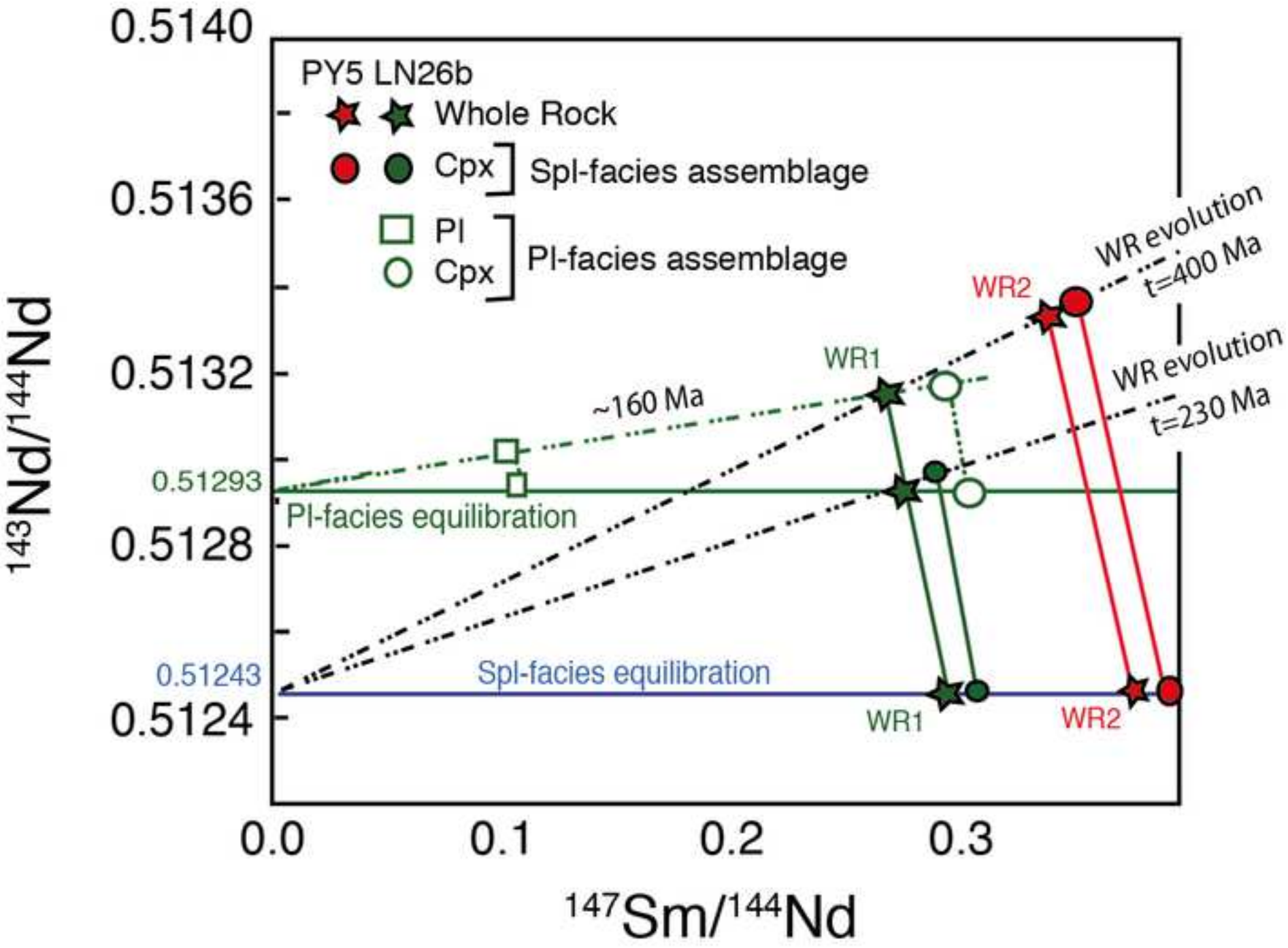

Figure 8

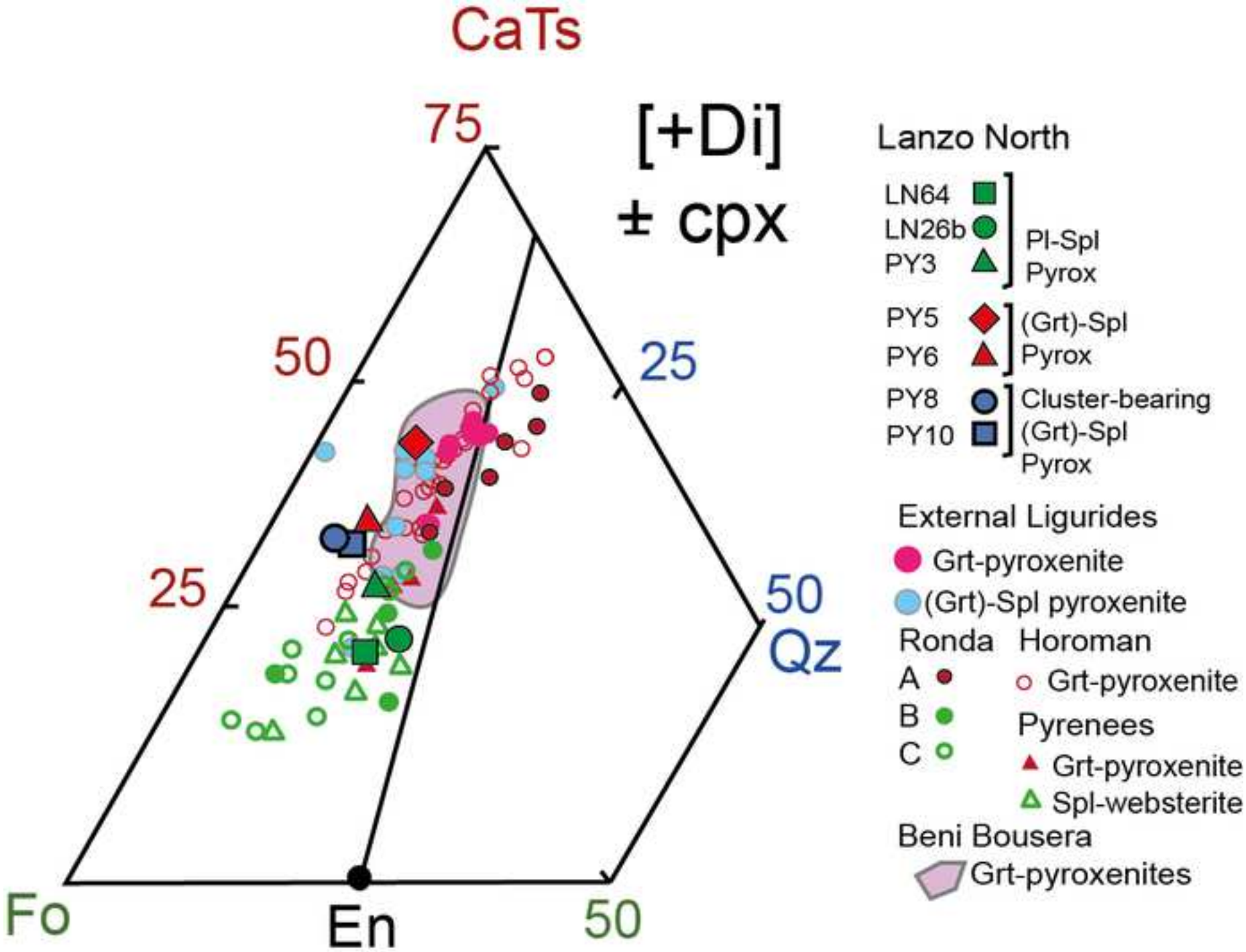

Figure 9

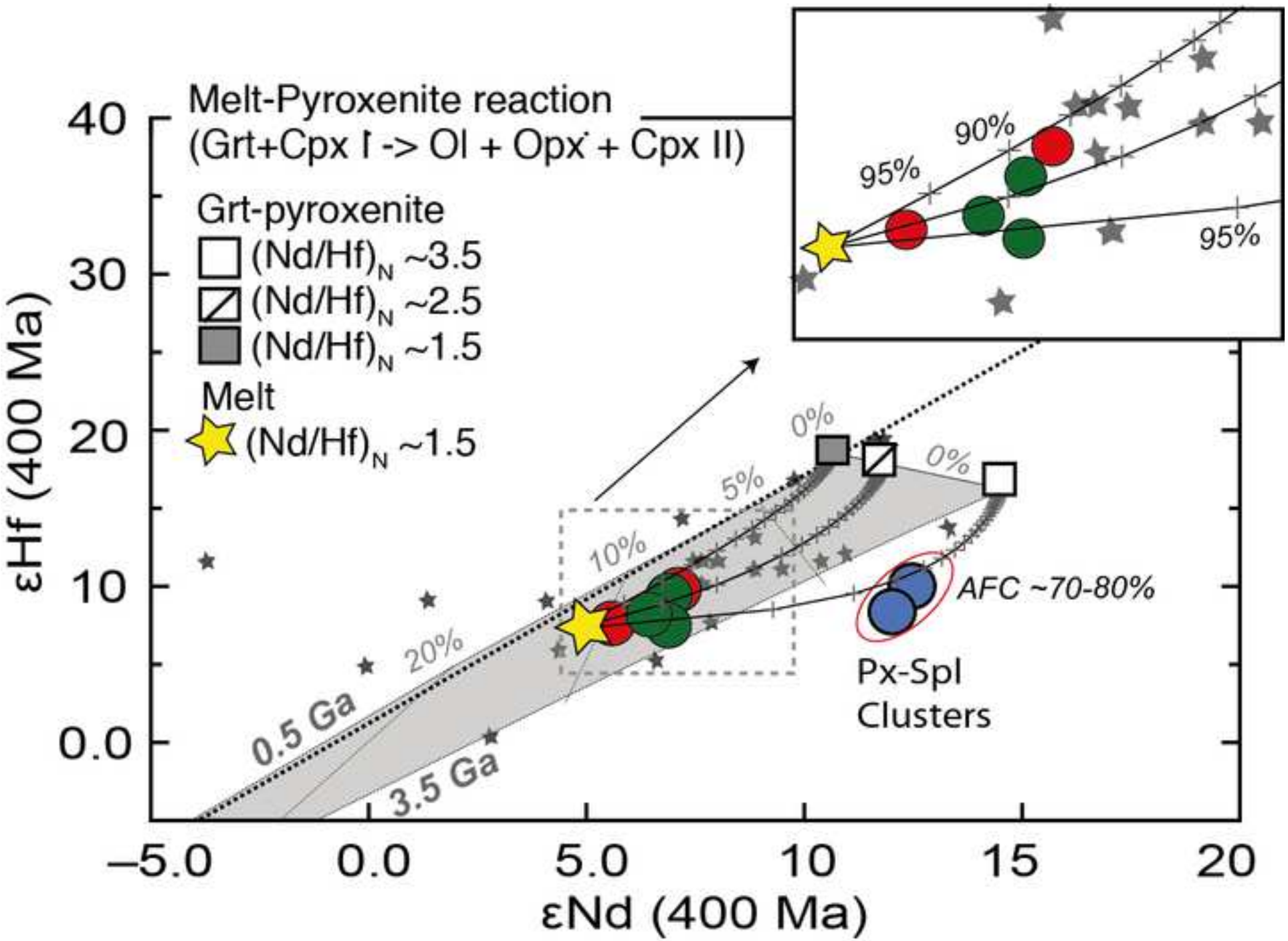

Table 1. Location and Nd and Hf isotopic data for clinopyroxenes and whole rocks from Lanzo North pyroxenites.

Sample name	Rock type	Coordinates		$^{143}Nd/^{144}Nd$	(2σ)	Sm (ppm)	Nd (ppm)	$^{147}Sm/^{144}Nd$	$^{176}Hf/^{177}Hf$	(2σ)	Lu (ppm)	Hf (ppm)	$^{176}Lu/^{177}Hf$
LN64	Spl-Pl pyroxenite	45° 15' 49.350" N 7° 27' 32.328" E	LN64 WR	0.513178	(8)	1.048	2.331	0.271848	0.283152	(6)	0.241	0.690	0.049579
			LN64 Cpx	0.513196	(7)	3.203	6.821	0.283961					
			LN64 Pl	0.513022	(9)	0.178	0.911	0.103761					
LN26	Spl-Pl pyroxenite	45° 16' 12.322" N 7° 27' 25.488" E	LN26b WR	0.513184	(9)	1.055	2.297	0.277743	0.283172	(3)	0.287	0.725	0.056192
			LN26b Cpx	0.513210	(8)	0.813	1.719	0.286089					
			LN26b Pl	0.513045	(6)	0.201	0.956	0.111794					
PY3	(Grt)-Spl pyroxenite	45° 15' 44.485" N 7° 27' 46.422" E	PY3 WR	0.513184	(5)	1.096	2.426	0.273115	0.283162	(12)	0.284	0.697	0.057842
			PY3 Cpx	0.513222	(7)	0.576	1.207	0.288671					
PY5	(Grt)-Spl pyroxenite	45° 15' 45.518" N 7° 27' 46.654" E	PY5 WR	0.513351	(9)	0.790	1.430	0.334145	0.283516	(7)	0.296	0.423	0.099378
			PY5 Cpx	0.513367	(8)	1.445	2.527	0.345668					
PY6	(Grt)-Spl pyroxenite	45° 15' 49.814" N 7° 27' 39.316" E	PY6 WR	0.513107	(7)	0.929	2.097	0.267945	0.283392	(9)	0.360	0.584	0.087582
			PY6 Cpx	0.513378	(7)	1.377	2.423	0.343647					
PY8	Cluster bearing (Grt)-Spl pyroxenite	45° 15' 56.338" N 7° 27' 46.731" E	PY8 WR	0.513403	(7)	0.720	1.557	0.245553	0.283663	(4)	0.340	0.411	0.117571
			PY8 Cpx	0.513365	(7)	1.430	3.328	0.228407					
PY10	Cluster bearing (Grt)-Spl pyroxenite	45° 15' 57.154" N 7° 27' 48.817" E	PY10 WR	0.513386	(6)	0.722	1.541	0.248962	0.283642	(4)	0.403	0.458	0.125003
			PY10 Cpx	0.513368	(7)	1.444	3.507	0.218831					

WR, whole rock; Cpx, clinopyroxene; Pl, plagioclase; details of analytical methods and errors (2σ) are given in the Methods section.

Declaration of interests

☒ The authors declare that they have no known competing financial interests or personal relationships that could have appeared to influence the work reported in this paper.

☐The authors declare the following financial interests/personal relationships which may be considered as potential competing interests: